

**Characterization of the neuronal proteolipids
M6A and M6B and the oligodendroglial tetraspans
PLP and TSPAN2 in neural cell process formation**

Dissertation

for the award of the degree

“Doctor rerum naturalium”

of the Georg-August-Universität Göttingen

submitted by

Patricia Irene de Monasterio Schrader

from Madrid, Spain

Göttingen, 28.6.2011

Prof. Klaus-Armin Nave Ph.D. (Reviewer)
Department of Neurogenetics / Max Planck Institute of Experimental Medicine

Prof. Dr. Gregor Bucher (Reviewer)
Department of Developmental Biology / Georg August University Göttingen

Dr. Dieter Klopfenstein
DFG Research Center for Molecular Physiology of the Brain (CMPB) /
Georg August University

Date of the oral examination: 20.7.2011

Declaration

I hereby declare that I prepared the PhD thesis entitled “Characterization of the neuronal proteolipids M6A and M6B and the oligodendroglial tetraspans PLP and TSPAN2 in neural cell process formation” has been written independently and with no other sources and aids than quoted. I would like to gratefully acknowledge Dr. Papiol for the statistical analysis and Dr. Mitkovski for the *in vivo* imaging of the cortical neurons.

Patricia Irene de Monasterio Schrader

Göttingen, 28th June 2011

To my family,
Especially my mother and father

Acknowledgement

I am sincerely grateful to Prof. Klaus-Armin Nave for his support, discussions and for giving me the possibility to work on this complex and challenging projects under such great conditions. He has shared his scientific experience with me and I could learn a lot.

I owe special thanks to Prof. Gregor Bucher and Dr. Dieter Klopfenstein, for their support, advices and fruitful discussions.

I am indebt to Hauke for his supervision in all the different stages of these two projects, for being a boss and a colleague, for his constant support and for everything he taught me.

Special thanks to Sergi and Miso for being the first aid team on statistical and confocal matters.

Many thanks to Ursula for restarting the M6-project and than giving it over to me.

Special thanks to Ulli for her support with the cell culture in general, and her tremendous help with the ES-cell culture in particular. And to Annette for all her help with the histology.

Many thanks to the animal facility: Kerstin, Marion and Franziska for their tremendous patience for standing my often times large animal cage numbers, Monika for her successful ES-cell injection, and Bianca for having always the proper mice for me.

Many thanks to the "Sequencing team" whom I visited so often at the beginning of this work: Fritz Benseler, Ivonne and Davana.

And special thanks to the computer experts: Beate, Lothar, Hajo and Rolf for having always time for me and my technical concerns.

I owe many thanks to Dr. Iñigo Azcoitia for introducing me firstly into the cell biology world and later on for walking with me my first steps into the neuroscience field.

I want to thank you for your moral and technical support and for the very nice time we spent together: Carolin, Foteini, Amit, Susanne, Maike, Olga, Anna, Viki, Mostafa, Julia, Ulrike and Georg and the entire Nave lab, for being so special.

Very special thanks to my dear friends Natalia, Noa and Burcu who have specially been able to stand me this last tense months and Burcu also for her support in the every-day-lab-issues.

....Ainhoa, Katja and Ajit.... I have felt your absence so much!

Many thanks to Sandra E. for being such sunshine.

Very special thanks goes to my great Spanish girls for showing me that there is no distance between us, in good and in bad times: Bárbara, Vanessa and Virginia.

I am very thankful to Sandra, Sergi and Viktor for being my Spanish family in Göttingen and giving me unconditional support. Without you I would not have been able to finish this adventure.

And last but not least, a big thanks to my beloved family, for being there always for me and helping me to become a better version of myself: my mother and father, Natalia, Tatiana, Angel and Andrés, Horst and Elke, and also Florian and Bettina. And the tiny Paula and Adrian for drawing always a big smile on my face.

Table of Content

List of figures	1
List of tables	2
Abbreviations	3
1. Abstract	6
2. Introduction	7
2.1. Development of the central nervous system	8
2.1.1. Neurons	9
2.1.2. Oligodendrocytes and myelin	14
2.2. Proteolipids	17
2.2.1. The oligodendroglial proteolipid protein PLP	18
2.2.2. The oligodendroglial and neuronal glycoprotein M6B	19
2.2.3. The neuronal glycoprotein M6A	21
2.3. Tetraspanins	24
2.3.1. Tetraspanins in myelin	26
2.3.2. Tetraspanin2: A role in myelination?	28
2.4. Aim of the study	30
3. Materials and Methods	31
3.1. Materials	31
3.1.1. Kits, chemicals and protocol source	31
3.1.2. Molecular biology buffers	31
3.1.3. Protein biochemistry buffers	32
3.1.4. SDS-PAGE and Immunoblotting	33
3.1.5. DNA and Protein markers	34
3.1.6. Immunocytochemistry buffers	34
3.1.7. Immunohistochemistry buffers	35
3.1.8. Histological stains and reagents	36
3.1.9. Oligonucleotides	37
3.1.10. Antibodies and recombinant proteins	38
3.1.11. Enzymes	39
3.1.12. Bacteria and bacterial culture media	39
3.1.13. Cell culture media	40
3.1.14. Mouse lines	41
3.2. Methods	41
3.2.1. Molecular biological methods	41
3.2.2. Generation of null-mutant mice	45
3.2.3. Protein biochemical methods	48
3.2.4. Animal breeding	51
3.2.5. Cell culture	51
3.2.6. Immunocytochemistry	52
3.2.7. Histology and immunohistochemistry	53
3.2.8. Confocal and light microscopy	54
3.2.9. Statistical analysis	55

4. Results	57
4.1. M6 Proteolipids in neuronal cell process formation	57
4.1.1. Localization of M6A and M6B on cortical neurons	57
4.1.2. Subcellular localization of M6A and M6B on cortical neurons	59
4.1.3. M6A defines F-actin free membrane protrusions	61
4.1.4. Altered growth cone morphology in Gpm6a ^{null*} Gpm6b ^{null} mice	64
4.1.5. M6A and M6B are required for normal reaction to ephrinA5	68
4.1.6. Impaired neurite outgrowth in the absence of M6 proteins	74
4.1.7. Neurite outgrowth and cholesterol	77
4.1.8. Growth cone morphology, adhesiveness and motility	79
4.1.9. Cortical development and corpus callosum width	84
4.2. Tetraspanin2 in CNS myelination	85
4.2.1. Tetraspanin2 expression in myelin	85
4.2.2. Targeted inactivation of the murine <i>Tspan2</i> gene	86
4.2.3. Characterization of TSPAN2 ^{null} mice	90
4.2.4. Weight increase in TSPAN2 ^{null} mice	92
4.2.5. Protein composition in TSPAN2 ^{null} mice	93
5. Discussion	97
5.1. Neuronal M6A and M6B proteolipids are abundant in cortical neurons	97
5.2. M6A defines F-actin free membrane protrusions	97
5.3. M6A and M6B are required for growth cone compartmentalization	98
5.4. M6A and M6B are required for normal reaction to ephrinA5	99
5.5. M6A and M6B are required for neurite outgrowth	101
5.6. M6A and M6B are required for the response to cholesterol in neurite outgrowth	101
5.7. M6A and M6B are not required for growth cone morphology, adhesiveness and motility	102
5.8. M6A and M6B are required for proper corpus callosum formation	103
5.9. Tetraspanin2 in CNS myelin	104
5.10. Targeted inactivation of the murine <i>Tspan2</i> gene	104
5.11. Weight increase in TSPAN2 ^{null} mice	105
5.12. Protein composition in TSPAN2 ^{null} mice	105
6. Summary and conclusions	107
7. References	108
Appendix 1: List of publications	117
Appendix 2: <i>Curriculum vitae</i>	118

List of figures

Figure 1. Growth cone drawings by Ramón y Cajal	10
Figure 2. Localization of F-actin and microtubules in axonal growth cones	12
Figure 3. Model of Eph receptors, ephexin and RhoA in growth cones	13
Figure 4. CNS myelination by oligodendrocytes	15
Figure 5. M6A is enriched at the leading edge of growth cones	22
Figure 6. Localization of TSPAN2 in brain sections	29
Figure 7. Evaluation of the <i>in vivo</i> motility of cortical neuron growth cones	55
Figure 8. Wild-type cortical neurons expressing M6A and M6B	57
Figure 9. Types of wild-type cortical neurons according to the M6-protein abundance	58
Figure 10. Subcellular localization of M6A and M6B on wild-type cortical neurons regarding tubulin and F-actin	60
Figure 11. M6A defines F-actin free membrane protrusions	62
Figure 12. M6B does not define F-actin free membrane protrusions	63
Figure 13. Classification of the neuronal growth cones according to three categories	65
Figure 14. Classification of the neuronal growth cones according to two categories	67
Figure 15. Altered growth cone morphology in Gpm6a ^{null*} Gpm6b ^{null} mice	67
Figure 16. Responsiveness to ephrinA5 induced growth cone collapse assay	69
Figure 17. Responsiveness to EphrinA5 induced growth cone collapse assay (diagram)	71
Figure 18. Abundance of axonal growth cones with lamellipodia	72
Figure 19. Immunoblot of cortical neuron lysates	73
Figure 20. Impaired neurite outgrowth of M6 mutant cortical neurons	74
Figure 21. Impaired neurite outgrowth in M6 deficient cortical neurons	76
Figure 22. Neurite outgrowth of cortical neurons upon cholesterol application	79
Figure 23. Morphometry of <i>in vivo</i> imaged cortical neuron growth cones	80
Figure 24. Adhesiveness of <i>in vivo</i> imaged cortical neuron growth cones	81
Figure 25. Motility of <i>in vivo</i> imaged cortical neuron growth cones	83
Figure 26. Reduced corpus callosum width at P5 in Gpm6a ^{null*} Gpm6b ^{null} mice	84
Figure 27. Tspan2 staining in the striatum of WT and PLP ^{null} mice	86
Figure 28. Generation of a C57BL/6 null-mutant mouse by gene targeting	87
Figure 29. Targeting strategy to inactivate the murine <i>Tspan2</i> gene	88
Figure 30. Homologous recombination and germline transmission after <i>Tspan2</i> gene targeting	89
Figure 31. Germline transmission and first TSPAN2 ^{null} mouse	90
Figure 32. Characterization of TSPAN2 ^{null} mice	91
Figure 33. Weight increase in wild-type, TSPAN2 ^{null} , PLP ^{null} and TSPAN2 ^{null*} PLP ^{null} mice	93
Figure 34. Silver staining of TSPAN2 ^{null} CNS myelin	94
Figure 35. Immunoblot analysis of TSPAN2 ^{null} mice	96

List of tables

Table 1. Neuronal growth cones classification according to their F-actin and tubulin compartmentalization, into three categories	65
Table 2. Neuronal growth cones classification according to their F-actin and tubulin compartmentalization	66
Table 3. Chi-square comparison of frequencies of classification of neuronal growth cones according to their F-actin and tubulin compartmentalization	66
Table 4. Quantification of the growth cone collapse assay induced by ephrinA5	70
Table 5. Chi-square comparison of the growth cone collapse assay induced by ephrinA5	71
Table 6. Abundance of axonal growth cones with lamellipodia	72
Table 7. Impaired neurite outgrowth of M6 mutant cortical neurons	75
Table 8. Impaired neurite outgrowth of M6 mutant cortical neurons	75
Table 9. Neurite outgrowth in cortical neurons upon cholesterol application	78
Table 10. Decreased corpus callosum width at P5 in Gpm6a ^{null*} Gpm6b ^{null} mice	85
Table 11. Reduced weight increase in PLP ^{null} and TSPAN2 ^{null*} PLP ^{null} mice	92

Abbreviations

°C	Degrees Celsius
bp	Base pairs
BSA	Bovine serum albumin
CD	cluster of differentiation
CNP	2'3'-cyclic nucleotide 3'phosphodiesterase
CNS	Central nervous system
Cy2	Cyanine Dye 2
Cy3	Cyanine Dye 3
DAB	3,3'- Diaminobenzidine
DAPI	4',6'-diamidino-2-phenylindole
ddDNA	Double stranded DNA
ddH ₂ O	Double distilled water
dH ₂ O	Distilled water
DIV	Days in vitro
dKO	Double null-mutant
DM20	Splice variant of PLP
DMEM	Dulbecco's Modified Eagles Medium
DMSO	Dimethylsulfoxide
DNase	Deoxyribonuclease
dNTPs	Deoxynucleotide Ttriphosphates
E	Embryonic day
EC	Extracellular loop
EDTA	Ethylened acid
ES	Embryonic stem cell
F generation	Filial generation
f.c.	Final concentration
F-actin	Filamentous actin
G418	Geneticin (gentamicin)
<i>Gpm6a</i>	Glycoprotein M6A-gene
<i>Gpm6ab</i>	Glycoprotein M6B-gene
HE	Haematoxylin-Eosin staining
HRP	Horseradish peroxidise
Ig	Immunoglobulin
Kb	Kilobases
kDa	Kilodalton
KO	Single-null mutant
LB	Luria-Bertani broth
M	Molar

M6A	Glycoprotein M6A
M6B	Glycoprotein M6B
mA	milliAmpere
MBP	Myelin basic protein
min	Minutes
ml	Milliliter
mM	Millimolar
mRNA	Messenger RNA
MT	Microtubules
ng	Nanogram
nm	Nanometer
OAP-1	OSP/claudin-11–associated protein 1, TSPAN3
OL	Oligodendrocytes
ON	Overnight
OPC	Oligodendrocyte precursor cells
OSP	Oligodendrocyte-specific protein (OSP)/ claudin-11
P	Postnatal day
PAGE	Polyacrylamidgelelektrophorese
PBS	Phosphate buffered saline
PCR	Polymerase chain reaction
PFA	Paraformaldehyde
PLL	Poly-L-lysine
PLP	Proteolipid protein
<i>PLP1</i> gene	Human Proteolipid protein gene
<i>Plp1</i> gene	Mouse Proteolipid protein gene
PMD	Pelizaeus-Merzbacher disease
PNS	Peripheral nervous system
PVDF	Polyvinylidene difluoride membranes
RhoA	Ras homolog gene family, member A
rpm	Rotations per minute
RT	Room temperature
SC	Schwann cell
SDS	Sodium dodecyl sulfate
sec	Seconds
SEM	Standard error mean
SERT	Serotonin transporter
SPG2	Spastic paraplegia type 2
ssDNA	Single stranded DNA
St. Dev.	Standard deviation

TBE	Tris-Borat/EDTA
TBS	Tris buffered saline
TEM	tetraspanin-enriched microdomains
TEMED	Tetramethyldiamin
TM4SF	Transmembrane four superfamily
Tris-HCl	Tris-(hydroxymethyl)-aminomethan titred with HCl
TSPAN2	Tetraspanin-2
U	Unit (for enzyme activities)
V	Volt
WT	Wild-type
µg	Microgram
µl	Microliter
µm	Micrometer

1. Abstract

The tetraspan-transmembrane proteins of the M6-proteolipid proteolipid protein family are among the most abundant cell surface proteins in neurons. Their cellular function has remained largely speculative, also because their analysis has been limited to acute alterations of their abundance levels *in vitro*. Based on expression analyses I have hypothesized that neuronal M6 proteolipids have a role in neuronal development. Indeed, the results presented in this thesis show that M6A defines an F-actin-free structural compartment at the tip of axonal growth cones while its homolog M6B is mainly present at actin-rich neurite domains. For the analysis of neurite extension upon chronic deficiency of M6-proteins, single-mutant M6A^{null} and M6B^{null} mice and M6A^{null}*M6B^{null} double-mutants were characterized. Importantly, lack of either neuronal M6-protein impaired the extension of neurites from cultured cortical neurons *ex vivo*. Mutant growth cones showed abnormal compartmentalization and did not display normal growth cone collapse upon ephrinA5-application. The mechanism of action is likely to involve Eph-receptor signalling, as the abundance of the effector molecule ephexin-1 is considerably reduced in the absence of M6-proteins. Preliminary analysis shows that the formation of neuronal processes is also impaired *in vivo*, at least affecting the long-projecting cortical neurons traversing the corpus callosum at an early postnatal stage. Together, M6-proteolipids contribute to the structural organization of neuronal growth cones that is prerequisite for normal reaction to guidance cues and neurite extension.

The third member of the M6-proteolipid proteolipid protein family, termed PLP, is the most abundant protein of CNS myelin. It has been surprising that myelin biogenesis is not obviously impaired in PLP^{null} mice. In a candidate approach the structurally related tetraspan tetraspanin-2 (TSPAN2), a known low-abundant myelin protein, was identified as a candidate to compensate for PLP-deficiency because of its considerably increased abundance in PLP^{null} myelin. To investigate the role of TSPAN2 in myelination, I generated TSPAN2^{null} mutant mice by homologous recombination in embryonic stem cells and TSPAN2^{null}*PLP^{null} double-mutant mice were bred. These mice are viable and fertile. Interestingly, the initial examination shows that the abundance of the closely related tetraspanin CD81 is increased in TSPAN2^{null} myelin, signifying a molecular change that may compensate for the absence of TSPAN2 function. Considering their spatio-temporal expression and that overexpression studies hint to a role of TSPAN2 and PLP in oligodendroglial processes formation it is likely that tetraspans of various protein families have overlapping and partially redundant functions as molecular facilitators of myelination.

2. Introduction

All our behaviours are orchestrated by brain function, which is performed by neurons and the connections between them. The proper performance facilitates a very complex behaviour. Brain function enables simple motor activities like breathing, smiling and walking, but also very complex ones as emotional and cognitive activities like feeling, thinking or writing a PhD Thesis (Kandel *et al.*, 2000).

The cellular unit of the brain is the neuron. At the end of the nineteenth century, Ramón y Cajal proved that the nervous system is a network of single cells, leading to the “neuron doctrine”. He demonstrated that neurons are the basic signalling unit of the nervous system: each neuron is one defined cell, which contacts other neurons at specific interaction points, the synapses (Ramón y Cajal, 2008). There are two distinct classes of cells in the nervous system, neurons and their glial support cells. In the human brain there are about 10^{11} neurons associated with over 10^{12} glial cells (Kandel *et al.*, 2000; Gilbert, 2003).

Neurons transmit electrical impulses from one region of the body to another. To prevent dispersion of the electrical signal and to facilitate its transmission to the target cells, the conducting part of large axons is insulated at intervals by oligodendrocytes (OL) in the central nervous system (CNS) and Schwann cells (SC) in the peripheral nervous system (PNS) (Sherman & Brophy, 2005). The OL wraps a process extension around the developing axon and produces a specialized plasma membrane called a myelin sheath. The myelin sheath is essential for fast nerve conduction. The axon has short non-myelinated segments that enable saltatory nerve impulse propagation, called the nodes of Ranvier (Sherman & Brophy, 2005). Myelin is indispensable for proper neural function, and demyelination of nerve fibres is associated with convulsions, paralysis and several debilitating or lethal afflictions (such as multiple sclerosis) (Gilbert, 2003).

The nervous system can be subdivided into the CNS and the PNS. The CNS comprises the brain and spinal cord, while the PNS is made up of all the remaining ganglia and peripheral nerves. The PNS has a somatic component (the sensory neurons form the dorsal root and cranial nerves) as well as an autonomic one (the sympathetic, parasympathetic and enteric nervous system). The CNS and PNS are anatomically separated but functionally connected (Kandel *et al.*, 2000).

2.1. Development of the central nervous system

After gastrulation the mammalian embryo has three embryonic layers, namely (1) the endoderm that gives rise to the gut, liver and lungs, (2) the mesoderm from which originates the connective tissue, muscles and vascular system, and (3) the ectoderm, the outermost layer that will give rise to the major tissues of the CNS and PNS as well as the epidermis. These three layers are part of the neural plate. Inside the gastrula is also the notochord that induces the neurulation (Kandel *et al.*, 2000; Gilbert, 2003).

During the following neurulation, the neural plate undergoes the neural induction so that it folds until forming the neural tube, which is the embryonic precursor of the six brain regions. The neuroectoderm produces neural precursor cells that will give rise to the neurons and glia of the CNS. The neuroblasts will migrate into the nervous system and differentiate into the neurons of the brain and spinal cord, while the glial progenitors give rise to OLs and astrocytes (Jessel, 2000). Cells within the neuroectoderm give rise to the neural crest; a transient group of migratory cells that emerge from the dorsal region of the neural tube and rapidly disperse along different pathways. They will give rise e.g. to neurons and SCs of the sensory and autonomic nervous system (Gilbert, 2003). Cell differentiation depends on a series of signals that ultimately control the differential activation of gene sets; each distinct cell type expresses a different subset of genes (proved by Monod and Jacob, late 1950s, cited after Kandel *et al.*, 2000). In the vertebrate neural development the cell-to-cell interactions are essential (Kandel *et al.*, 2000).

Subsequently the organogenesis occurs, in which the rostral segment of the neural tube gives rise to the brain and the caudal segment to the spinal cord. The rostral neural tube transforms initially into the three primary brain vesicles: forebrain, midbrain and hindbrain (Jessel, 2000), and with several flexures (cervical, cephalic and pontine) and further subdivision, the CNS is finally constituted of six main parts. From the forebrain arises (1) the telencephalon, which includes the cerebral hemispheres that are involved in perception and cognition and (2) the diencephalon that contains the thalamus and hypothalamus, integration centres, as well as the retina and optic nerves. The midbrain gives rise to (3) the mesencephalon that controls sensory and motor functions like eye movement. The hindbrain forms (4) the metencephalon which includes the pons and the cerebellum, related to movement modulation and learning of motor skills, and (5) the myelencephalon that forms the medulla oblongata, involved e.g. in breathing. The caudal part of the neural tube stays undivided and becomes (6) the spinal cord that controls movements of the limbs and trunk and receives and processes sensory information from the skin, joints and muscles of these (Kandel *et al.*, 2000; Squire *et al.*, 2002; Gilbert, 2003).

2.1.1. Neurons

Neurons are compartmentalized into three functionally different domains: the soma, where the cellular metabolism takes place, the dendrites and the axon. The dendrites receive signals from other neurons, which are conducted into the axon that transmits the signal to other neurons with an all-or-none propagating system, the action potential, a transient electrical signal. Axons may have up to one meter length, e.g. the pain sensing cells at the toes that transmit their impulses all the way to the spinal cord. The presynaptic terminal at the axon's end transmits neurotransmitters to the adjacent neuron at the synapses (Kandel *et al.*, 2000; Gilbert, 2003).

Neurons are the signalling unit and their interconnection allows the processing of information. The functioning of the mature nervous system depends on the action of distinct neuronal circuits. The neuronal connections are established during development and in the CNS of vertebrates it is an intimidating complex system: millions of neurons project their axons throughout the brain and establish thousands of connections with different target neurons. The diversity of connections by one single neuron distinguishes it from other cells (Tessier-Lavigne & Goodman, 1996; Kandel *et al.*, 2000).

The neurogenesis comprises several partially overlapping steps that include proliferation, migration, cell differentiation, maturation and cell death (Kandel *et al.*, 2000). The migration pattern of neurons establishes the basic plan of the CNS. Neural stem cells in the ventricular zone of the neural tube divide and form precursor cells, the neuroblasts. These migrate from the proliferation site at the ventricular zones of the neuroectoderm to their final positions along a scaffold of radial glial cells. Different neuroblasts migrate at different stages, before or after extending their axons (Kandel *et al.*, 2000; Squire *et al.*, 2002; Gilbert, 2003). For example, in the cerebral cortex, neurons of different morphology and connections are orderly arranged into well-defined layers. The layering of cortical neurons is associated to the moment they emerged: neurons born at early stages of cortical development end up in the deepest cortical layers, and those born at later times end up in progressively more superficial layers. Meaning that later born neurons must migrate through the existing layers of neurons that have already reached their final position in the cortex. Cortical layer organization is thereby an inside-out sequence of neuronal differentiation (López-Bendito & Molnár, 2003).

Once a neuron has migrated to its final position and sometimes even before, it begins to extend an axon. The axon extension takes place at its growing tip by means of the growth cones (GCs). Ramón y Cajal (1890) postulated that the axon was an outgrowth of the neuronal soma and described for the first time the growing tips of neuronal axons and named

them growth cones (Fig. 1). In a unique assumption based on morphological observations of fixed material he described their behaviour (Ramón y Cajal, 1890):

“Desde el punto de vista funcional, puede estimarse el cono de crecimiento como una especie de mata ó ariete, dotado de exquisita sensibilidad química, de rápidos movimientos ameboides, y de cierta fuerza impulsiva, merced á la cual es susceptible de empujar y franquear los obstáculos hallado á su paso, forzando los intersticios celulares hasta arribar a su destino.” (Cited after Ramón y Cajal, 2008).

[Translation of the citation of Ramón y Cajal, cited after Squire *et al.*, 2002.]

“From the functional point of view, one might say that the growth cone is like a club or battering ram endowed with exquisite chemical sensitivity, rapid amoeboid movements, and a certain motive force allowing it to circumvent obstacles in its path, thus coursing between various cells until reaching its destination.”

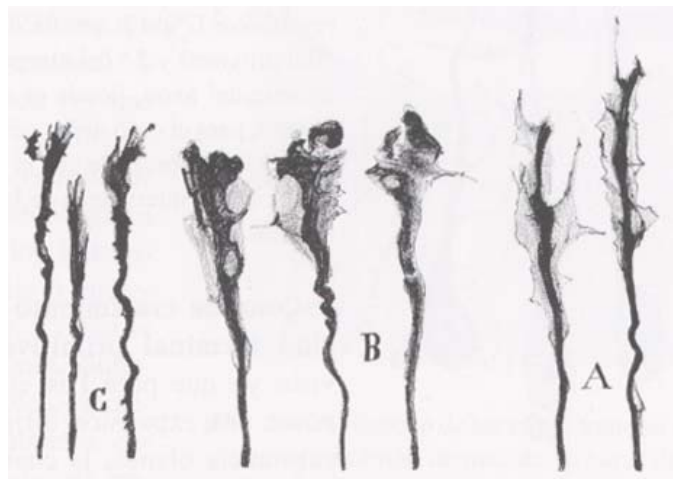


Figure 1. Growth cone drawings by Ramón y Cajal.

Growth cones of chicken spinal cord embryos of four days of age, stained by the Golgi method. Depicted are growth cones of the gray matter (A), close to the anterior commissure (B) and of the white matter (C) (Taken from Ramón y Cajal, 2008).

Hence, Ramón y Cajal suggested that the growth cones lead the advancing axon to its targets, thereby presenting the first instance of growth cones being involved in axon pathfinding. Two decades later, Harrison (1909) demonstrated the outgrowth theory. He observed living tissue in culture, deduced that growth of axons occurs by extension of the growth cones, and demonstrated the truth of Ramón y Cajal's description of a highly motile, amoeboid specialization at the tips of growing axons (Kandel *et al.*, 2000; Gilbert, 2003). Shortly after, Speidel (Squire *et al.*, 2002) took advantage of the thinness and transparency of tadpole fins and examined living growth cones extending *in situ*. The pioneering studies of Ramón y Cajal, Harrison and Speidel identified the growth cone as the key decision-making component in the elaboration of axonal pathways.

The neuronal growth cones lead the neuron's outgrowth by sensing environmental cues along the substrate. The force that extends the axon derives from changes that occur within the growth cone (reviewed in Dickson, 2002). Growth cones appear as an enlargement of the distal axon shaft, where the structural support is provided by microtubules (MT). In tissue culture growth cones are flattened into a thin fan-shaped sheet with many long, very thin spikes radiating forward. The veil-like extensions at the periphery of the growth cone are called lamellipodia, and the narrow cylindrical extensions capable of extending tens of microns from the periphery of the growth cone are called filopodia or microspikes. The lamellipodia are motile and give the growth cone its characteristic ruffled appearance. The filopodia (finger-like extensions) project from the growth cones, are highly motile and continually extend and retract. The sensitive capacity of the growth cones depends largely on the filopodia: by fanning out in front of them, each filopodium samples the microenvironment and sends signals back to the soma. Different second-messenger pathways are activated in growth cones by environmental signals and regulate their motility by modifying the structure or function of cytoskeletal and other proteins in the growth cone (reviewed in Dent & Gertler, 2003). Lamellipodia and filopodia of growth cones contain a high density of filamentous (F-) actin, and there is evidence that the degree of actin polymerization regulates growth cone motility. Actin is mainly present in the growth cone periphery with filopodia containing mainly F-actin bundles and lamellipodia an F-actin meshwork (Dent *et al.*, 2010). MTs are also present in growth cones, essentially in the axon shaft and the growth cone centre, and the regulation of the MT assembly also contributes to the extension and orientation of growth cone (Fig. 2). A bidirectional signalling between actin and MT is necessary for coordinating their polymerization for the directed axon growth from the growth cone, but is not required for axon extension *per se* (Dent & Kalil, 2001; Dent & Gertler, 2003).

As the axon extends the surface of the neuronal membrane increases tremendously. New membrane is synthesized in the cell body and transported in vesicles along MT into the growth cone. There, vesicles fuse and are incorporated into the plasma membrane. Although the growth cones also recycle membrane via endocytosis, there is a net addition of new plasma membrane (Pfenninger, 2009).

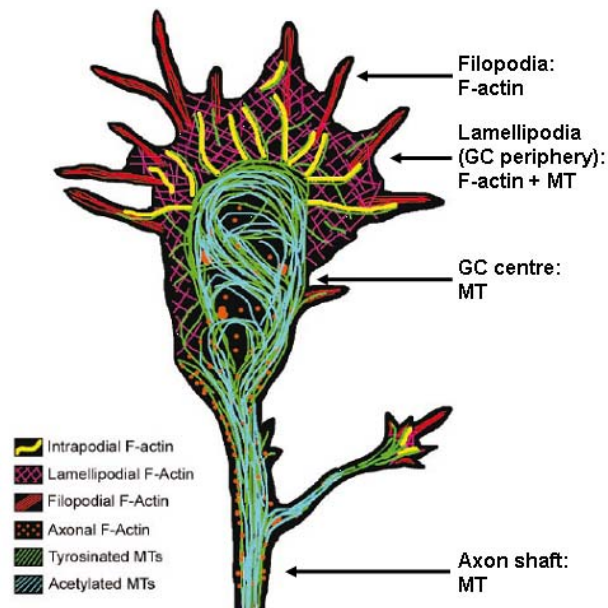


Figure 2. Localization of F-actin and microtubules in axonal growth cones.

Scheme representing the F-actin and MTs localization in an enlarged growth cone. MTs are present in the axon shaft and the central region of the growth cone and some tyrosinated-MTs extend into the lamellipodium and proximal domains of filopodia. F-actin is found in a mesh-like structure in the lamellipodium and as F-actin bundles in the filopodia. Note that filopodia are mainly formed by F-actin bundles (Taken from Dent & Kalil, 2001).

The specificity of the neuronal connections is one of the most striking physical aspects of the nervous system. How do the axons of developing neurons reach their targets? The specificity of axonal pathfinding is largely attributable to Sperry (1940s and 1950s), who demonstrated the high degree of preciseness in the formation of synaptic connections (cited after Kandel *et al.*, 2000). Axon guidance, the directed axonal growth early in development contributes to the specificity of neuronal connections, as the axons are guided from their origin to their appropriate destiny where they establish functionally appropriate connections with their synaptic partners. The selectivity of synaptic connections depends on the recognition of specific molecular cues in the vicinity of the target (Benson *et al.*, 2001).

Axons are guided along specific pathways by guidance molecules located in the extracellular space (Dickson, 2002). This takes place by the simultaneous and coordinated action of four types of guidance mechanism: contact attraction, chemoattraction, contact repulsion and chemorepulsion. A single growth cone might be “pushed” from behind by a chemorepellent, “pulled” from in front by a chemoattractant and “hemmed in” by attractive and repulsive local cues. “Push, pull and hem: these forces get together to guarantee accurate guidance” (cited after Tessier-Lavigne & Goodman, 1996). Guidance cues include molecules that are soluble, membrane-bound or from the extracellular matrix. There are four major families of signalling molecules that contribute to axon guidance: netrins, Slits, semaphorins and ephrins (Dickson, 2002). Many guidance cues are multifunctional, as they can be attractive but also

repellent. The growth cone guides the axon by converting the positive and negative cues into orders that regulate the cytoskeleton and determine the trajectory and speed of the axon's growth. Axon guidance specificity may depend on the balance between the attractive and repellent molecules (Tessier-Lavigne & Goodman, 1996; Dickson, 2002). Therefore, molecular gradients help axons to find their correct location within a target field, like opposing gradients of EphAs (ephrin receptors) and ephrin-As in the nasotemporal axis in the retina determine the final axon's termination and topographic map of the developing retinotectal system (reviewed in Feldheim & O'Leary, 2010). The axonal pathfinding depends not only on the guidance molecules *per se*, but also on their precise spatiotemporal distribution. Moreover, axonal outgrowth may be controlled independently of the guidance cues themselves. For example, when no ephrin is bound, the Eph receptor recruits the guanine nucleotide exchange factor (GEF) ephexin to the plasma membrane, where it activates RhoGTPases like Cdc42, Rac or RhoA (Fig. 3). Thereby the receptor without the ligand leads to a balance in the GTPase activation, which promotes axonal growth. Once ephrin binds to its Eph receptor and provokes the assembly of several ligand-receptor units in a cluster, the tyrosine kinase of the Eph receptor phosphorylates ephexin, RhoA gets inactivated and acts on the F-actin disassembly (reviewed by Egea & Klein, 2007; Lowery & Van Vactor, 2009). Thus, not only the type of guidance cue is decisive for the neuronal growth, but also its presence or absence.

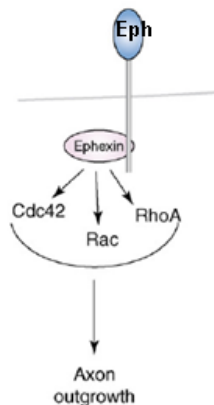


Figure 3. Model of Eph receptors, ephexin and RhoA in growth cones. The Eph receptor recruits the guanine nucleotide exchange factor ephexin to the plasma membrane, where it will activate RhoGTPases like Cdc42, Rac or RhoA. When the GTPases are balanced in this manner axonal outgrowth is promoted (Taken from Egea & Klein, 2007).

Axons have a non-constant growth rate as they often pause while they project to their targets. In decision regions, growth cones change their appearance, become more expanded and with a greater number of filopodia (Dent & Kalil, 2001). These changes have been suggested to reflect that the growth cone is actively searching for specific guidance cues. Once the immature neurons migrate from the germinal zones to their final position, the axons will form synaptic connections with a selected group of target cells. The initial synapse formation is often accurate, but some synapses are exuberant and superfluous and will be eliminated or modified partially during later stages of development, until the mature pattern of neural connections is completed (Innocenti & Price, 2005).

2.1.2. Oligodendrocytes and myelin

Neuroglial cells were first recognized over a century ago as connective elements in the CNS that fill the space between nerve elements or glue the nerve elements together (Greek, *glia* = "glue") (reviewed in Zhang, 2001). The three major glial cell types in the CNS are OLs, astrocytes and microglia. Many other types of glia cell are associated with them, evolutionarily or functionally. Astrocytes and oligodendrocytes both develop from the neuroectoderm, whereas the origin of microglia remains controversial, with the majority favouring a haematopoietic derivation. It is estimated that glial cells occupy half of the brain space, but outnumber neurons by ten to one (Zhang, 2001). Glial cells are involved in almost every aspect of neural function. During development, glia cells are implicated in guiding neuronal migration (radial glia), removing superfluous cells (microglia), myelinating axons (OLs) and forming the blood–brain barrier (pericytes). Under normal conditions, glial cells maintain the homeostatic environment for proper neuronal functions by storing energy, buffering pH, balancing ion concentrations and recycling neurotransmitters after neuronal excitation. Recent findings even indicate a synaptic communication with neurons, one of the hallmarks of neuronal identity. Under pathological conditions, glia cells act as a defence system collaborating with the immune system and producing trophic factors (Zhang, 2001).

In general, gliogenesis begins after neurogenesis but overlaps with it in several brain regions, and persists long after neurogenesis has ceased (Lee *et al.*, 2000). In the vertebrate CNS, OLs are derived from oligodendrocyte precursor cells (OPCs), which originate from the subventricular zone (Sherman & Brophy, 2005; Klämbt, 2009). The differentiation of OLs from their progenitors follows a stepwise morphological transformation from bipolar progenitors to pro-OLs bearing multiple processes (immature), membrane sheath-bearing mature OLs and, finally, to myelinating OLs. Accompanying this morphological change is a sequential expression of molecular markers (Zhang, 2001). The OPCs move as individual cells through the neural tube in a saltatory migration mode. Time-lapse imaging of cultured mammalian OPCs and *in vivo* imaging of developing zebrafish have shown that migrating OPCs have a rapidly remodelling tip that resembles an axonal growth cone. Interestingly, OPCs retract their processes upon contacting another OPC and change their migration direction. In addition to chemoattractants that are secreted by the target tissue and guide OPC's migration, such repulsive interactions between OPCs eventually result in their even distribution in the brain tissue. OPCs also divide during their passage through the brain. Because of the contact inhibition described above, the two daughter cells usually grow away from each other. This migration behaviour continues in adults and ensures that brain areas lacking oligodendrocytes, such as lesioned areas, can be efficiently repopulated (reviewed in Klämbt, 2009).

Myelin is a multilamellar isolating membrane that is formed by OLs in the CNS. The OLs enwrap tightly the axon with their membranous processes in segments that are separated by the nodes of Ranvier. An OL may envelope up to 60 internodes (Sherman & Brophy, 2005). The myelin sheath reduces current flow across the axonal membrane by lowering its capacitance and increasing its transverse resistance, thereby allowing the fast, saltatory movement of nerve impulses from node to node. As a consequence, a large number of axons with high conduction velocities (up to 100-fold increase) could be placed in a limited space, a feature that permitted the development of more complex nervous systems (Arroyo & Scherer, 2000; Poliak & Peles, 2003). Myelin and the confinement of voltage-dependent sodium channels to the nodes of Ranvier allowed the fast saltatory conduction of action potentials (Hartline & Colman, 2007). In addition, saltatory conduction eliminates the need for regenerating the action potential at every point of the axonal membrane, therefore reducing the metabolic requirements for neuronal activity (Poliak & Peles, 2003). When the OLs ensheath the axon they cover them at intervals (the internodes) leaving bare gaps, the nodes of Ranvier (Fig. 4). The nodes are flanked on either side by the paranodes where myelin loops form septate-like junctions with the adjacent axonal membrane. The following juxtaparanodal domain, as well as the internodes, extends underneath the compact myelin. These domains have different protein composition and compaction level (Poliak & Peles, 2003).

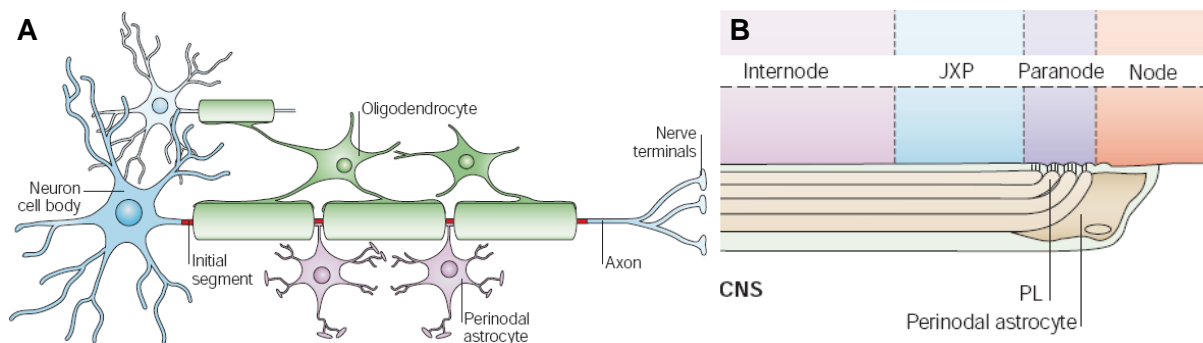


Figure 4. CNS myelination by oligodendrocytes.

A) In the CNS OLs myelinate numerous axon segments by enwrapping them with several myelin sheath layers at the internodes. The gaps they leave are the nodes of Ranvier.

B) Scheme of a longitudinal section of a node of Ranvier. At the nodes perinodal astrocytes contact the axon, and at the paranode the paranodal loops (PL) of the myelin sheaths end up. Following is the juxtaparanode that is beneath the compact myelin. The internode is also beneath the compact myelin and extends between two juxtaparanodal regions (Taken from Poliak & Peles, 2003).

Myelin is not only essential for the fast conduction of the action potential but also for the maintenance of axonal integrity, function, protection and survival. Several mouse mutants deficient in oligodendroglial proteins like proteolipid protein (PLP) and 2'3'-cyclic nucleotide 3'-phosphodiesterase (CNP) (Griffiths *et al.*, 1998a; Lappe-Siefke *et al.*, 2003) show normal myelination, but a secondary axonal loss, highlighting the importance of myelinating glia in the maintenance of axonal integrity. Myelinating glia communicates lifelong with axons and glia is required for the long-term integrity and survival of axons (Nave & Trapp, 2008; Nave, 2010b). The clinical relevance of myelin is very considerable. Aberrant myelin is a central feature of several neurological disorders, including multiple sclerosis, inherited leukodystrophies of the CNS and various peripheral neuropathies. Apart from to the primary axonal degeneration that occurs in some forms of multiple sclerosis and neuropathies, it is the secondary axonal degeneration that seems to be the major cause of continuous clinical impairment. Minor myelin abnormalities appear to also contribute to more complex disorders like schizophrenia, where patients seems to have myelin and white matter alterations (Nave, 2010a).

There are several crucial stages during myelination and some of them occur partially simultaneously. A first glia-to-axon contact is set at which the selection of axons and initiation of cell-cell interactions takes place. After the establishment of stable intercellular contact the spiral enwrapping starts (with up to 50 membrane layers) and the nodes of Ranvier are assembled. Subsequently, a radial and longitudinal expansion of myelin occurs and myelin thickness is regulated by compaction. The glia-to-axon support will last lifelong (Sherman & Brophy, 2005). Myelination has its onset in humans around the fourth intrauterine month and continues in the postnatal period, until nearly all the fibres are myelinated the moment the child starts to walk. Nonetheless, myelination is maximal at five years of age and still occurs in the fifth decade of life (Snell, 2001). In mice e.g. myelination starts early postnatal, making it an advantageous and excellent model organism for studying myelination.

The CNS myelin has a particularly unique composition in comparison to other plasma membranes. Some myelin proteins are present in high abundance (Jahn *et al.*, 2009), although the complexity of the myelin protein composition may not be below that of other membranes. Another prominent feature of myelin is the high enrichment of lipids that constitute about 70% to 80% of its dry weight (Norton, 1984), in contrast to most plasma membranes that show a lipid to protein ratio of around 1:1 (cited after Saher *et al.*, 2011). One of the most abundant ones, cholesterol, has been shown to be rate-limiting for myelin membrane biogenesis (Saher *et al.*, 2005).

The formation of myelin sheaths correlates with major changes of the gene expression profiles of differentiating glia in the CNS (Nielsen *et al.*, 2006; Dugas *et al.*, 2006). Only few ultrastructural features of compact myelin have been related to specific myelin proteins. Myelin is structured in compacted, concentric layers with a periodic ultrastructure. The compaction requires the abundant expression of structural proteins, such as PLP and myelin basic protein (MBP) in the CNS. Proteome analyses have revealed that the diversity of proteins in myelin is much more prominent than thought (Taylor *et al.*, 2004; Vanrobaeys *et al.*, 2005; Roth *et al.*, 2006; Werner *et al.*, 2007; Dhaunchak *et al.*, 2010). A recent quantification of myelin protein abundance based on mass-spectrometry demonstrated that all the previously known myelin proteins account only for 35% of the total myelin. Thereby, 65% of myelin corresponds to novel identified myelin-associated proteins. PLP and MBP that were thought to comprehend ~40% and ~30%, respectively, of total myelin protein, represent a still very high 17% and 8% of total CNS myelin protein (Jahn *et al.*, 2009). The function of the recently identified myelin-associated proteins is not well understood. A fraction of these proteins may reflect intracellular biogenesis and transport of myelin components that have a slow turnover rate (Nave, 2010b).

2.2. Proteolipids

The proteolipids received their name because of their high hydrophobicity (Folch & Lees, 1951), as a protein fraction that was isolated from white matter and that behaved like a lipid, being insoluble in water but soluble in organic solvents. The protein family of the proteolipid proteins includes the major CNS myelin protein proteolipid protein (PLP) and its smaller isoform DM20 (Nave *et al.*, 1987), as well as the homologs M6A and M6B. All have four transmembrane-domains (Popot *et al.*, 1991) and share a high similarity and homology at the nucleotide and amino acid level (Yan *et al.*, 1993). The proteolipid PLP/DM20 is expressed in OLs, M6A in neurons and M6B in both neurons and glia (Yan *et al.*, 1996). PLP, M6A and M6B are among the most abundantly expressed genes in brain (Huminiacki *et al.*, 2003).

The phylogeny of the proteolipids shows that orthologs do also exist in invertebrates like in the bilaterian groups of the platyhelminthes, molluscs, annelids and nematodes. They are also present in arthropods like the fruit fly *Drosophila melanogaster* (Möbius *et al.*, 2009). It has been recently shown that the *Drosophila* M6, the only proteolipid family member present in *Drosophila* and ortholog to M6a, is essential in the follicular epithelium maintenance involving membrane remodelling during oogenesis (Zappia *et al.*, 2011). In vertebrates PLP, M6A and M6B emerged in an ancestor of cartilaginous fish and are present in all non-mammalian groups (reviewed in Möbius *et al.*, 2009).

2.2.1. The oligodendroglial proteolipid protein PLP

The proteolipid protein was discovered in a brain protein fraction isolation that behaved similarly to lipids (Folch & Lees, 1951). PLP is a four transmembrane domain protein (Popot *et al.*, 1991) of 30 kDa (Nave *et al.*, 1987), with two extracellular loops (EC), EC1 and EC2. There are two disulfide bridges in EC2 that are essential for the proper protein function (Dhaunchak & Nave, 2007). DM20, the smaller isoform of PLP, is produced by alternative splicing and has a 35 amino acids deletion in the intracellular loop, resulting in a 26.5 kDa protein (Nave *et al.*, 1987). As previously mentioned, PLP is the most abundant protein in CNS myelin (Jahn *et al.*, 2009).

DM20 mRNA transcripts are expressed before the onset of myelination (Timsit *et al.*, 1992). During the OL development, the expression of DM20 decreases and PLP's increases largely, so that the presence of PLP defines the mature myelinating OL. In the myelinated CNS, PLP is found in the compact myelin sheets (reviewed in Griffiths *et al.*, 1998a). This indicates a role of PLP in the early development of OLs as well as in myelination itself. It has been recently shown a novel function for DM20 in increasing filopodium formation by overexpression in COS7 cells (Fernández *et al.*, 2010).

PLP binds cholesterol and this is very important for the association of PLP with lipid rafts (Simons *et al.*, 2000; Krämer-Albers *et al.*, 2006). Lipid rafts are cholesterol- and sphingolipid-rich membrane domains that form platforms for concrete proteins and regulate thereby functions like e.g. intracellular membrane transport and cell signalling (Simons & Ikonen, 1997; Simons & Toomre, 2000). When PLP cannot bind cholesterol the proper sorting and assembly of myelin in OLs (Simons *et al.* 2002; Krämer-Albers *et al.*, 2006) is distorted. PLP is as well palmitoylated and this is required for the sorting of PLP into myelin (Schneider *et al.*, 2005).

Since long PLP/DM20 has been proposed to act as an "adhesive strut" in myelin (cited after Kirschner *et al.*, 1984, in Kitagawa *et al.*, 1993), even though there were no indications for them being adhesion proteins. The analysis of the PLP^{null} mice at the ultrastructural level illustrated an altered membrane compaction in CNS myelin (Klugmann *et al.*, 1997; Rosenbluth *et al.*, 2006). But recently, it has been shown that this has been probably mainly a fixation artefact, to which the PLP-deficient myelin is particularly vulnerable. So, X-ray diffraction analysis on optic nerve of PLP^{null} mice suggested a normal compact myelin periodicity (Yin *et al.*, 2006). Additionally, high-pressure freezing and freeze substitution, in which the *in vivo* morphology is better preserved, on PLP^{null} optic nerves has also not shown an altered periodicity in myelin (Möbius *et al.*, 2009). Thereby, the suggested role of PLP as

an adhesive strut in myelin is still under debate. But PLP^{null} mice do show a progressive axonal degeneration, mainly in small diameter myelinated axons (Griffiths *et al.*, 1998b), as well as an impaired fast retrograde and anterograde axonal transport (Edgar *et al.*, 2004). This axonopathy demonstrates the importance of PLP in preserving integrity of CNS axons. The neuroprotective effect of PLP on CNS axons has also been proven when exchanging PLP and P0 in CNS myelin (Yin *et al.*, 2006). P0, the major PNS myelin protein was evolutionary replaced by PLP in the CNS. All in all, PLP by its abundance, lipid-binding properties and axonal protective effects, does contribute to the proper myelin formation and maintenance.

There are several natural *Plp1*-gene mutations that cause different degrees of dysmyelination. The *rumpshaker* mouse (Schneider *et al.*, 1992) has a point mutation that leads to an amino acid substitution and shows a mild affection with tremors. But, e.g., in the *jimpy* mouse a point mutation at a splice site (Nave *et al.*, 1986) leads to a deletion and thereby to an altered C-terminus of the PLP protein. The *jimpy* mice have a severe dysmyelination and die prematurely (reviewed in Griffith *et al.*, 1998). The pathology of these mutant PLP mice is due to the toxicity of the misfolded mutated PLP protein (Klugmann *et al.*, 1997). There have also been generated two-fold overexpressing *Plp1* mice that show a severe hypomyelination and premature death (Readhead *et al.*, 1994). This mouse models prove that alterations in the *Plp1* gene lead to an aberrant myelination, thereby confirming again the importance of PLP in myelin biogenesis. There are as well several leukodystrophies due to the mutation of the X-linked gene encoding PLP in humans. The PLP-deficiency is observed in spastic paraplegia type 2 (SPG2, OMIM no. 312920) patients. While Pelizaeus–Merzbacher disease (PMD, OMIM no. 312080) is most commonly caused by duplications of the *PLP1* gene, but also by deletions, triplications and point mutations. Both are CNS dysmyelinating pathologies, but with a broad clinical spectrum: from the mild SPG2 forms to the severe congenital PMD (reviewed in Garbern, 2006; Woodward, 2008).

2.2.2. The oligodendroglial and neuronal glycoprotein M6B

The glycoprotein M6B, and ortholog to PLP, with 2 potential N-linked glycosylation sites (Yan *et al.*, 1993), was lately proven to be actually a glycosylated protein (Fünfschilling U., pers. comm.). The mammalian *Gpm6b* gene has a complex transcription and splice scheme and encodes eight different protein isoforms, differentially expressed. The subcellular localization depends on the N-termini and the presence of transmembrane domains (Werner *et al.*, 2001).

Abundant M6B expression has been detected in both neurons and OLs (Yan *et al.*, 1993, 1996; Werner *et al.*, 2001) and its expression is throughout the brain and spinal cord (Yan *et al.*, 1996). There are also faint expression levels of M6B mRNA in many non-neuronal tissues, including testis, liver, spleen, kidney, muscle, heart and lung (Werner *et al.*, 2001; Isensee *et al.*, 2008). During CNS development, M6B mRNA has first been detected in the ventricular zone; as early as at embryonic (E) day 10 (Yan *et al.*, 1996), indicating its expression in proliferating and differentiating cells.

M6B has been detected by immunoblotting in a myelin-enriched brain fraction (Klugmann *et al.*, 1997), without presenting abundance differences between wild-type and PLP^{null} mice; and M6B represents approximately 1% of total CNS myelin proteins (citing Jahn *et al.*, 2009, from Möbius *et al.*, 2009). M6B is functionally redundant to PLP with respect to myelin biogenesis (Werner *et al.*, pers. comm.).

In primary cultures of hippocampal neurons the overexpression of M6B induces filopodia formation, similar to M6A (see below). Chronic restraint stress in mice leads to a decrease in M6B mRNA levels in the hippocampus (Fernández *et al.*, 2010).

Recently, it has been shown that M6B interacts with the serotonin transporter (SERT), a sodium- and chloride dependent transporter that mediates active re-uptake of the neurotransmitter serotonin at the synapses. Co-expression of SERT with M6B led to a reduced SERT expression at the cell surface and diminished the serotonin uptake *in vitro* (Fjorback *et al.*, 2008). M6B may therefore regulate serotonin uptake by regulating the trafficking of the serotonin transporter.

The human M6B gene (*GPM6B*) is located at Xp22.2 (Olinsky *et al.*, 1996) and has been associated with a susceptibility locus for sickle cell anemia (OMIM no. 603903) (Sebastiani *et al.*, 2008). *GPM6B* has also been considered a candidate to cause neurological diseases that have been mapped to the Xp22 region, but no *GPM6B* mutations were detected in analyses of patients with Rett syndrome (OMIM no. 312750) (Narayanan *et al.*, 1998) or Xp22-linked recessive mental retardation (OMIM no. 309530) (Turner *et al.*, 2003). It is also unlikely that mutations in *GPM6B* are involved in the Pelizaeus–Merzbacher-like disease (PMLD, OMIM no. 608804), a subgroup of human hypomyelination disorders (Henneke *et al.*, 2004; Combes *et al.*, 2006). PMLD is a leukodystrophy with diffuse hypomyelination. The patients have a clinical course very similar to PMD and represent about 20% of all cases with a clinical PMD phenotype, but lack *PLP1* gene duplications or mutations (Henneke *et al.*, 2004). Nevertheless, it was recently found a decreased expression of the *GPM6B* gene in

male suicide completers in a population of French Canadians (Fiori *et al.*, 2011). In female mammals most genes are silenced on one X chromosome as a result of the X-chromosome inactivation. However, some genes escape this and are then expressed in both, leading to potential sexual dimorphisms. The human *GPM6B* has been proven to escape this X-inactivation (Carrel *et al.*, 2005) and shows decreased expression in females (Isensse *et al.*, 2008).

Together, it is known that M6B is important and partially functionally redundant to PLP in CNS compact myelin. Moreover, by its neuronal expression, it has been related mainly to filopodia formation *in vitro* and to the regulation of the SERT.

2.2.3. The neuronal glycoprotein M6A

M6A, also known as glycoprotein M6A (GPM6A), because of its N-glycosylation (Lagenauer *et al.*, 1992; Baumrind *et al.*, 1992) or edge membrane antigen (EMA) (Baumrind *et al.*, 1992), was cloned as the antigen of the monoclonal M6 antibody, and has 30 kDa (Yan *et al.*, 1993). The human *GPM6A* gene is located at 4q34 (Olinsky *et al.*, 1996) and there are two splice variants in rodents and humans: M6a-1a and M6a-1b, being M6a-1b more predominantly expressed in the brain (Cooper *et al.*, 2009). The two isoforms differ in their N-terminal cytoplasmic domain (Werner *et al.*, 2001).

M6A is an abundant cell surface protein on postmitotic neurons in the CNS and is not present in OLs or glial precursors (Lagenauer *et al.*, 1992; Baumrind *et al.*, 1992). It is expressed already at E10 in postmitotic neurons of the developing neural tube and at E11 M6A is detected throughout the brain (Baumrind *et al.*, 1992) and spinal cord, where it is maintained throughout adult life (Lagenauer *et al.*, 1992; Yan *et al.*, 1996). M6A is also expressed in the retina of adult mice (Lagenauer *et al.*, 1992). Immunohistochemistry reveals a wide expression in the CNS (Lagenauer *et al.*, 1992; Baumrind *et al.*, 1992). M6A is also expressed in cells of the epithelial layer of the choroid plexus and in renal proximal tubules, but not in PNS neurons (Lagenauer *et al.*, 1992; Baumrind *et al.*, 1992). The abundance of M6A augments strongly during neuronal differentiation, when the neurite outgrowth takes place in postmitotic neurons (Lund *et al.*, 1986; Yan *et al.*, 1996). During the maturation of the CNS the expression of M6A decreases, coinciding with myelination, in e.g. the pyramidal tract, corpus callosum, optic nerve and retina (Mi *et al.*, 1998). However, it remains extensively in non-myelinated axons like cortical pyramidal neurons, cerebellar granule cells and glutamatergic presynaptic terminals (Lund *et al.*, 1986; Cooper *et al.*, 2008).

In the early 1990's it was revealed in cultured cortical neurons (by immuno-fluorescence and freeze-etch immuno-electron microscopy) that although M6A is present on the plasma membrane of neuronal cell bodies and processes, it has an enriched and non-uniform distribution (Fig. 5) on lamellipodia and filopodia at the leading edges of the neuronal growth cones (Sheetz *et al.*, 1990; Baumrind *et al.*, 1992).

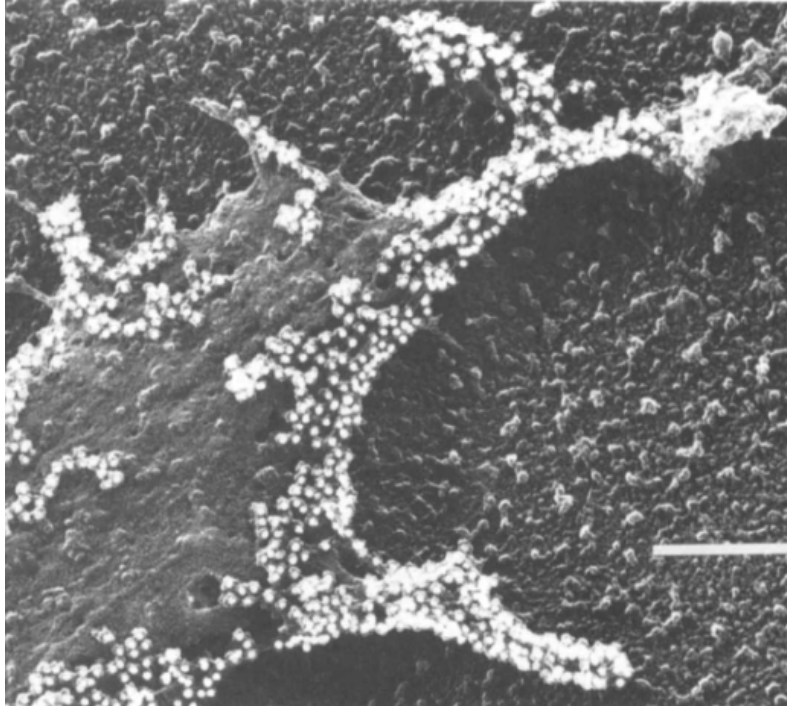


Figure 5. M6A is enriched at the leading edge of growth cones.

Freeze-etch immuno-electron micrograph revealing M6A labelling on neuronal growth cones. There is an enriched M6A labelling at the leading edge of lamellipodia and along filopodia. Scale bar = 0.2 μm (Taken from Baumrind *et al.*, 1992).

At that time it was also realized that upon acute addition of the monoclonal M6 antibody, cultured cerebellar neurons experienced a reduced neurite extension, without altering the motility of the filopodia or lamellipodia from the growth cones and without presenting a growth cone collapse (Lagenauer *et al.*, 1992). This result suggested for the first time that M6A could be involved in neurite elongation. *In vitro* studies overexpressing M6A in primary hippocampal neurons revealed an increased number of neurites (Alfonso *et al.*, 2005). An augment in neurite outgrowth has also been shown in M6A overexpressing mouse retinal progenitor cells (Zhao *et al.*, 2008). Thereby, by *in vitro* experiments, M6A seems to be involved in neurite outgrowth.

Regarding filopodia, *in vitro* studies overexpressing M6A in primary hippocampal neurons revealed an increased number of filopodia (Alfonso *et al.*, 2005) and an increased motility of them (Brocco *et al.*, 2010). The loss-of-function experiment (with small interference RNA) decreased the number of filopodia (Alfonso *et al.*, 2005). The importance of the glycosylation

status was investigated by Fuchsova *et al.* (2009) by overexpressing M6A with mutations that abolish the two N-glycosylation sites of the extracellular domain (EC) EC2 in the neuroblastoma cell line N2a. This did not alter the induction of filopodia nor cell surface expression of M6A. Recently it was shown that the Src and MAPK kinases seem to be involved in the filopodia formation after M6A overexpression (Scorticati *et al.*, 2011). Consequently, it appears that M6A, as well as M6B, is involved in filopodia formation in *in vitro* systems.

The suppression of M6A mRNA in mouse and human embryonic stem (ES) cells inhibits their differentiation and proliferation (Michibata *et al.*, 2008, 2009). While the overexpression of the human M6A in human ES cell lines enhanced their differentiation and proliferation. Additionally, this overexpression led to an increased neuronal migration, and *vice versa* in the suppression (Michibata *et al.*, 2009). This points to a role of M6A in differentiation and neuronal migration of neurons derived from ES cells. On the other hand, overexpression of M6A in mouse retinal progenitor cells did not affect their differentiation and proliferation (Zhao *et al.*, 2008).

The association of M6A and lipid rafts has been assessed in cultured hippocampal neurons (Scorticati *et al.*, 2011) and it has also been shown to be palmitoylated (Kang *et al.*, 2008). The involvement of lipid rafts and palmitoylation in proteolipid biology has also been described above PLP (see 2.2.1.), and could provide a link on the molecular functioning of this protein family.

Also in primary hippocampal neurons the suppression of M6A mRNA decreased the density of synaptophysin-positive presynaptic clusters (Alfonso *et al.*, 2005). And it seems that in hippocampal neurons the EC2 plays an important role in synaptogenesis (Fuchsova *et al.* 2009). M6A has been detected in the presynaptic membrane and synaptic vesicles by immuno-electron microscopy (Roussel *et al.*, 1998) and in a synaptosomal rat brain fraction by mass-spectrometry (Takamori *et al.*, 2006). M6A affects endocytosis at the mature presynapses and subcellular sorting of G-protein-coupled receptors such as the μ -opioid receptor (Wu *et al.*, 2007; Liang *et al.*, 2008). M6A associates with the μ -opioid receptor and enhances its endocytosis and sorting into the recycling pathway. M6A also interacts with other G protein-coupled receptors such as the δ -opioid receptor, the cannabinoid type 1 receptor and the somatostatin receptor sst2A (Wu *et al.*, 2007).

M6A mRNA levels were found to be significantly reduced in the adult hippocampus in response to chronic psychosocial and restraint stress, an effect that is conserved across

species and that can be prevented by antidepressant treatment. It has been shown before that stress can lead to disorders like depression (Alfonso *et al.*, 2004, 2006; Cooper *et al.*, 2009). These experiments indicate a role of M6A in neuronal plasticity. An association of the *GPM6A* gene with a subgroup of schizophrenia patients with high levels of depression was found (Boks *et al.*, 2008). This supports that M6A is involved in alterations that take place in the hippocampus upon stress induction, like in many psychiatric disorders as depression or schizophrenia.

Although M6A and M6B seem to play significant roles in neuronal development and function, initial evaluation of the single-null mutant mice (*Gpm6a*^{null} and *Gpm6b*^{null}) did not reveal any major differences in the CNS histology in mature animals. Also in *Gpm6a*^{null}**Gpm6b*^{null} mice, no abnormalities were found at the adult histological level. However, *Gpm6a*^{null}**Gpm6b*^{null} mice do show an increased mortality after weaning (of approximately 20%) and they have a reduced motor performance at the rotarod test at one month of age (Burzynska A., Fünfschilling U., Werner H., pers. comm.). This results show that there are some *in vivo* abnormalities when the neuronal M6 proteins lack chronically, but the involvement of the M6 proteins in the CNS biology has to be further examined.

2.3. Tetraspanins

The tetraspanins also termed transmembrane four superfamily (TM4SF) members are small (20-30 kDa), membrane proteins that are expressed ubiquitously and are evolutionary highly conserved (Hemler, 2008).

Tetraspanins comprise a large family of cell-surface proteins expressed in protozoan amoebae, some sponges, fungi, plants and metazoans. They seem to have an evolutionary role in the transition from uni- to multicellularity (Huang *et al.*, 2005; Hemler, 2005). There are 33 tetraspanins in humans, 35 in *D. melanogaster* and 20 in *Caenorhabditis elegans* (García-España *et al.*, 2008). The *Drosophila* tetraspanin *late bloomer (lbl)* is expressed during development at the growth cones and terminal arbores of motor axons. It has been shown that it acts as a cell adhesion protein important for synapse formation at the neuromuscular junction (Kopczynski *et al.*, 1996) and that other tetraspanins expressed on motor neurons have a redundant function and can compensate when Late Bloomer is absent (Fradkin *et al.*, 2002).

Structurally, tetraspanins have four transmembrane domains with polar residues close to these and four to six conserved Cys residues in their EC2 (Stipp *et al.*, 2003, Levy &

Shoham, 2005a) that lead to protein structure stabilizing disulfide bridges (Levy & Shoham, 2005b) This structure is similar to the structure of proteolipids, where the two disulfide bridges have been proven e.g. to be essential for the proper PLP function (Dhaunchak & Nave, 2007). The polar charges of the transmembrane domains mediate hydrophobic tetraspanin-tetraspanin interactions (Kovalenko *et al.*, 2005). Apart from these characteristics they possess a small EC1, a much larger EC2 with consensus N-glycosylation sites (Hemler, 2005) and short N- and C-terminal termini (Stipp *et al.*, 2003; Kovalenko *et al.*, 2005). The EC2 is compartmentalized into two regions: the constant region (ABE α -helices) and the variable region (CD α -helices), the latter being essential for protein-protein interactions (Seigneuret *et al.*, 2001; Stipp *et al.*, 2003, reviewed in Hemler, 2005). The cytoplasmic domain is less conserved and there are sorting signals in some tetraspanins, which probably links them to cytoskeletal and signalling molecules. There are several highly conserved membrane-proximal palmitoylation sites that are required for the initial tetraspanin-tetraspanin complex formation (Stipp *et al.*, 2003; Levy & Shoham, 2005b). The S-palmitoylation is reversible, increases the hydrophobicity of the proteins and was shown to influence the subcellular distribution and lateral associations of tetraspanins and their partner proteins (Levy & Shoham, 2005a). So, e.g., the tetraspanins tetraspanin2 (TSPAN2), CD9 (cluster of differentiation 9) and CD81 have six possible palmitoylated Cys (Stipp *et al.*, 2003).

Tetraspanins have been associated with a large number of biological processes such as the regulation of cell motility, invasion and fusion, proliferation and differentiation as well as signalling and protein trafficking (Hemler, 2008). They accomplish these functions e.g. during infectious diseases and fertilization and in the immune and nervous system (Hemler, 2008). The most distinct characteristic of the tetraspanins is the ability to organize multimolecular membrane complexes by establishing dynamic lateral associations with each other and multiple partner proteins and assembling them into the so called “tetraspanin web” (Rubinstein *et al.*, 1996) or “tetraspanin-enriched microdomains” (TEMs), which are cell-type specific, regarding their exact molecular composition (Hemler, 2005). Unusually, they can also act as cell-surface receptors, like e.g. the tetraspanin CD81 that has been identified as the receptor for the hepatitis C virus envelope protein E2 (reviewed in Levy & Shoham, 2005a).

The levels of TEM interactions can be subdivided into different classes as a simplified approach to its complexity (this has been excellently reviewed by Hemler, 2005). The first level would consider the robust and direct homo and hetero protein-protein interactions that can take place extra- as well as intracellularly, as e.g. the CD9-CD9 interaction. These are

specific and soluble interactions (Hemler, 2005). The second level describes the indirect protein interactions in which several direct homophilic and heterophilic primary complexes assemble into a network of secondary interactions (Tarrant *et al.*, 2003). Potential tetraspanin partners are e.g. integrins and members of the immunoglobulin superfamily. Through this mechanism, different partner proteins get recruited through tetraspanins into functionally important complexes. Palmitoylation seems to be very important for the maintenance of this type of interactions (Levy & Shoham, 2005a). It is specific for tetraspanins that they can take part in different protein-protein interaction according to the cell type (Levy & Shoham, 2005b). The class three interactions account for the formation of insoluble complexes, when milder non-ionic detergents are used and tetraspanin complexes begin to show partial insolubility. These last two types of interactions are potentially very relevant due to their dynamic status (Tarrant *et al.*, 2003). Functionally, these interactions cluster in TEMs, enabling lateral dynamic organization in the membrane and the connection with intracellular signalling and cytoskeletal structures (Levy & Shoham, 2005a; Yáñez-Mó *et al.*, 2009). Thereby the robust level one interaction represents specific functions for concrete tetraspanins, while level two and three interactions are weaker and embody the general function of tetraspanin in TEMs: acting as “molecular facilitators” (Maecker *et al.*, 1997) that enable the lateral dynamical organization in the membrane and the cross-talk with intracellular signalling and cytoskeletal structures (Hemler, 2001). This complex and multiple levels of interaction explain how tetraspanins can be involved in this plethora of cell functions.

Tetraspanins can also associate with three different types of lipids: cholesterol (Charrin *et al.*, 2003), gangliosides and palmitate (Levy & Shoham, 2005a, Hemler, 2005). Tetraspanin complexes are resistant to solubilisation by milder detergents, thereby they have been proposed to form membrane microdomains distinct from lipid rafts (Hemler, 2005; Israels & McMillan-Ward, 2007). In contrary to lipid rafts, TEMs are not disrupted at 37°C, they are resistant to cholesterol depletion, mostly soluble in non-ionic detergents and they do not comprehend GPI-linked proteins or caveolin (Hemler, 2005).

2.3.1. Tetraspanins in myelin

The tetraspanin proteins that are known today to be in CNS myelin are: TSPAN2 (Birling *et al.*, 1999), CD9 (Tole & Patterson, 1993), CD81 (Sullivan & Geisert, 1998), CD82 (Jahn *et al.*, 2009), OAP-1 (Bronstein *et al.*, 2004), CD63 and CD151 (Baer *et al.*, 2009).

CD63 and CD151 have, until now, only appeared in a CNS myelin blue native experiment (Baer *et al.*, 2009), but there is no further literature explaining their role in OLs or myelin. CD63 was the first characterized tetraspanin and is abundant in late endosomes and lysosomes. As a tetraspanin it interacts with many proteins like integrins, kinases and also other tetraspanins like CD9, CD81, CD82 and CD151 (reviewed in Pols & Klumperman, 2008). CD151 is present in most epithelial and fibroblastic cells and has been proven to act in an integrin-dependent manner on cell morphology, adhesion and motility (reviewed in Hemler, 2005). Until now, CD63 and CD151 have been vastly examined outside the nervous system and further studies involving neural cells will demonstrate the function of these proteins in the CNS.

The myelin tetraspanins CD9, CD81 and CD82 have been all shown to directly interact with cholesterol (Charrin *et al.*, 2003), what already gives a hint of their potential function and importance in myelination.

Phylogenetic analysis has shown that CD9, CD81 and TSPAN2 form a cluster, thereby being all very closely related orthologs (Garcia-España *et al.*, 2008). All the three members of this subgroup of tetraspanins contain two disulfide bridges in their EC2 (Charrin *et al.*, 2009). By immunoprecipitation it was found out that CD9 interacts with β 1 integrin, CD81 and TSPAN2 (Terada *et al.*, 2002). And this stands again for a similar and partially simultaneous role of CD9, CD81 and TSPAN2 in the OL biology.

During development CD9 (TSPAN29) is expressed in motoneurons (Tole & Patterson, 1993) and glia precursor cells (Deissler *et al.*, 1996), but in the adult its expression is mainly in CNS and PNS glia (Tole & Patterson, 1993), and it seems that it is more abundant in the PNS than in the CNS (Ishibashi *et al.*, 2004). CD9 is present in human CNS and PNS myelin (Nakamura *et al.*, 1996) and in premyelinating OLs and mature myelinating OLs (Terada *et al.*, 2002). In the course of CNS myelination, CD9 appears when myelination is very advanced, after PLP (Kagawa *et al.*, 1997), and ultrastructural analysis have confirmed that in the CNS CD9 is detected at the outermost membrane of compact myelin (Nakamura *et al.*, 1996), in the PNS in non-compact regions (Tole & Patterson, 1993) and in both it is found as a paranodal protein (Ishibashi *et al.*, 2004). By studying the CD9^{null} mutant mice it was revealed that CD9 does have a role in organizing the paranode, but the CNS myelin showed no aberrant compaction and there was only a restricted hypermyelination in the PNS (Ishibashi *et al.*, 2004). This demonstrate a different role and implication of CD9 in CNS Vs PNS myelination and indicates the possible function of CD9 being a tetraspanin in organizing the interaction with and of different proteins.

CD81 (TSPAN28) is expressed in the CNS by the major glia cell types: OLs, astrocytes and microglia (Geisert *et al.*, 2002). CD81 has a very broad tissue expression (peripheral nerve, muscle, liver, kidney, skin, testicle, etc.), but it is particularly abundant in the brain. Its expression is upregulated during early postnatal development, at the time of glial development and maturation, and at P14 the levels approach those of the adult (Sullivan & Geisert, 1998). CD81^{null} mutants encompass brain enlargement and augmentation in the number of astrocytes and microglia, while the number of OLs is unaltered. The general myelination pattern is similar to wild-type mice (Geisert *et al.*, 2002).

CD82 (TSPAN27) has been recently revealed to play a role in CNS myelination. Apart from the high expression of CD82 in mature OLs *in vitro* and *in vivo*, CD82 is an important factor in promoting the differentiation from pre-myelinating OLs to myelinating OLs (Mela & Goodman, 2009). Further studies will probably reveal that this function of CD82 relies on assembling protein networks, as most tetraspanins do.

OAP-1 (OSP/claudin-11-associated protein 1 or TSPAN3) is an interaction partner of the tetraspan oligodendrocyte-specific protein (OSP)/ claudin-11, a main component of CNS myelin that forms tight junctions within myelin sheaths (Tiwari-Woodruff *et al.*, 2001). It is N-glycosylated and broadly expressed, e.g. spinal cord, brain, testes, skeletal muscle and heart, in neurons, astrocytes and OLs (Tiwari-Woodruff *et al.*, 2001; Bronstein *et al.*, 2004), and in all stages of OL development (Bronstein *et al.*, 2004). In the CNS, its expression increases during development and OAP-1 is found in the germinal zones and is still broadly expressed in the adult, also in myelin (Bronstein *et al.*, 2004). *In vitro* studies demonstrated a role of OAP-1 in OL proliferation and, through the complex of OAP-1/OSP/ β 1integrin, also in OL migration (Tiwari-Woodruff *et al.*, 2001). The interaction of OAP-1 with OSP/claudin-11 and integrins points to a possible role in the fine-tuning of the interaction of different cells, with an involvement in migration and proliferation.

2.3.2. Tetraspanin2: A role in myelination?

The murine TSPAN2 is a nervous system specific protein that is present in OLs and CNS myelin. It has 24 kDa and one potential N-glycosylation site at EC2 (Birling *et al.*, 1999). The mRNA expression commences just when myelination starts (at P3, before PLP) mainly in the hindbrain and increases caudorostrally until it peaks at P22, coinciding with the major myelination phase, and is then reduced to the adult level. TSPAN2 is found also in some neuronal subpopulation of cerebellar nuclei (Birling *et al.*, 1999). The mRNA is found in brain tissue as well as in sciatic nerve (Birling *et al.*, 1999), although the protein has not been

detected so far in the PNS (Werner H., pers. comm.). The TSPAN2 protein is found in the white matter tracts and in compact myelin of the CNS (Fig.6; Birling *et al.*, 1999).

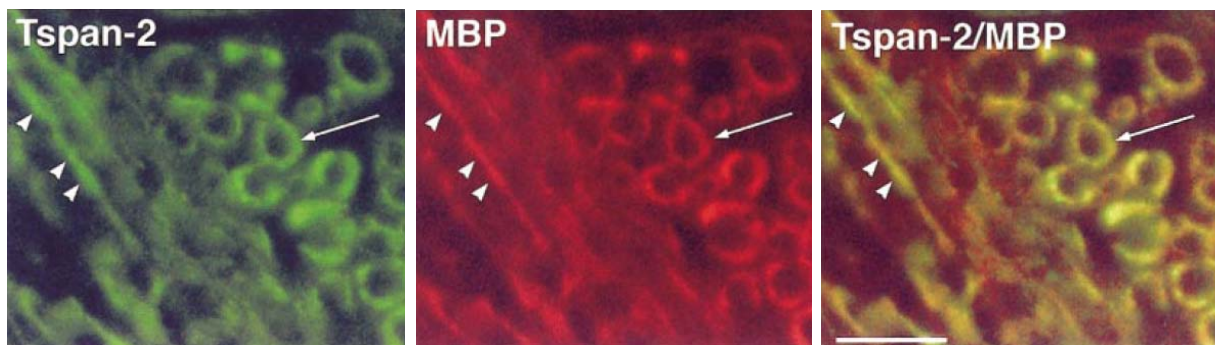


Figure 6. Localization of TSPAN2 in brain sections.

Confocal microscopy performed on sagittal sections from P31 rat brain stained against TSPAN2. The expression is found in compact myelin as it colocalizes widely with MBP (marker for compact myelin). Depicted are cross-sections (arrows) and longitudinal sections (arrowheads) of individual axons surrounded by myelin. Scale bar = 5 μ m (Taken from Birling *et al.*, 1999).

Different transcriptomic analyses have demonstrated an upregulation of TSPAN2 during OL differentiation (Nielsen *et al.*, 2006; Dugas *et al.*, 2006). And there has been shown an upregulation of cortical mRNA levels of TSPAN2 after the application of a traditional Chinese medicinal treatment (Huang-Lian-Jie-Du decoction) that improves learning and memory function in the senescence-accelerated mouse/prone 8 mice, a model for age-related learning and memory deficits (Yue *et al.*, 2008). Additionally, OLs cultured under oxygen glucose deprivation conditions have a decrease in TSPAN2 mRNA. While OLs cultured under these conditions and treated with human umbilical cord blood cells that have a protective effect on white matter tracts, show an increase in their TSPAN2 mRNA expression levels (Rowe *et al.*, 2010).

Thereby, until now it is known that TSPAN2 is present during OL differentiation and in CNS compact myelin. But how TSPAN2 could act on OL differentiation as well as myelination or myelin maintenance is completely unidentified. Because of being a member of the tetraspanin family it is straightforward to speculate about an involvement in signalling and in coordinating and arranging interacting proteins in the OL plasma membranes and myelin sheaths.

A surprising discovery was the drastic increase of the TSPAN2 levels in a CNS myelin-enriched fraction of PLP^{null} mutant mice (Werner H., pers. comm.). As PLP and TSPAN2 are both structurally similar tetraspan proteins and expressed in OLs in a similar spatiotemporal pattern, this leads to the hypothesis that TSPAN2 could compensate for PLP in its absence.

2.4. Aim of the study

Neuronal development involves the interplay of a large number of cell surface proteins. Two members of the M6-proteolipid protein family of tetraspan-transmembrane proteins are among the most abundant cell surface proteins in neurons, but their physiological role has remained largely obscure despite over 25 years of analysis. The majority of studies relied on acute reduction or augmentation of their abundance levels *in vitro*, and knowledge on their cellular function *in vivo* is entirely lacking. To achieve a better understanding of the function of M6 proteolipids (termed M6A, official gene name *Gpm6a*, and M6B, official gene name *Gpm6b*) during neuronal development I will analyse available GPM6A^{null} and GPM6B^{null} mutant mice. Since both proteins are closely related orthologs, a partially redundant function has to be considered, and therefore GPM6A^{null}*GPM6B^{null} double null mutant mice will be included. I will utilize an *ex vivo* cell culture system of primary cortical neurons in which both proteins are highly abundant. The study will involve life cell microscopy, immunocytochemistry, confocal analysis, as well as functional assays. Thereby I want to assess the detailed subcellular localization in neurons, as well as their functional involvement in neuronal development. Furthermore, I aim to investigate the consequences of the chronic lack of M6 proteins in long-projecting neurons at an early postnatal stage *in vivo*.

A structurally related superfamily of tetraspan transmembrane proteins, the tetraspanins, has been related to various features of cell biology, including myelination of axons by the cellular processes of oligodendrocytes in the CNS. Tetraspanin-2 (TSPAN2) is particularly abundant at the onset of myelination and a constituent of mature compact CNS myelin, in which its abundance is very strongly increased in mutant mice that lack the most abundant myelin protein, proteolipid protein (PLP). I hypothesized that TSPAN2 can partially compensate for the absence of PLP in myelination, which would also explain that the abnormalities observed in PLP^{null} mutant mice are minor. To this aim I will generate TSPAN2^{null} mutant mice by inactivating the *Tspan2* gene using homologous recombination in embryonic stem cells. I will also generate TSPAN2^{null}*PLP^{null} double null mutant with the aim to test for a possible cumulative effect of the lack of both tetraspan proteins in CNS myelin. The myelin protein composition will be characterized using biochemical methods.

The aim of this thesis is to assess the role of the neuronal proteolipids M6A and M6B, as well as of the oligodendroglial proteolipid protein PLP and TSPAN2 in the growth of cellular processes in neurons and oligodendrocytes, respectively.

3. Materials and Methods

3.1. Materials

3.1.1. Kits, chemicals and protocol source

All chemicals used were purchased from the Sigma-Aldrich and Merck unless stated otherwise and all molecular biology kits were purchased from Qiagen, Macherey-Nagel, Promega or Sigma-Aldrich, while cell culture and general laboratory material were purchased from Falcon, Nunc and Eppendorf.

3.1.2. Molecular biology buffers

DNA-sample buffer (6x)

20 % glycerol in TAE buffer

0.025 % bromophenol blue

dNTP-stock solutions (100 mM)

25 mM of each dATP, dCTP, dGTP, dTTP (Boehringer, Mannheim)

Ethidiumbromide

1 - 1.5 µg/ml for agarose gels in 1x TAE

Modified Gitschier buffer (MGB, 10x)

6.7 ml 1 M Tris-HCl (pH 8.8)

1.66 ml 1 M (NH₄)₂SO₄

650 µl 1 M MgCl₂

add dH₂O up to 10ml

MGB buffer (1x, working solution)

1 ml 10x MGB

100 µl β-mercaptoethanol

500 µl 10 % Triton X-100

8.4 ml dH₂O

TAE (50x, 1000ml)

2 M Tris-acetate, pH 8.0
50 mM EDTA
57.1 ml glacial acetic acid
add dH₂O up to 1000ml

TE (1x)

10 mM Tris-HCl, pH 8.0
1 mM EDTA

3.1.3. Protein biochemistry buffers**10x Phosphate buffered saline (PBS)**

1.7 M NaCl
34 mM KCl
40 mM Na₂HPO₄ x 2H₂O
18 mM K₂HPO₄
Adjust pH 7.2 with 1N NaOH.

Modified RIPA buffer (protein lysis buffer)

50 mM Tris-HCl, pH 7.4
150 mM NaCl
1 mM EDTA
0.1 % SDS
1.0 % sodium deoxycholate
1.0 % TritonX-100

Solutions for CNS-myelin enriched fraction

0.32 M sucrose
0.85 M sucrose (filtered sterile)

Complete Mini protease inhibitors (Roche) 1 tablet/10 ml of RIPA buffer

3.1.4. SDS-PAGE and Immunoblotting

Separating SDS gel (for 4 gels, 12 %, 1.5 mm thickness)

13 ml dH₂O
15 ml 30 % Acrylamide (BioRad, 29.1)
9.4 ml 1.5 M Tris-HCl (pH 8.8)
370 µl 10 % SDS
125 µl 10 % APS (Ammonium persulfate)
30 µl TEMED (BioRad)

Stacking SDS gel (4 gels)

6.1 ml dH₂O
1.3 ml 30 % Acrylamide (BioRad, 29.1)
2.5 ml 0.5 M Tris-HCl (pH 6.8)
100 µl 10 % SDS
50 µl 10 % APS (Ammonium persulfate)
10 µl TEMED
SDS running buffer (Laemmli buffer, 1x)
25 mM Tris-HCl
192 mM Glycine
1 % (w/v) SDS

SDS sample buffer (6x)

7 ml 0.5M Tris-HCl buffer (pH 6.8)
3 ml Glycerol (30 % final concentration)
1 g SDS
1.2 ml 1 % Bromophenol blue
0.2 - 2 % β-Mercaptoethanol (add fresh)

Transfer buffer (1x)

48 mM Tris base
39 mM Glycine
10-20 % Methanol

Blocking Buffer

5 % non-fat dry milk powder in TBS or PBS (1x)

Western blot stripping buffer

0.2 M Glycine-HCl, pH 2.5

0.1 % Tween-20

Tris buffered saline (TBS, 20x)

1 M Tris base

3 M NaCl

Adjust pH 7.4 (with HCl)

TBS with Tween-20 (TBST, 1x)

50 mM Tris-HCl (pH 7.4 - 7.6)

150 mM NaCl

0.05 % - 0.15 % Tween-20

Enhanced Chemiluminescence (ECL) Western-blot detection kit

Western Lightning™ Plus-ECL, Enhanced luminol reagent plus (Perkin Elmer Life Sciences, Inc.).

ECL-Hyperfilms (Amersham Biosciences)

PVDF membrane -Hybond P pore size 0.45 µm (Amersham)

3.1.5. DNA and Protein markers

GeneRuler 1 kb DNA ladder (Fermentas)

GeneRuler 100 bp DNA ladder (Fermentas)

Prestained Page Ruler Plus (Fermentas)

3.1.6. Immunocytochemistry buffers

4 % Paraformaldehyde in PBS/TBS

100 ml 0.2 M NaH₂PO₄ (Sodiumdihydrogenphosphate)

400 ml 0.2 M Na₂HPO₄ (di-Sodiumhydrogenphosphate)

108 ml 37 % Formalin

392 ml dH₂O

Filtered with a 500 ml Nalgene sterile filter unit

Blocking Buffer

2 % BSA in PBS

Mounting Agent

Aqua polymount (Polysciences)

3.1.7. Immunohistochemistry buffers**Phosphate buffer (stock solution)**

0.2 M NaH_2PO_4

0.2 M Na_2HPO_4

Phosphate buffer (working solution, pH 7.4)

20 ml 0.2 M NaH_2PO_4

80 ml 0.2 M Na_2HPO_4

100 ml dH_2O

Bovine Serum Albumin (PBS/BSA)

20 ml 0.2 M NaH_2PO_4

80 ml 0.2 M Na_2HPO_4

1.8 g NaCl

1 g BSA

100 ml dH_2O

Citrate Buffer (stock solution, stored 4°C)

0.1 M Citric acid ($\text{C}_6\text{H}_8\text{O}_7 \cdot \text{H}_2\text{O}$)

0.1 M Sodium citrate ($\text{C}_6\text{H}_5\text{O}_7\text{Na}_3 \cdot 2\text{H}_2\text{O}$)

Citrate Buffer (working solution, 0.01 M, pH 6.0, prepared freshly)

9 ml 0.1 M Citric acid ($\text{C}_6\text{H}_8\text{O}_7 \cdot \text{H}_2\text{O}$)

41 ml 0.1 M Sodium citrate ($\text{C}_6\text{H}_5\text{O}_7\text{Na}_3 \cdot 2\text{H}_2\text{O}$)

450 ml dH_2O

Tris Buffer (stock solution, stored 4°C)

0.5 M Tris base

Adjust pH 7.6 with HCl

Tris Buffer (working solution, prepared freshly)

100 ml 0.5M Tris base (pH 7.6)

9 g NaCl

Add up to 1000 ml with dH₂O

Blocking buffer (2 % milk powder in Tris Buffer)

20 g of non-fat milk powder

Add up to 1000 ml with Tris buffer

3.1.8. Histological stains and reagents**Mayer's Haematoxylin solution**

1 g Haematoxylin (Merck) was dissolved in 1000 ml dH₂O and 0.2 g sodium iodate and 50 g potassium aluminium sulphate (K₂Al₂(SO₄)₄*24H₂O) was added under constant shaking. Finally, 50 g chloralhydrate and 1 g citric acid were added and the solution was filtered before use.

Eosin solution

Stock solution (10x)

10 g of Eosin were dissolved in 100 ml of dH₂O and left to mature.

Working solution

2.5 ml stock solution

250 ml dH₂O

12 drops glacial acetic

Scott's solution

2 g KHCO₃ (potassiumhydrogencarbonate)

20 g MgSO₄ (magnesium sulphate)

Add up to 1000 ml with dH₂O

HCl- Alcohol

1.25 ml HCl

350 ml Ethanol

150 ml dH₂O

3.1.9. Oligonucleotides

Oligonucleotides were synthesized in the “DNA core Facility” of the Max-Planck-Institute of Experimental Medicine.

Genotyping primers

Nested external PCR:

Forward: 5'-CTTCATCTTTGTCTCCAGTT -3'

Reverse: 5'-GCAATCCATCTTGTTCAATGGC -3'

Nested internal PCR:

Forward: 5'-CTCCTTAATCTTCACAACCTCTT -3'

Reverse: 5'-CCATCTTGTTCAATGGCCGATC -3'

Amplification product: 2.1 kb in control vector and 1.6 kb in homologous recombined ES cells

TSPAN2^{null}:

Forward: 5'-CCATAGACACGCAGGATAACTTCAACCA -3'

Reverse: 5'-GGCTTTTTGCTTCCTCTTGA -3'

Reverse: 5'-GTTGGGAGGGGCGTGACCTGT -3'

Amplification product: 196 bp for mutant and 286 bp for wild-type

PLP^{null}:

Forward: 5'-TTG GCG GCG AAT GGG CTG AC-3'

Forward: 5'-GGA GAG GAG GAG GGA AAC GAG-3'

Reverse: 5'-TCT GTT TTG CGG CTG ACT TTG-3'

Amplification product: 300 bp for mutant and 150 bp for wild-type

GPM6A^{null}:

Forward: 5'-TTGCTCTTCTACAGGGTGCT-3'

Reverse: 5'-CCTCCATCCTCTGTCATTCC-3'

Reverse: 5'-GCAATCCATCTTGTTCAATGGC-3'

Amplification product: 310 bp for mutant and 560 bp for wild-type

GPM6B^{null}:

Forward: 5'-CCAGGGAGGCATAGGGAACT-3'

Reverse: 5'-CCCTTTGCCTCCCAGTCAGTTG-3'

Reverse: 5'-GCAATCCATCTTGTTCAATGGC-3'

Amplification product: 700 bp for mutant and 400 bp for wild-type

3.1.10. Antibodies and recombinant proteins

Primary antibodies for immunocytochemistry:

M6A	Rat	1:1500	MBLInternational Corporation.
M6B (#8547)	Rabbit	1:500	(Werner <i>et al.</i> , 2001)
Tuj1	Mouse	1:500	Sigma

Primary antibodies for immunoblot:

A431 (PLP)	Rabbit	1:5000	(Jung <i>et al.</i> , 1996)
Actin	Mouse	1:500	Sigma
CD9	Rat	1:250	BD Pharmingen
CD63	Mouse	1:1000	Calbiochem
CD81	Hamster	1:2000	BD Pharmingen
CD82	Rabbit	1:500	Novus Biologicals
CNP	Mouse	1:1000	Sigma
Ephexin-1	Rabbit	1:1000	ECM Biosciences
Fyn	Rabbit	1:500	Santa Cruz
MBP	Mouse	1:500	Chemicon
RhoA	Rabbit	1:1000	Cell signalling
TSPAN2	Rabbit	1:600	(Biriling <i>et al.</i> , 1999)
Tubulin	Mouse	1:5000	Sigma

Primary antibodies for immunohistochemistry:

TSPAN2	Rabbit	1:1000	(Biriling <i>et al.</i> , 1999)
--------	--------	--------	---------------------------------

Secondary antibodies:

HRP-anti mouse	1:5000	Dianova
HRP-anti rabbit	1:5000	Dianova
HRP-anti rat	1:2000	Dianova
HRP-anti hamster	1:2000	abcam
Cy2-anti rat	1:100	Dianova
Cy3-anti mouse	1:1000	Dianova
Cy5-anti rat	1:1000	Dianova

Others :

Rhodamine-Phalloidin	1:100	Invitrogen
----------------------	-------	------------

Recombinant proteins for the ephrinA5 “growth cone collapse assay”:

Recombinant human ephrin-A5/Fc Chimera, CF, R&D systems

Recombinant human IgG1 Fc, R&D systems
Anti-human IgG; Fc specific, Sigma

3.1.11. Enzymes

CIP (alkaline phosphatase)	Roche
DNase	Qiagen
GoTaq polymerase	Promega
Pfu high fidelity DNA polymerase	Stratagene
Proteinase K	Roth
REDTaqDNA polymerase	Sigma-Aldrich
Restriction enzymes	New England Biolabs
T4 DNA ligase	Promega

3.1.12. Bacteria and bacterial culture media

Bacterial strains

Escherichia coli XL1-Blue (Stratagene)

LB medium (Luria and Bertani medium)

1 % Bacto-Pepton

0.5 % Yeast extract

1 % NaCl

pH7.5, adjusted with 10 N NaOH and autoclaved.

Selective LB media was supplemented with following antibiotics:

100 µg/ml Ampicillin

50 µg/ml Kanamycin

LB-Agar plates

1 % Bacto-Pepton

0.5 % Yeast extract

1 % NaCl

1.2% Bacto-agar

pH7.5, adjusted, autoclaved and left to cool to 55°C

desired antibiotics are added.

3.1.13. Cell culture media

Components were purchased from GIBCO or Lonza.

Neurobasal complete medium for cortical neurons

100ml Neurobasal medium

2ml B27 Supplement

1ml Glutamax 10x

1ml 1 % Penicillin/Streptomycin

Hank's Balanced Salt Solution (HBSS+) for preparation of brains

500 ml HBSS

7.5 ml 10 % MgSO₄

DNase in HBSS (0.05 %)

Dilute 100 mg in 200 ml HBSS, Freeze aliquots at -20°C

Papain in PBS (20U/ml)

Cholesterol (C3045, Sigma)

diluted in ethanol

ES-cell medium (600 ml)

474 ml DMEM (4,5 g Glucose/l)

6 ml aminoacids (100x)

6 ml Sodiumpyruvat (100x)

6 ml Penicillin/Streptomycin (100x)

6 ml L-Glutamin (100x)

6 ml β-mercaptoethanol (10 mM in PBS)

6 ml LIF (10⁷ U/ml)

90 ml FCS

Gelatine (500 ml)

0.5 mg gelatine

500 ml dH₂O, autoclaved

3.1.14. Mouse lines

PLP^{null} mice (Klugmann *et al.*, 1997)

GPM6A^{null} mice (generated by Klugmann M.)

GPM6B^{null} mice (generated by Werner H.)

3.2. Methods

3.2.1. Molecular biological methods

3.2.1.1. Transformation of chemical competent *E. coli* (XL-1 blue)

100 µl of chemical competent *Escherichia coli* (*E. coli*) were thawed on ice, transferred into 14 ml Falcon tubes, 50 ng of plasmid DNA was added and incubated for 30 min on ice. A heat shock was performed at 42°C during 40 sec and then the bacteria were put back on ice for 2 min. Afterwards, 800 µl of LB-medium without antibiotic was added to the tube and the bacteria were incubated under rotation at 37°C for 30 min. 50 to 200 µl of this culture were plated on LB plates with the appropriate antibiotic, and incubated ON at 37°C.

3.2.1.2. DNA purification at small scale (“mini prep”)

For preparing small amounts of plasmid DNA, the “QIAprep 8 Miniprep kit” (Qiagen) or “NucleoSpin Plasmid QuickPure kit” (Macherey-Nagel) were employed. The protocol is in accordance with the modified “alkaline lysis” protocol (Birnboim & Doly, 1979), in which the DNA binds to an anion-exchange resin and is subsequently washed and eluted. This occurs under specific pH levels and at low-salt conditions. Bacteria inoculated with a single transformed colony were grown ON at 37°C with gentle shaking in 3 ml LB medium with the appropriate antibiotic. 2 ml of these cultures were transferred into 2 ml microfuge tubes and centrifuged at 5000 rpm for 5 min, so that the bacteria were pelleted. The DNA of these bacteria was isolated according to the manufacturer’s protocol, and in the last step the DNA bound to an anion-exchange resin column was eluted in 100 µl of ddH₂O.

3.2.1.3. DNA purification at large scale (“maxi preps”)

For preparing large amounts of plasmid DNA, the “NucleoBond PC500 EF Maxi kit” (Macherey-Nagel) was used, which is based as well as the “mini preps” (3.2.1.2.) on the “alkaline lysis” protocol (Birnboim & Doly, 1979). The RNA and low-molecular weight contaminations were removed with medium salt washes. The plasmid DNA is as in the “mini prep” eluted from an anion-exchange resin column, then precipitated with isopropanol and washed several times to remove remaining salts from the elution buffer. For this procedure, 2 ml of plasmid DNA grown ON in 3 ml LB-medium with the appropriate antibiotic were inoculated in 250 ml of LB-medium with again the appropriate antibiotic and grown ON at 37°C with gentle shaking. Bacteria were pelleted by centrifugation at 6000g for 30 min at 4°C (SLA-1500 rotor). The “maxi prep” protocol was applied and the DNA was finally resuspended in 250 µl of endotoxin free ddH₂O.

3.2.1.4. Murine genomic DNA preparation

Murine genomic DNA was prepared for genotyping, out of 5 mm large tail biopsies. Each tail was carefully placed into microfuge tubes with 200 µl lysis buffer (180 µl of 1xMGB, 20 µl proteinase K (10 mg/ml)) and incubated at 55°C ON with strong shaking. The proteinase K of the genomic DNA lysates was heat-inactivated (95°C, 15 min), and then the lysates were centrifuged at 5000 rpm for 10 min to pellet the non-lysed debris. The supernatant was used for the genotyping PCRs.

3.2.1.5. DNA restriction digest

The DNA restriction digest is performed with restriction endonucleases, which recognize specific dsDNA sequences and cut the DNA at those sites, leaving sticky or blunt ends. The resulting dsDNA with 5' and 3' sticky ends can be further ligated to other digested dsDNA fragments, what gives them their relevance as an essential tool in molecular biology. In general, in an analytical digest, in a 20 µl digestion reaction with approximately 500 ng of DNA, 1 to 10 units of restriction enzyme were added and incubated at 37°C for 1 hour. The restriction enzymes can be heat-inactivated (65°C, 20 min) or removed by electrophoretic gel extraction.

3.2.1.6. Digested DNA dephosphorylation

By employing the calf intestinal phosphatase (CIP), 5' phosphoryl groups were removed from digested DNA, to avoid their religation. 1 to 2 units of CIP were added to the digested DNA (with CIP buffer and the necessary ddH₂O for a 1x concentration) and incubated at 37°C for 30 min. The CIP is removed by DNA agarose gel extraction.

3.2.1.7. DNA ligation

The ligation of DNA fragments was performed in 10 µl reactions by mixing 25 to 50 ng of vector DNA, insert DNA in a 1:3 ratio, 0.5 µl of T4-ligase and 1 µl of 10x ligation buffer (Promega). It was incubated at RT for 1 hour, and the resulting product could be used directly for transformation.

3.2.1.8. DNA gel-electrophoresis

DNA gel electrophoresis was performed in order to separate DNA fragments, from 200 bp to 6 kb, with gels containing 0.8 % to 2 % agarose concentration. The proper amount of agarose was dissolved in 1xTAE buffer and heated in a microwave. Once it had solved and cooled down ethidiumbromide was added (1 µg/ml) and the agarose was poured into custom-made gel trays and combs were placed in them to allow forming wells in the gel. Once the gel was solidified, it was transferred into a gel loading chamber and the DNA samples as well as standard DNA markers (100 bp or 1 kb ladder) (all containing sample buffer) were loaded. Gels were run under constant current (approximately 10 V/cm length) until the appropriate DNA band separation. For documentation, snapshots of UV-trans-illuminated gels were taken.

3.2.1.9. DNA extraction from agarose gels

DNA fragments were excised under UV light from agarose gels according to the manufacturer's protocols, and the "QIAquick Gel Extraction kit" (Qiagen) or "NucleoSpin Extract II kit" (Macherey-Nagel) were used. They are based on the DNA capacity to bind to silica-membranes under high-salt conditions at pH 7.5. At the last step, DNA was eluted in 25 µl of ddH₂O.

3.2.1.10. Determination of DNA concentrations

The DNA concentrations were determined spectrophotometrically, according to the Lambert-Beer law, as a substance in solution is proportional to its absorption. The DNA was diluted 1:100 with water and the solution was pipetted into a cuvette and analysed in a UV spectrophotometer (Biophotometer, Eppendorf). The concentration was determined by measuring the absorbance at 260 nm, 280 nm and 320 nm. A ratio of A₂₆₀/A₂₈₀ between 1.8 and 2 implies sufficient DNA purity.

3.2.1.11. DNA sequencing

16 µl of DNA samples (100 ng/µl in ddH₂O) were sequenced at the “DNA core Facility” of the Max-Planck-Institute of Experimental Medicine. The resulting sequence was analyzed with the DNASTar (SeqMan) software package and verified on public domain databases such as the “National Centre for Biotechnology Information” (NCBI).

3.2.1.12. Primer design

The sense and antisense DNA primers were designed manually based on appropriate melting points (50°C to 65°C) and GC content. They were verified with the DNASTar (PrimerSelect, SeqMan, EditSeq) software package and synthesized at the “DNA core Facility” of the Max-Planck-Institute of Experimental Medicine.

3.2.1.13. DNA amplification by employing polymerase chain reaction (PCR)

The polymerase chain reaction permits the *in vitro* amplification of a specific DNA sequence (Mullis *et al.*, 1986). DNA synthesis starts at two primers that flank the sequence to be amplified. One of them anneals to the sense and the other one to the antisense strand of the amplicon.

The DNA polymerase of the thermophilic bacterium *Thermus aquaticus* (taq polymerase) catalyzes the reaction at 72°C and is stable at 95°C. DNA synthesis is carried out in a thermocycler (Thermocycler T3, Biometra) that changes temperatures between 95°C, the specific annealing temperature of the primers, and 72°C for the synthesis reaction. The reaction mixture contains the DNA template, primers dNTPs and the taq polymerase with corresponding salt and optimal pH conditions. Multiple reaction cycles are necessary to

obtain sufficient quantities of the DNA fragment for further studies. Standard PCR reactions were performed as following:

1 μ l DNA (100 pg to 100 ng)
1 μ l sense primer (10 pM)
1 μ l antisense primer (10 pM)
2 μ l dNTP mix (2 mM)
2 μ l 10x RedTaq buffer
1 μ l RedTaq polymerase (1 U/ μ l)
12 μ l ddH₂O

As the taq polymerase does not possess a 3'-5' exonuclease activity ("proofreading"), and thereby introduces about 0.8 mismatches per 1 kb per amplification cycle. Therefore, the proofreading DNA polymerase of *Pyrococcus furiosus* (Pfu polymerase) was employed and the number of cycles was reduced, when necessary. To visualize the amplified PCR product, these were separated on an agarose gel.

3.2.2. Generation of null-mutant mice

3.2.2.1. DNA preparation for electroporation into embryonic stem cells

150 μ g of the targeting vector were linearized with the ClaI restriction enzyme ON at 37°C and this was confirmed by the electrophoretic separation of a little amount (5 μ l) of the digest in a 0.8 % agarose gel. The linearized vector was purified by isopropanol precipitation and column filtration. In a 1:1 ratio the linearized vector and isopropanol were added, and the precipitated DNA fragments were pelleted by centrifugation at 13000 rpm for 10 min at RT. The resulting pellet was washed twice with 70 % ethanol, with a further centrifugation step between each washing. By air-drying the pellet at RT for 20 min, the traces of ethanol were removed, and then the pellet was dissolved in 80 μ l of 10 mM Tris-HCl (pH 8.5) at 50°C for 30 min. The following column filtration purification was performed in C-30 columns (BioRad), according to the manufacturer's protocol. The column tip had to be broken and then the columns were centrifuged at 2000 rpm for 3 min, to release the storage buffer. 80 μ l of linearized DNA were added on the C-30 column and centrifuged at 2000 rpm for 3 min. The eluted fraction was collected in a microfuge tube. Than 40 μ l of 10mM Tris-HCl (pH 8.5) were added onto the C-30 column and centrifuged at 2000 rpm for 3 min. The eluted fraction was

collected in the same microfuge tube as the previous. Finally to recover any remaining DNA, further 40 μl of 10mM Tris-HCl (pH 8.5) was added on the column and centrifuged at 2000 rpm for 3 min. This fraction was collected in a clean microfuge tube and stored at -20°C . The DNA concentration was measured spectrophotometrically and 1 μl was separated on a 0.8 % agarose gel to confirm the concentration and integrity of the DNA. Once that was assessed, the linearized fragment ($\sim 50 \mu\text{g}$) was ready for the electroporation into ES cells.

3.2.2.2. Electroporation and selection of ES cells

One vial of frozen ES cells ($5 \cdot 10^6$ cells) was plated on a 6 cm dish and incubated for 36 to 48 hours at 37°C and 5 % CO_2 . Cells were splitted on two 10 cm dishes and kept in culture for 2 to 3 days prior to electroporation. Thereby, sufficient cells 10 to $15 \cdot 10^6$ ES cells/plate (i.e. confluent plate) were available for various transfections. Several hours before the transfection, the culture medium was changed, as actively growing cells are a prerequisite for successful transfection. Cells were trypsinized (2 ml/dish) and spun down at 900 rpm for 5 min. The cell pellet was resuspended in the medium, pre-plated on 10 cm dishes covered with gelatine, to get rid of feeders (fibroblast cells), and incubated at 37°C for 45 min and 5 % CO_2 . The supernatant medium containing mainly ES cells, as feeders were attaching to the gelatin, was transferred to a 15 ml falcon tube. ES cells were spun down at 900 rpm for 5 min and the pellet was immediately resuspended in 1 ml of cold PBS. Cells were counted using a Neubauer chamber and the cell number was adjusted to about 10 to $14 \cdot 10^6$ cells/ml. From these ES cell suspension, 0.7 ml (i.e. 7 to $10 \cdot 10^6$ cells) was transferred to a microfuge tube and kept on ice. Then, 100 μl (0.5 $\mu\text{g}/\mu\text{l}$) of the linearized targeting vector DNA were added and mixed thoroughly. This mix was transferred to an electroporation cuvette (pre-cooled on ice) and was pulsed (240 V, 500 μF) with an electroporator (BioRad). After the pulse the cuvette was incubated on ice for 20 min. The cell suspension was then transferred to a fresh tube, 30 ml of ES cell medium were added and the cells were plated on three 10 cm dishes. After 24 hours the medium was changed and selection was started with G418 (f.c. 300 $\mu\text{g}/\text{ml}$). Approximately at day 10 of selection large isolated ES cell clones were picked up.

3.2.2.3. DNA isolation of ES cells

When picking the ES clones, a fraction was kept for DNA recovery. These cells were pelleted by centrifugation at 13000 rpm for 10 to 15 min at RT, the supernatant was carefully aspirated out and the pellet was washed with 100 μl of sterile 1xDPBS. Cells were then

repelleted by centrifugation at 13000 rpm for 5 min at RT and the resulting pellet was resuspended in 50 µl of ddH₂O. This cell suspension was kept at 95°C for 10 min and centrifuged shortly to spin down the evaporated liquid. After cooling down on ice, cells were digested with 1 µl of proteinase K (20 µg/µl) at 56°C for 30 min, with strong shaking. The lysed cells were then incubated at 95°C for 15 min to heat inactivate the proteinase K, and were finally centrifuged shortly to evaporated liquid on the microfuge tube sides. 5 µl of these DNA preparations were used for PCR amplification.

3.2.2.4. PCR amplification of ES cell DNA

The ES cell DNA had to be amplified by PCR, for assessing if homologous recombination had taken place. Therefore, a nested PCR based screening strategy was employed. For establishing the primer pairs capable of efficient amplification of a homologous recombined target sequence and the PCR conditions, a control vector was used. This control vector had a homologous sequence 5' to the short arm and lacked the 3' long arm of the targeting vector. The nested PCR is a two-step reaction, where the amplification product of the outer primer pair is used as the template for the amplification reaction of the inner primer pair. The nested PCR amplification yielded a product of about 2.1 kb in the control vector and of 1.6 kb in homologous recombined ES cells, confirming that the homologous recombination had taken place.

Nested external PCR:

5 µl template ES cell DNA	94°C, 2 min 30 sec
1.5 µl SE primer (10 pmol/µl)	56°C, 30 sec
1.5 µl AS primer (10 pmol/µl)	72°C, 2 min 30 sec
2 µl betain	94°C, 30 sec, 20 cycle repetition
2 µl dNTP mix (2 mM)	56°C, 1 min
4 µl 5xGoTaq buffer	72°C, 5min
0.15 µl Go Taq polymerase	4°C
0.1 µl Pfu turbo polymerase	
3.75 µl ddH ₂ O	

Nested internal PCR:

2 µl template of the external PCR reaction	94°C, 2 min 30 sec
1.5 µl SE primer (10 pmol/µl)	56°C, 30 sec
1.5 µl AS primer (10 pmol/µl)	72°C, 2 min 30 sec
2 µl betain	94°C, 30 sec, 36 cycle repetitions

2 µl dNTP mix (2 mM)	56°C, 1 min
4.4 µl 5xGoTaq buffer	72°C, 5 min
0.15 µl Go Taq polymerase	
0.1 µl Pfu turbo polymerase	
8.35 µl ddH ₂ O	

3.2.3. Protein biochemical methods

3.2.3.1 Preparation of protein lysates from cell cultures

Primary cortical neurons (plated $\sim 1 \cdot 10^6$ cells) kept in culture for 2 DIV on 10 cm dishes were lysed in RIPA buffer to obtain proteins for subsequent immunoblot analysis. The dish was washed once with cold PBS, 200 µl of RIPA buffer was applied and cells were scraped from the dish with a cell-scraper. The obtained cells were placed into a microfuge tube and left on ice for 20 min to lyse. Cell lysates were centrifuged at 4°C for 20 min at 13000rpm maximum speed, to pellet the undigested material. The supernatant containing the soluble proteins was transferred into a new tube and kept at -20°C. The pellet containing the cell debris and unsolubilized material was as well stored at -20°C.

3.2.3.2. Preparation of a CNS-myelin enriched fraction

Mice were sacrificed by spinal cord dislocation and decapitated. The brains were removed, collected and homogenated in 0.32 M sucrose. This preparation of the CNS-myelin enriched fraction was according to Norton & Poduslo (1973). All centrifugation steps were performed in a SW28 rotor in a Beckman ultracentrifuge. The brains were homogenated with an Ultra-Turrax in 0.32 M sucrose and then layered over a 0.85 M sucrose solution in centrifuging tubes (Beckmann). It was then centrifuged at 23800 rpm for 30 min and the interphase was collected with a Pasteur pipette and put into a clean tube. Then the interphase was washed with dH₂O, by filling the tubes with dH₂O and centrifuging at 23800 rpm for 15 min. The supernatant was discarded, the pellet was resuspended in dH₂O while vortexing. Then the first osmotic shock took place, by filling the tubes with dH₂O, incubating for 10 min and centrifuging at 9500 rpm for 15 min. For the second osmotic shock, the resulting pellet was resuspended in dH₂O and centrifuged again at 9500 rpm for 15 min. The pellet was then resuspended in 0.32 M sucrose and layered over 0.85 M sucrose in a clean centrifuge tube.

This was centrifuged at 23800 rpm for 30 min. The second interphase is collected than, and washed with water, by filling the tubes with dH₂O and centrifuging at 23800 rpm for 15 min. The resulting pellet was the purified myelin fraction, which was resuspended in TBS with protease inhibitors, aliquoted and kept at -80°C until further use.

3.2.3.3. Protein concentration measurement by Lowry assay

The protein concentrations were assessed in 96-well plates (flat bottom) with the “DC Protein Assay kit” (BioRad) according to the manufacturer’s 'microplate assay' protocol, which is based on the Lowry assay (Lowry *et al.*, 1951). The assay is based on two subsequent reactions between the proteins and a copper in alkaline medium, followed by the reduction of the Folin reagent that produces several reduced species of a characteristic blue colour with a maximum absorbance at 750 nm. The colour development is primarily due to the oxidation of the amino acids tyrosine and tryptophan, and to a lesser extent, cystine, cysteine, and histidine. The absorbance was measured at 650 nm in a microtitre plate reader.

3.2.3.4. SDS-polyacrylamide gel electrophoresis

The separation of proteins was performed using the discontinuous SDS-polyacrylamide gel electrophoresis (SDS-PAGE) of the Mini-Protean-3 system (BioRad), based on the description of Laemmli (1970). The chamber and gels were assembled as described by the manufactures protocol. A separating gel of desired thickness and percentage of acrylamide was layered with isobutanol. Before casting a stacking gel, the residual alcohol was removed and the future interphase between the two gels was rinsed twice with dH₂O. 5 µl of prestained Page Ruler Plus (Fermentas) was loaded on each gel as a molecular weight standard and to monitor the electrophoresis. A maximum of 40 µl sample was loaded in a single pocket and the gels were run with a constant current of 30 mA per gel, and a maximum voltage of 150 V. Gels were subjected to immunoblotting, once the bromophenol blue of the loading dye reached the lower end of the gel.

3.2.3.5. Immunoblot

The proteins were transferred from the SDS-gel onto a PVDF membrane (pore size 0.45 µm, Amersham/Millipore) by electrophoresis with the Invitrogen blotting apparatus (based on the original description of Towbin *et al.*, 1979). PVDF membranes were activated for 30 sec in

methanol and incubated 5 to 15 min in transfer buffer. Blotting paper and blotting pads presoaked in transfer buffer were assembled according to the manufacturer's protocol, although the blotting buffer differs from the manufacturers recommended. Proteins were transferred at a constant voltage of 38 V and a maximum current of 275 mA, for 1 hour at RT. Afterwards, the immunodetection of the proteins on PVDF membranes was performed. The membranes were rinsed briefly in TBS and blocked for at least 1 hour at RT in blocking buffer (5 % non-fat dry milk in TBS). Primary antibody diluted in blocking buffer was applied ON at 4°C. After four washes in TBS-T (0.05 % Tween-20 in TBS), HRP-conjugated secondary antibodies were applied for at least 1 hour, followed by four washes with TBS-T. Membranes were exposed using the Enhanced Chemiluminescence Detection kit (PerkinElmer), according to the manufacturer's instructions. ECL photographic films (Hyperfilm™, Amersham Biosciences) were used to expose the membranes. The time of exposure varied depending on the signal intensity. To reprobe the same membrane with a second antibody, the membrane was incubated with stripping buffer for 1 hour at 55°C with rigorous shaking. After one wash with TBS-T, the membrane was incubated in blocking buffer for 30 min before probing with the second primary antibody.

3.2.3.6. Silver staining

The silver staining was performed according to the modified protocols of Blum *et al.* (1987) and Mortz *et al.* (2001). The proteins were separated by SDS-polyacrylamide gel electrophoresis (section 3.2.3.4.) and then the gel was incubated in different solutions. All steps were performed on a shaking table. The silver staining was performed according to the following incubation steps: fixed in 40 % ethanol, 10 % acetic acid for 1 hour, washed twice with 30 % ethanol for 20 min each, and once with dH₂O for 20 min, sensitized in sodium thiosulfate for 1 min, rinsed trice with dH₂O for 20 sec each, impregnated with 0.2 % silver nitrate, 0.05 % formaldehyde solution (37 %) for 20 min and rinsed again trice in dH₂O for 20 sec. Then the development took place, and this step needed to be performed under visual inspection for evaluating when the staining is sufficient. The gel was incubated with 3 % sodium carbonate, 0.05 % formaldehyde solution (37 %) for 2 to 10 min, and once the staining was prominent enough, the gel was rinsed in dH₂O for 20 sec and the staining reaction was stopped by incubation with 5 % acetic acid for 10 min. Finally, the gel was washed trice with dH₂O for 10 min each and could be stored without drying out for long time at RT.

3.2.4. Animal breeding

The TSPAN2^{null} mice were generated in C57BL/6 ES cells and a backcrossing was therefore not necessary. The PLP^{null}, GPM6A^{null}, GPM6B^{null}, GPM6A^{null}*GPM6B^{null} mice had already been bred into the C57BL/6 background for more than ten generations using mice from the breeding colony of the Max-Planck-Institute of Experimental Medicine. And consequently the TSPAN2^{null}*PLP^{null} did also not require specific backcrossing. Wild-type animals were obtained from the breeding colony of the Max-Planck-Institute of Experimental Medicine. All animals used for this work were kept and treated in accordance with the guidelines for animal welfare of the Max-Planck-Institute of Experimental Medicine, approved by the German Federal State of Lower Saxony.

3.2.5. Cell culture

3.2.5.1. Primary cortical neuron cultures

Primary cortical neurons were prepared from brain hemispheres of E15 to E17 embryos. Briefly, the dissect hemispheres were removed from their meninges on HBSS+ and transferred into a 15 ml Falcon tube with HBSS+. This medium was removed and 1 ml of a 1:1:1 dilution of papain (20 U/ml), HBSS and DNase was added and incubated at RT for 6 min. The reaction was stopped by adding 1 ml of 10 % FCS in HBSS. HBSS was added until reaching 10 ml and the cells were centrifuged at 900 rpm for 5 min. The supernatant was removed, 2 ml of Neurobasal complete medium were added and the cells were carefully dissociated with a fire-polished Pasteur pipette. A 1:10 dilution was performed to determine the cell number in a Neubauer chamber. The appropriate cell were plated onto 10 cm dishes ($5 \cdot 10^6$ cells) or onto 24-well plates ($5 \cdot 10^4$ cells/well) (Falcon) containing PLL-coated (0.2 mg/ml, 37°C for at least 30 min) glass coverslips, and cultured at 37°C with 5 % CO₂.

3.2.5.2. Growth cone collapse assay

The “growth cone collapse assay” was performed on primary cortical neurons, cultured for 2 DIV of wild-type, GPM6A^{null}, GPM6B^{null} and GPM6A^{null}*GPM6B^{null} mice. The assay is based on the protocol applied by Knöll *et al.* (2006). Briefly, primary cortical neurons were cultured for 2 DIV with 500 µl medium in 24-well plates. The ephrin-A5-Fc (1 µg/ml) was preincubated with the anti-human IgG (10 µg/ml), as well as the recombinant Fc (1 µg/ml) with anti-human

IgG, which serves as a control condition, at RT for 30 min. These were added to the cultures, mixed carefully and incubated for 30 to 45 min at 37°C, 5 % CO₂. When the increased ephrinA5 dose was applied, double amounts of ephrinA5 were preclustered to the anti-human IgG. Then, cells had to be fixed with 4 % PFA including 10 % sucrose in a very fast manner, by adding the fixative directly to the side of the well and including no prior washing step, as these could abolish the effect of the collapse agents. After 5 min, the PFA/sucrose was refreshed, and 5 min later washed twice with PBS. The cortical neurons were then immunostained against tubulin and F-actin to visualize the collapse effect. The collapse was assessed on the axonal growth cones and defined as the absence of a lamellipodium.

In order to quantitatively assess the response to the growth cone collapse assay, cortical neurons were randomly imaged with a Leica SP2 confocal microscope, with a 63x oil objective. For each genotype n = 3 was used and ~ 75 growth cones were quantified per condition. The images were analyzed using the ImageJ software. The collapse was assessed on the axonal growth cones and defined as the absence of a lamellipodium. The statistical significance of the differences between experimental groups was assessed by performing a Chi-square comparison, using the SPSS software package.

3.2.6. Immunocytochemistry

Immunostainings were carried out at the time mentioned in the experiment, and all steps were performed at RT. Cortical neurons grown on PLL-coated coverslips were washed once (unless otherwise stated) with PBS and fixed for 10 min with 4 % PFA and 10 % sucrose. Cells were then washed three times for 10 min in PBS, permeabilized for 5 min with 0.1 % TritonX-100 in PBS and washed twice with PBS. They were then blocked for 30 min in blocking solution (2 % BSA in PBS) and the primary antibody was applied for 1 hour in blocking solution. Afterwards they were washed three times with PBS and the fluorochrome-conjugated secondary antibody was applied and kept in darkness for 1 hour. When phalloidin-rhodamine was used, it was added to the secondary antibody dilution. After four washings, including 4',6'-diamidino-2-phenylindole (DAPI) in the second-last one, the coverslips were rinsed in dH₂O and mounted with AquaPolyMount (Polysciences, Warrington, PA) on glass slides.

3.2.7. Histology and immunohistochemistry

3.2.7.1. Perfusion and fixation of mouse tissue

Mice were deeply anaesthetized by injecting 2.5 % avertin (0.017 ml/g of body weight) intraperitoneally. Once anaesthetized, the mice were washed with 70 % ethanol on the stomach and the skin was removed from the ventral side. A transversal cut was made just below the diaphragm and slowly opened until the heart was visible. A 27-gauge needle was inserted into the left ventricle and, immediately after starting the perfusion, a small incision was made in the right auricle to allow the blood to flow out of the body. Perfusion was carried out with HBSS and changed from HBSS to fixative (4 % PFA in PB). The perfusion was carried out with ~ 50 ml of fixative. The brain were removed carefully and collected into vials with fixative and stored in it ON at 4°C and then in 1 % PFA/PBS until further use.

3.2.7.2. Paraplast impregnation and embedding of the tissue

After post-fixation, the tissue was washed 3 to 4 times with PBS, the brains were cut into half and transferred into plastic chambers for dehydration and paraplast impregnation. The dehydration consisted in incubating the brains in the following solutions: 50 % ethanol for 1 hour, twice in 70 % ethanol for 2 hours, twice in 96 % ethanol for 1 hour and twice in 100 % ethanol for 1 hour each. Then, they were incubated in isopropanol for 1 hour, twice in xylol for 2 hours and the tissues were impregnated with paraplast at 60°C for 2 hours. Finally, the tissue was embedded in molten paraplast and left to harden. Blocks were removed from the moulds and could be stored stably for years.

3.2.7.3. Haematoxylin-Eosin (HE) staining

From the paraffinized blocks, 7 µm thick sections were cut using a microtome. The sections were floated on a warm water bath (42°C), placed on positively charged glass slides and then dried ON at 37°C. The sections were then incubated at 60°C for 10 min before being deparaffinized and rehydrated in the following steps: twice in xylol and once in xylol/isopropanol (1:1) for 10 min each, then, 100 % - 90 % - 70 % - 50 % ethanol for 5 min each and were than rinsed in dH₂O. The sections were incubated with 0.1 % haematoxylin for 5 min staining the basic cell nuclear compartment blue. After a wash with dH₂O, the

sections were dipped in a HCl-alcohol solution once for 5 to 10 sec and then in Scott's solution for 5 min. They were shortly rinsed with dH₂O, counterstained with 0.1 % eosin for 3 to 5 min and then rinsed with dH₂O. Sections were dehydrated by incubating them in increasing alcohol concentrations (50 %, 70 %, 90 %, and 100 %) for 2 min each, then in xylol/isopropanol (1:1) and twice in xylol for 5 min. Finally, they were mounted with 'Eukitt' (Kindler GmbH).

3.2.7.4. DAB-based immunodetection on paraffin sections

The sections were processed as above (section 3.2.7.3.) until rehydration, when they were incubated for 5 min in citrate buffer before being "cooked" for 10 min in boiling citrate buffer in a microwave. After this, the sections were left in the citrate buffer for about 20 min to cool down and subsequently rinsed in Tris buffer/2 % milk for 5 min. Endogenous peroxidases were inactivated by incubating the sections with 100 µl of 3 % hydrogen peroxide for 5 min. Then, the sections were incubated with 100 µl of goat-serum diluted in PBS/BSA (1:5) for 20 min at RT before proceeding with the 100 µl of the primary antibody diluted in PBS/BSA. After an ON incubation at 4°C, the sections were washed with Tris buffer/2 % milk and incubated with 100 µl of bridging antibody, i.e. biotinylated secondary antibody (Dako) for 10 min. They were then rinsed with Tris buffer/2 % milk and probed with 100 µl of tertiary antibody, i.e. Horseradish Peroxidase streptavidin complex (Dako), by incubating the sections for 10 min. They were then rinsed with the Tris buffer and incubated with 100 µl of DAB for 10 min. Finally, the sections were rinsed twice with dH₂O for 5 min each and counterstained for 30 sec with haematoxylin following the steps until mounting (section 3.2.7.3). The enzymatic reaction between the HRP and DAB yielded a very a stable brown precipitate.

3.2.8. Confocal and light microscopy

The light microscopic observations were performed on a Zeiss Axiophot microscope using the following objectives: 4x (achroplan, 4x/0.10), 10x (achroplan, 10x/0.30) and 20x (plan-neofluar, 20x/0.50) and the images were captured by a Kappa camera system (Kappa optoelectronics GmbH, Gleichen, Germany). The images were taken with the Kappa Image Base Software (version 2.7.2.).

Fluorescent images were captured on a Leica TCS-SP2 confocal microscope (Leica Microsystems Heidelberg GmbH, Germany) with a 63x (plan-apochromat, 63x/1.4) oil

objective. For final analysis, captured Leica images were exported as TIF, and analysed and processed with the Leica Confocal Software (LCS, version 2.61) and ImageJ software (version 1.45). The plugin NeuronJ (version 1.4.1, Meijering E.) was employed for the neurite length quantification.

3.2.8.1. *In vivo* imaging of cortical neuron growth cones

For the *in vivo* imaging of cortical neuron growth cones, the cells were plated on 8-well glass slides (Ibidi GmbH) to allow the confocal imaging on them. Growth cones were imaged for 10 min, taking one image every 3 sec, thereby resulting in a video of 201 frames. A 40x oil objective was used and the 633 nm laser was utilized for the reflection microscopy.

The images were further analysed with the ImageJ software. The images were processed as following: a 2 pixel Gauss filter was applied, the images were thresholded and by differences in the intensity levels they areas were classified into “adhesive” and “non-adhesive”. For the motility evaluation, the analysis was performed as depicted in the following figure (Fig. 7):

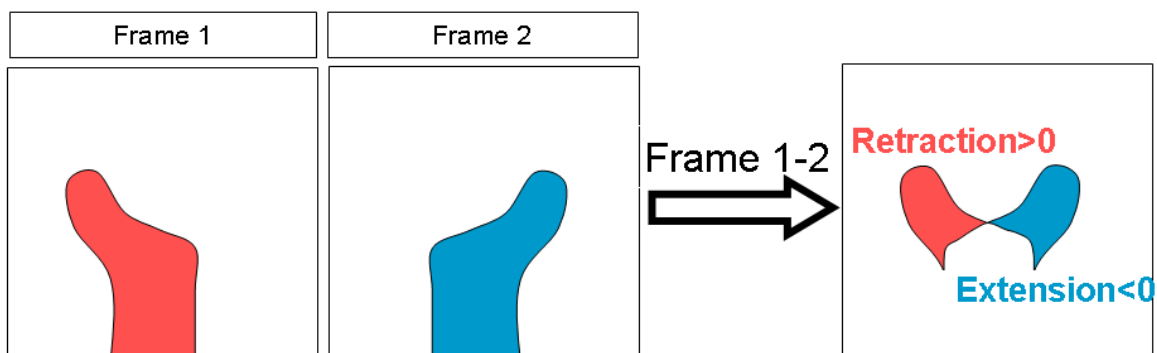


Figure 7. Evaluation of the *in vivo* motility of cortical neuron growth cones.

In each movie of the neuronal growth cones, the first frame was subtracted from the second, the second from the third, etc. Thereby the retraction between each frame could be evaluated as positive values and the extension as negative values.

In each movie, the first frame (binarized after subtracting the background) was subtracted from the second, the second from the third, etc. Thereby the retraction between each frame could be evaluated as positive values and the extension as negative values. This allowed assessing the motility of these growth cones.

3.2.9. Statistical analysis

The statistical analyses have been performed with the Microsoft Office Excel 2003 and the SPSS 13.0 software. Briefly, the Student's t-tests were applied to compare the mean values

of quantitative variables. The chi-square tests were applied in order to determine whether the frequency counts in each category were equally distributed. The ANOVA and the ANOVA with repeated measurements were performed to compare the variances. In the case of the ANOVA with repeated measurements, the sphericity could not be assumed and thereby the Greenhouse-Geiser test was used.

4. Results

4.1. M6 Proteolipids in neuronal cell process formation

The neuronal proteolipids M6A and M6B are transmembrane proteins highly expressed in the neurons of the CNS (Huminięcki *et al.*, 2003) and located throughout the brain (Baumrind *et al.*, 1992; Yan *et al.*, 1996). Acute antibody applications or over- and underexpression have implicated these proteins in neurite outgrowth (Lagenauer *et al.*, 1992; Zhao *et al.*, 2008) and filopodia formation (Alfonso *et al.*, 2005; Fernández *et al.*, 2010), but little is known about their function *in vivo* or about the consequences of their chronic lack.

4.1.1. Localization of M6A and M6B on cortical neurons

To characterize the expression of M6A and M6B in the culture system that has been subsequently used for functional investigations, immunocytochemical analysis was performed on wild-type primary cortical neurons of embryonic day 17 (E17) old mice embryos at 3 days in vitro (DIV). The *ex vivo* culture system was chosen, because it allows a simplified approach to study the importance of neuronal proteolipids in the neuronal biology.

The cortical neurons were immunostained using antibodies against M6A and M6B. The staining revealed the presence of a mixed population of cortical neurons expressing the neuronal proteolipids (Fig. 8).

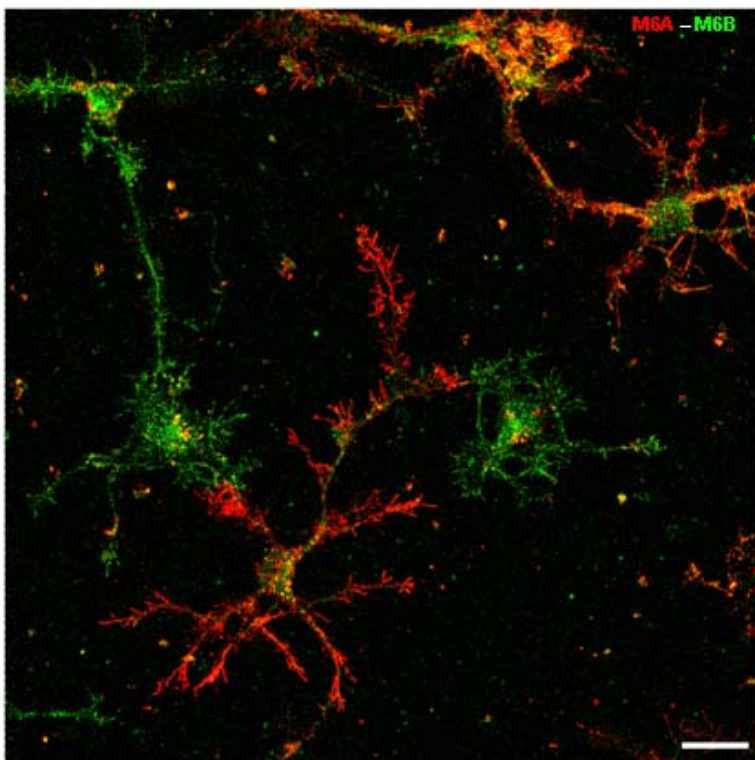


Figure 8. Wild-type cortical neurons expressing M6A and M6B.

Confocal image illustrating the immunocytochemical localization of M6A (red) and M6B (green) proteins in cultured cortical neurons prepared from E17 mice and maintained for 3 DIV. Most cortical neurons express both proteins, but their expression levels vary. Scale bar = 20 μ m.

Distinct neurons differ regarding their staining towards M6A and M6B (Fig.8). Most cortical neurons express both proteins (Fig. 9A), but their expression levels vary.

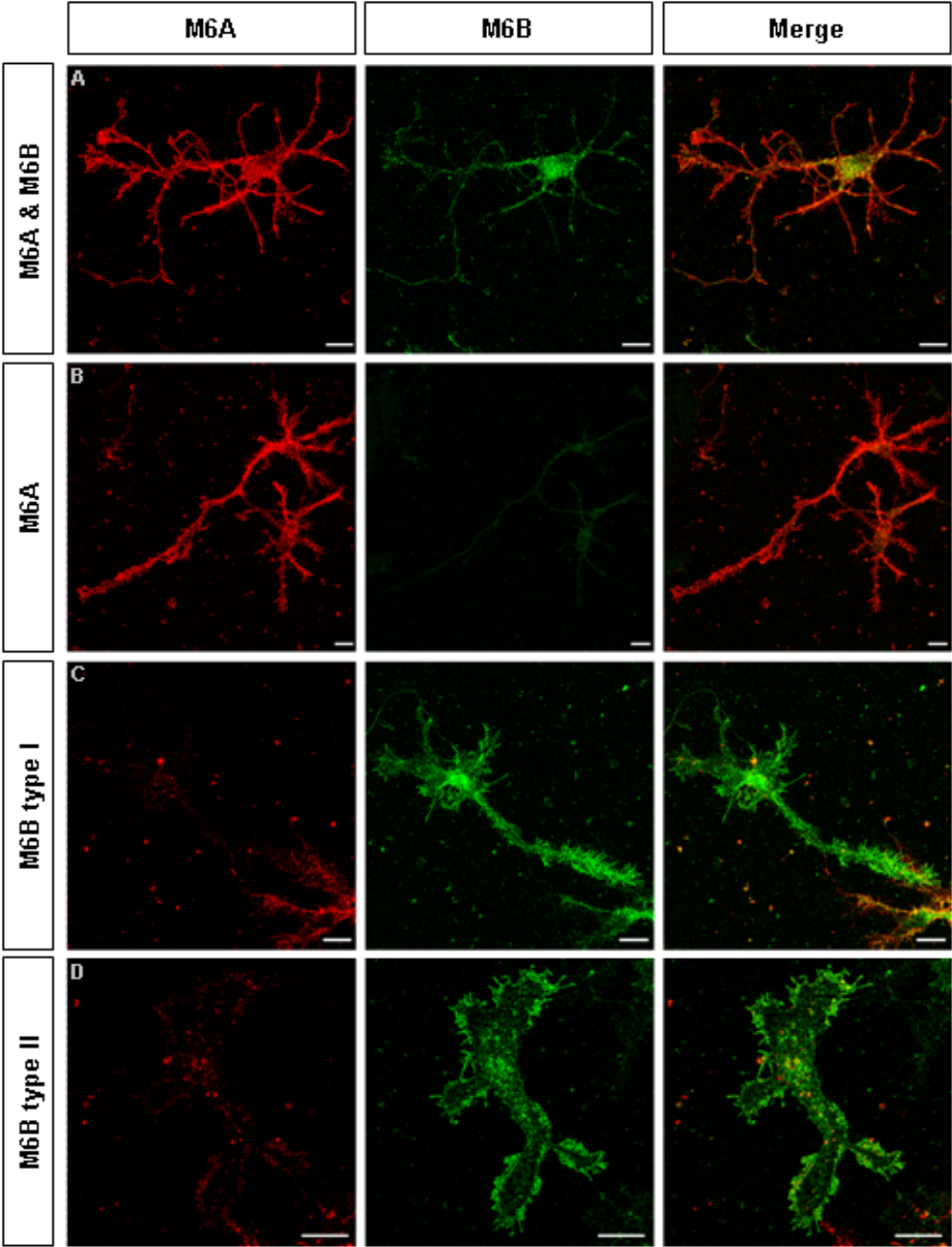


Figure 9. Types of wild-type cortical neurons according to the M6-protein abundance. Mouse cortical neurons (E17) were cultured for 3 DIV, immunostained against M6A (red) and M6B (green) and confocal images were taken. There is a mixed population of neurons expressing the neuronal proteolipids. There are cells expressing similar levels of both proteins (A), others expressing mainly M6A (B) or M6B (C, D). There are two subtypes of cortical neurons regarding their M6B expression pattern, either M6B has an overall broad localization in the cell (C) or it localizes mainly to the outer plasma membrane (D). Scale bars = 15 μ m.

Thereby there are cortical neurons that do express predominantly M6A (Fig. 9B) or M6B proteolipid protein. Interestingly, in the case of neurons expressing predominantly M6B, there are two subtypes of cortical neurons regarding this expression pattern: some neurons express M6B in a broad manner all over the cell (Fig. 9C), whereas in other neurons M6B is confined mainly to the external plasma membrane of the cell (Fig. 9D). In the cortical neurons that do express similar levels of both proteins, these co-localize extensively in axons and dendrites and partially in the somata, where M6B is more abundant (Fig. 9A). The M6A as well as the M6B staining demonstrates the presence of the neuronal proteolipids on all neurite processes, therefore in axons as well as in dendrites, with no difference in their expression levels between these. These results validate this culture system for the study of neuronal M6 proteins in neuronal development.

4.1.2. Subcellular localization of M6A and M6B on cortical neurons

To elucidate the localization of the neuronal proteolipids in more detail, co-localization studies were accomplished. It is known that tubulin as well as F-actin are major components of neurons, and that they define neuronal structures. Tubulin is mainly found in the axonal and dendritic shafts, while F-actin is mainly found in the peripheral growth cone regions (Dent *et al.*, 2010).

To investigate the subcellular localization of the neuronal proteolipids M6A and M6B, immunocytochemistry was performed to observe their co-localization regarding tubulin and F-actin. For these, the antibody Tuj-1 (against neuron-specific class III beta-tubulin) and the toxin phalloidin that binds to F-actin were used. These experiments were performed on wild-type cortical neurons of E15 old mice embryos at 3 DIV.

M6A as well as M6B are mainly expressed in tubulin rich compartments (Fig. 10A, B) including the axon and dendrites. When comparing their localization with F-actin, M6A co-localizes with F-actin positive structures such as the neurite tips and growth cones, but is also prominently detected at F-actin free membrane extensions (Fig. 10C). The M6B expression is confined to F-actin-rich domains, but not outside these (Fig. 10D). Thereby, M6A and M6B show overlapping but non-identical localizations.

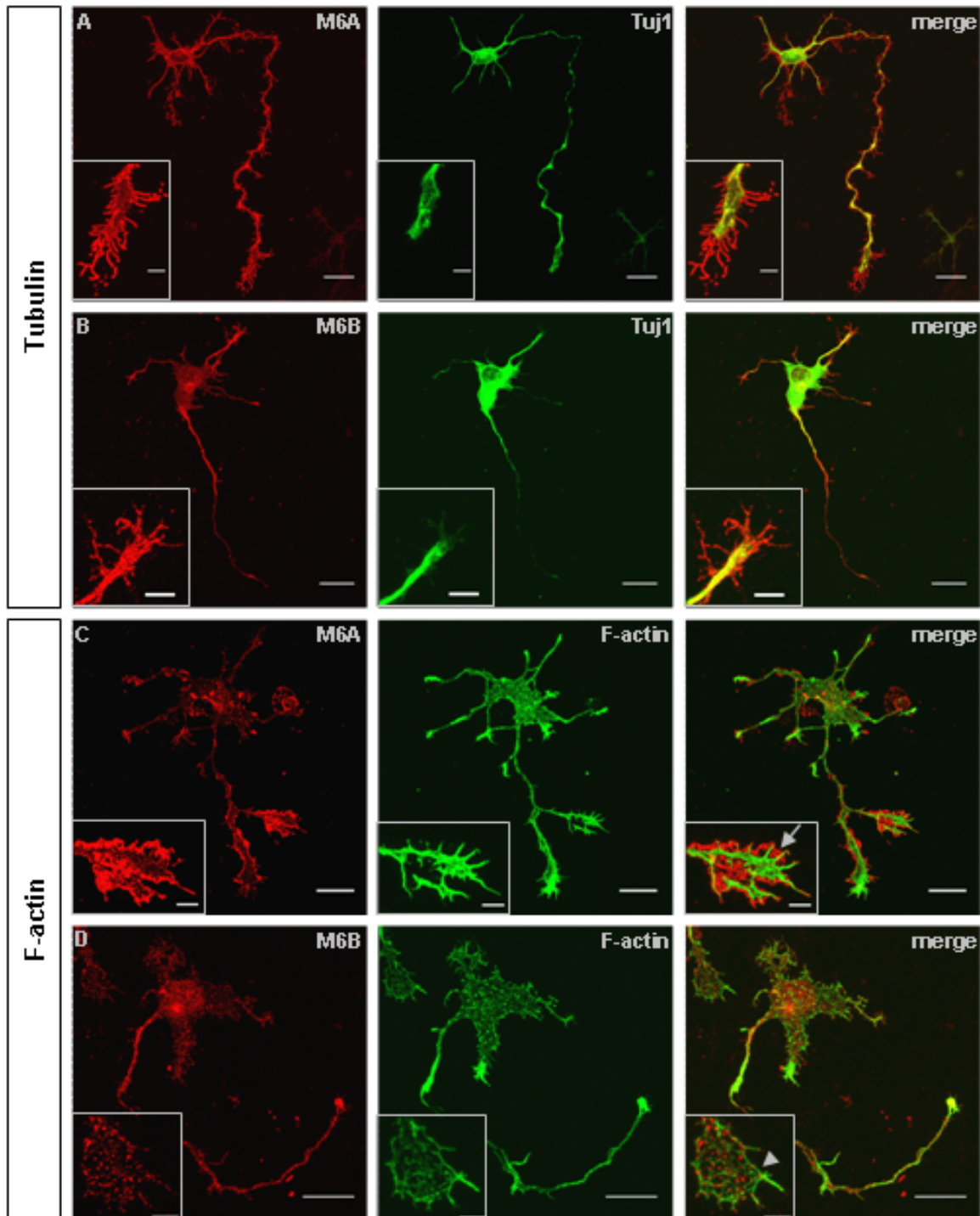


Figure 10. Subcellular localization of M6A and M6B on wild-type cortical neurons regarding tubulin and F-actin.

Immunocytochemistry was performed on mouse cortical neurons (E15) at 3 DIV and confocal images were taken. M6A (A) and M6B (B) localization in contrast to neuron-specific class III beta-tubulin (Tuj1) revealed that M6A as well as M6B co-localize with tubulin-rich structures. M6A also co-localized with F-actin positive regions (C), but was also found on F-actin free membrane extensions (arrow). M6B was also found in F-actin positive regions (D), but not extending into F-actin free membrane extensions (arrowhead). Images in false colour representation; scale bars = 50 μm ; scale bars of inset = 5 μm .

4.1.3. M6A defines F-actin free membrane protrusions

To further investigate the localization of M6 proteins at F-actin free membrane extensions a more detailed analysis was performed. According to the current knowledge, lamellipodia and filopodia have a high content in F-actin, and filopodia contain by abundance mainly F-actin, which also gives them their finger-shaped structure (Dent *et al.*, 2010).

Wild-type cortical neurons of E17 old mice embryos were cultured, fixed at 2 DIV and cells were stained against M6A or M6B and against F-actin with the toxin phalloidin. Confocal imaging that included not only the conventional laser-driven signal, but also simultaneous reflection confocal microscopy was performed. This allowed the examination of the signals from the immunocytochemistry, as well as the membrane surface and outer membrane demarcation. This was essential for being able to define outer tubules and membrane extensions, on which the presence or absence of F-actin and M6A or M6B were analysed.

On primary cortical neurons stained against M6A and F-actin co-localization was found on many tubular structures (filopodia) as well as on growth cone tips. However, there were frequent cases in which M6A was found in F-actin free outward tubules that clearly showed a membrane continuation at the reflection microscopy level, indicating that the M6A-positive F-actin-negative outer membrane tips were in contact with the full cell membrane (Fig. 11). In some neurite tips the majority of the process tips were M6A-positive and F-actin-negative (Fig. 11A). However, there were also cells in which there was diversity regarding the type of neurite tips. Some were positive for M6A and F-actin (Fig. 11B star), while close by others lack F-actin all over the process (Fig. 11 open arrow). Additionally, there were cases in which M6A and F-actin were both present in one subcompartment, while in the other compartment there was M6A labelling in the absence of F-actin. Hence, in particular in small processes the presence of M6A was found (Fig. 11B arrow). In some cases, process-ending tips showed M6A labelling and no F-actin one, thereby M6A was defining the end of these tip (Fig. 11B arrowhead). M6A-positive F-actin-negative membrane extensions were various in length (Fig. 11A arrow, B arrow and open arrow). There were also cases in which the M6A-positive membrane process extended more than 10 μm without the presence of F-actin (Fig. 11C). Besides there were also neurons in which membrane flattened extensions lack F-actin but show a clear M6A presence (Fig. 11D).

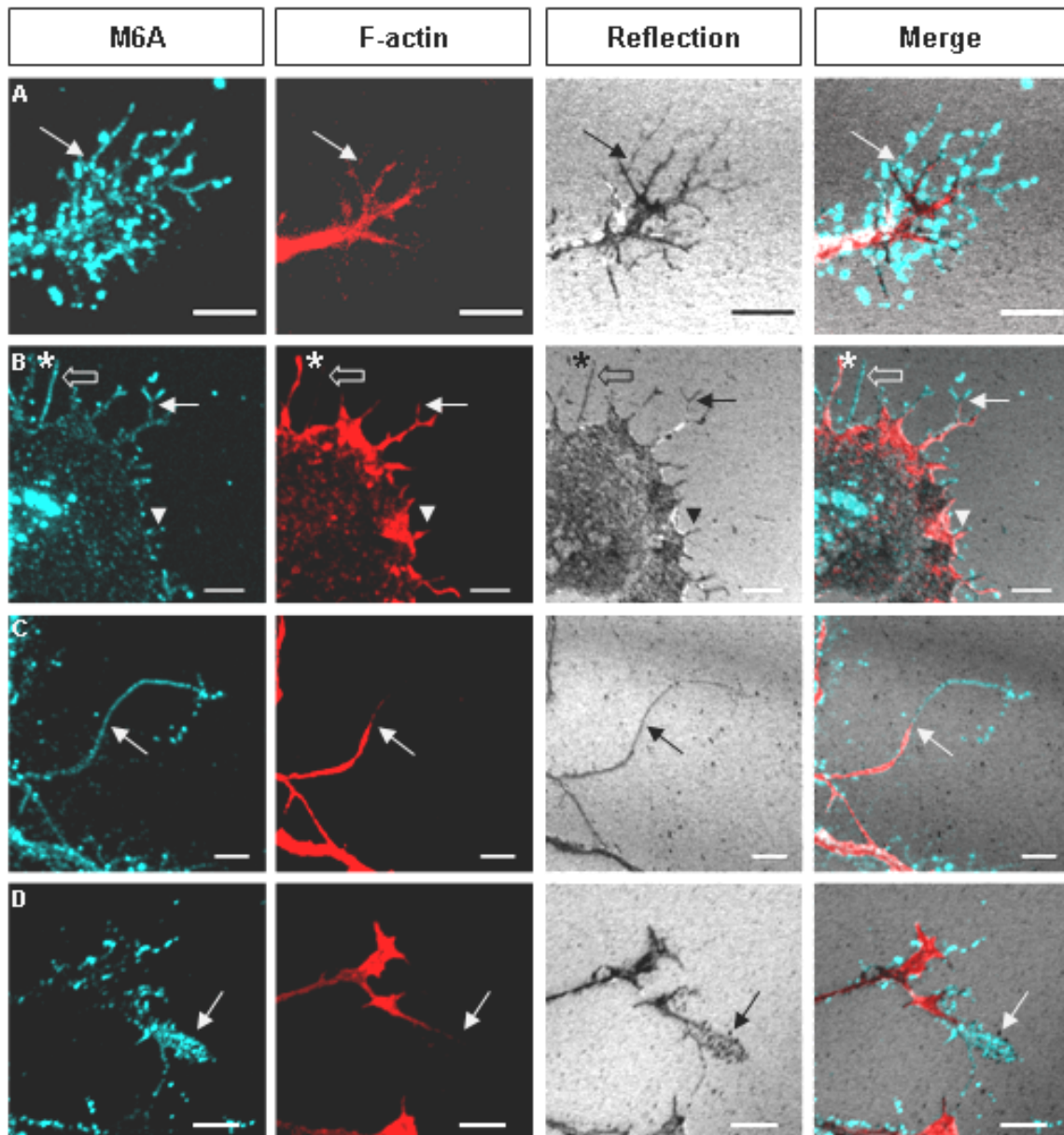


Figure 11. M6A defines F-actin free membrane protrusions.

E17 mouse cortical neurons were immunostained at 2 DIV against M6A (cyan) and F-actin (phalloidin toxin, red). Confocal microscopy and simultaneous reflection microscopy (gray) were performed to visualize the immunocytochemistry and the outer cell membrane delimitation. M6A co-localizes with F-actin at membrane extensions and growth cone regions, but is also found at membrane extensions that lack F-actin. In some neurites all membrane outer tips are M6A-positive and F-actin-negative (A, arrow). While in other membrane extensions there are a variety of events: M6A and F-actin positive protrusions (B, star); M6A and F-actin-positive extensions up to a position from which only M6A is present at the periphery, either at complete tips (B, arrow) or at final endpoints of the tip (B, arrowhead); as well as entire M6A-positive and F-actin negative processes (B, open arrow). The extension of the neurite tip at the absence of F-actin can extend more than 10 μm (C, arrow). There are also flat membrane extensions that are M6A-positive and F-actin negative (D, arrow). Scale bars = 5 μm .

Taken together, M6A defines a novel structure, as F-actin has been assumed “to compose the core of filopodia” (cited after Dent & Gertler, 2003). Consequently the M6A-rich domain in F-actin free membrane extensions of neuronal growth cones defines novel F-actin free M6A-rich membrane protrusions.

On the other hand, this is not the case for M6B. M6B was always confined to F-actin-rich regions and did not define F-actin free domains at the cell tips (Fig. 12). Very seldom M6B seemed present in F-actin free membrane tips, but this could be excluded upon more careful microscopic assessment (Fig. 12A arrowhead). Occasionally there were membrane tips that lacked either M6B as well as F-actin staining (Fig. 12 arrow), most likely these protrusions were M6A-positive. In general the majority of the tips were positive for M6B as well as for F-actin (Fig. 12 arrow).

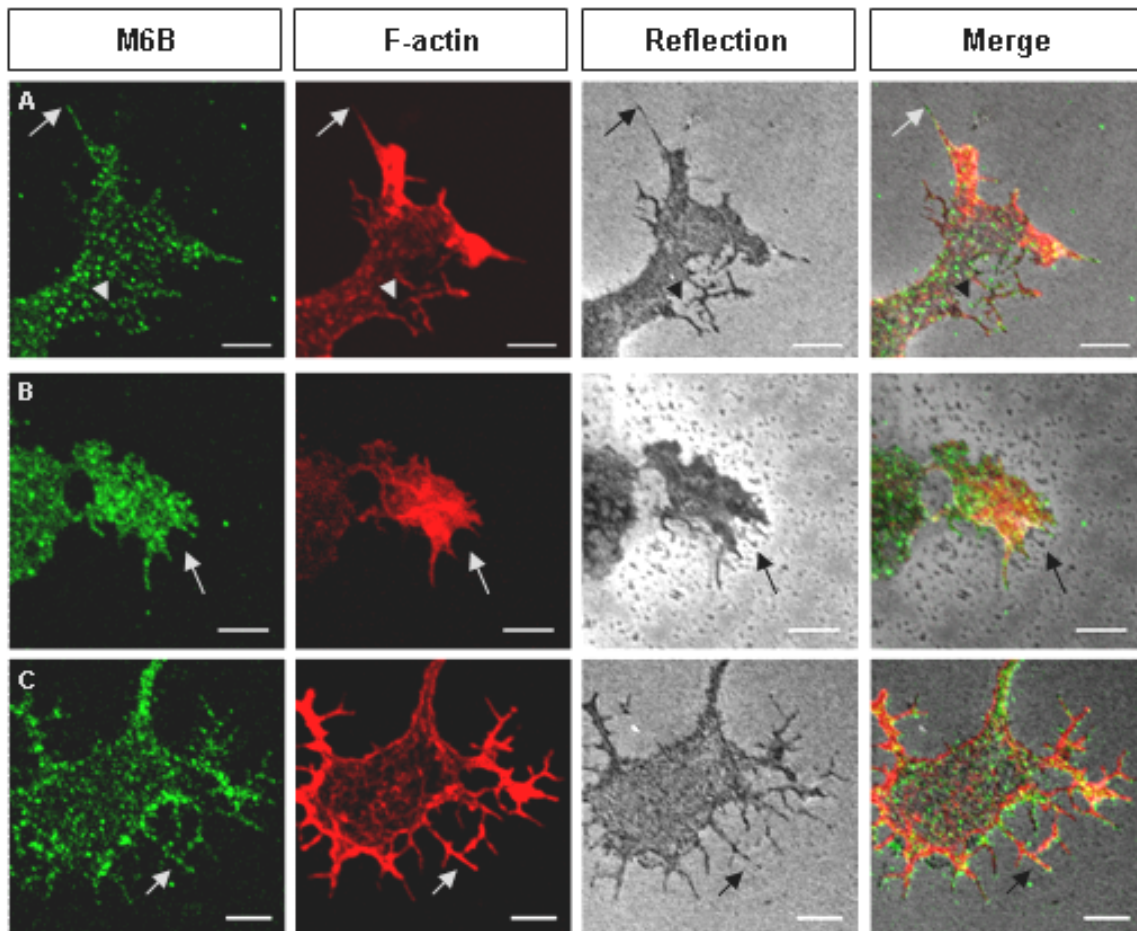


Figure 12. M6B does not define F-actin free membrane protrusions.

Mouse cortical neurons (E17) were immunostained at 2 DIV against M6B (green) and F-actin (phalloidin toxin, red). Conventional confocal microscopy and simultaneous reflection microscopy (gray) were performed to visualize the staining and the outer cell membrane delimitation. M6B does co-localize with F-actin at membrane extensions and growth cone regions, but is not found at membrane extensions that lack F-actin. In some neurite tip M6B seemed present without an F-actin co-labelling, but upon more careful examination this was excluded (A, arrow). Some tips lack M6B as well as F-actin staining (B, arrow). Most of the membrane extensions were positive for M6B as well as for F-actin (C, arrow). Scale bars = 5 μ m.

Accordingly, M6A does define F-actin free membrane protrusions while M6B does not. And in wild-type cortical neurons, essentially all membrane protrusions express the neuronal M6 proteolipid proteins.

4.1.4. Altered growth cone morphology in $Gpm6a^{null*}Gpm6b^{null}$ mice

Actin and tubulin define two different compartments in neuronal growth cones. This compartmentalization is known since long. There are MTs (thereby tubulin) in the axon shaft as well as in the centre of the neuronal growth cone. In the growth cone periphery, the lamellipodia, there are only few MTs but mainly a network of F-actin filaments. Finally, at the growth cone tips, the filopodia, F-actin is found mostly in them, hence also defining them (see Fig. 2, Dent & Kalil, 2001; Dent & Gertler, 2003). Sometimes, in pausing growth cones, it can occur that tubulin reaches partially into the actin domain (Dent *et al.*, 2010).

As a high expression of the M6 proteins had already been observed in cortical neuronal growth cones as well as a distinct localization of the M6A proteolipid protein regarding F-actin at the growth cone tip, an investigation involving the actin and tubulin compartmentalization was performed. For this purpose, primary cortical neurons of E17 wild-type as well as $Gpm6a^{null*}Gpm6b^{null}$ mice were cultured and immunostained at 2 DIV against tubulin (Tuj1; Neuron-specific class III beta-tubulin) and F-actin (phalloidin). For each genotype (wild-type or $Gpm6a^{null*}Gpm6b^{null}$ mice) the analysis was performed on cortical neurons deriving from four different embryos ($n = 4$) at E17, with ≥ 15 neurons per individual. Overall 63 wild-type and 61 $Gpm6a^{null*}Gpm6b^{null}$ neurons were analysed, resulting, respectively, in a total of 167 and 137 analyzed growth cones.

To evaluate the different localization of tubulin and F-actin, three categories were established: (1) tubulin and F-actin are together in one compartment, superimposed or partially superimposed, (2) tubulin and F-actin are separated into two compartments, as described in literature, being F-actin at the tips, and (3) tubulin is expressed at the end of the tips, beyond F-actin. For increased precision, it was distinguished between the growth cone or tip of the axon –or longest neurite in case of doubt– or the growth cone or tip of the remaining neurites. As expected, wild-type cortical neurites fell mainly into category two (Table 1). This is the case for the axonal growth cones (83 %) as well as for the tips of the remaining neurites (88 %). Some growth cones could be classified into the category of tubulin and F-actin being partially superimposed (17 % for axonal growth cone, 11 % for the remaining), while a localization of tubulin distal to F-actin is extremely unusual (0 - 1 %) in wild-type cortical neurons. Interestingly, this was very different in the cortical neurons of the $Gpm6a^{null*}Gpm6b^{null}$ mice (Table 1). Indeed, the majority of their growth cones were categorized into the group of tubulin being superimposed over F-actin (57 % in axonal growth cones, 56 % in remaining growth cones). Surprisingly, there were frequent growth cones in which tubulin defined the most distal point (11 %, 16 %).

Table 1. Neuronal growth cones classification according to their F-actin and tubulin compartmentalization, into three categories.

Proportion of wild-type (WT) and *Gpm6a^{null}*Gpm6b^{null}* (dKO) growth cones of the axon (Axonal GC) as well as the remaining growth cones (Remaining GCs) and the totality of the growth cones (All GCs), according to three categories: (1) tubulin and F-actin in one compartment, (2) tubulin proximal to F-actin localization, and (3) tubulin distal to F-actin localization. Display of the absolute numbers and the percentages in parenthesis. The star designates categories that excluded a statistical analysis.

Cat.	Axonal GC		Remaining GCs		All GCs	
	WT	dKO	WT	dKO	WT	dKO
1	11 (17%)	35 (57%)	18 (11%)	77 (56%)	29 (13%)	112 (57%)
2	52 (83%)	19 (31%)	147 (88%)	38 (28%)	199 (87%)	57 (29%)
3	0 (0%)*	7 (11%)	2 (1%)*	22 (16%)	2 (1%)*	29 (15%)

The following bar diagram (Fig. 13) shows the grouping of the growth cones of wild-type as well as *Gpm6a^{null}*Gpm6b^{null}* mice according to the three categories (see above). There is an obvious difference regarding the distribution over the categories between the genotypes in all growth cones, no matter they belong to the axon or to a dendrite.

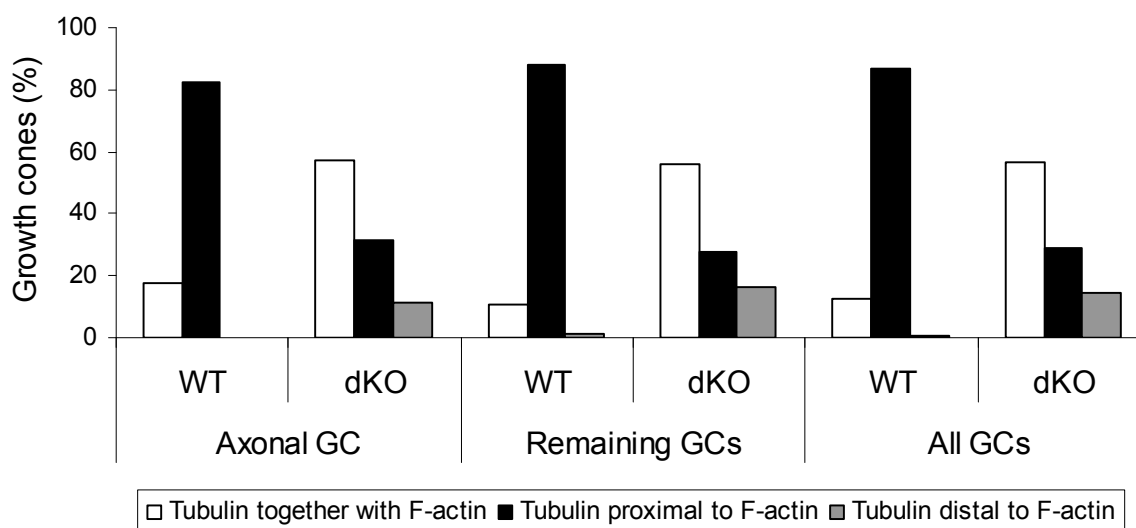


Figure 13. Classification of the neuronal growth cones according to three categories.

Evaluation of the tubulin and F-actin localization in 2 DIV cultured primary cortical neurons of E17 mice. Percentage of wild-type (WT) and *Gpm6a^{null}*Gpm6b^{null}* (dKO) growth cones of the axon (Axonal GC) as well as the remaining growth cones (Remaining GCs) and the totality of the growth cones (All GCs), according to three categories: (1) tubulin and F-actin in one compartment, (2) tubulin proximal to F-actin localization, and (3) tubulin distal to F-actin localization.

The fact that the third category of growth cones (with tubulin at the most distal endpoint) was only found in *Gpm6a^{null}*Gpm6b^{null}* cortical neurons impeded a statistical analysis, as the data points were zero or one in the wild-type (Table 1, star), thereby not fulfilling the minimal requirement for a meaningful statistical analysis.

Consequently, to perform a statistical analysis the categories were merged, so that there were two remaining groups: (1) tubulin and F-actin in one compartment, partially superimposed or tubulin at the distal endpoint of the tip, and (2) tubulin and F-actin in two

separated compartments (with F-actin at the distal end). Briefly, merging the prior category one with number three and maintaining number two. The resulting data are given in Table 2.

Table 2. Neuronal growth cones classification according to their F-actin and tubulin compartmentalization.

Proportion of wild-type (WT) and Gpm6a^{null*}Gpm6b^{null} (dKO) growth cones of the axon (Axonal GC) as well as the remaining growth cones (Remaining GCs) and the totality of the growth cones (All GCs), according to two categories: (1) tubulin and F-actin in one compartment, superimposed or with tubulin at the distal endpoint, and (2) tubulin proximal to F-actin localization. Display of the absolute numbers and the percentages in parenthesis.

Cat.	Axonal GC		Remaining GC		All GCs	
	WT	dKO	WT	dKO	WT	dKO
1	11 (17%)	42 (69%)	20 (12%)	99 (72%)	31 (13%)	141 (71%)
2	52 (83%)	19 (3%1)	147 (88%)	38 (28%)	199 (87%)	57 (29%)

On this dataset it was possible to perform a chi-square test comparison of the frequencies of the growth cones being grouped into one category or the other (Table 3).

Table 3. Chi-square comparison of frequencies of classification of neuronal growth cones according to their F-actin and tubulin compartmentalization.

Representation of the result of the statistical analysis of the comparison of tubulin and F-actin localization on neuronal growth cones of wild-type and Gpm6a^{null*}Gpm6b^{null} mice, according to two categories. Either tubulin and F-actin are in the same compartment, or into two different ones, with F-actin at the distal tip. Chi-square test performed on data resulting from n = 4 per genotype with ≥ 15 neurons per n, with a total of 167 and 137 growth cones, respectively. It is shown the Pearson X² statistic (Pearson X²), the degrees of freedom (df) and the P-value (P) for each comparison.

	Pearson X ²	df	P
Axonal GC	33.447	1	7.325 · 10 ⁻⁹
Remaining GCs	114.825	1	8.597 · 10 ⁻²⁷
All GCs	147.547	1	5.960 · 10 ⁻³⁴

The result of the chi-square test demonstrates a very highly significant difference between wild-type and Gpm6a^{null*}Gpm6b^{null} cortical neurons regarding the distribution of tubulin and F-actin at the growth cones. No matter if the focus is on the growth cones or tips of the axons or the dendrites (Fig. 14). There is a very clear difference in all the neurite tips. In the Gpm6a^{null*}Gpm6b^{null} cortical neurons it is significantly more frequent that tubulin is partially or totally superimposed over the F-actin compartment, or beyond the limits of the F-actin localization. This is a very profound breakage of the normal growth cone morphology, as tubulin and F-actin define the regions (morphologically and functionally) of the neuronal growth cone in a very distinctive manner.

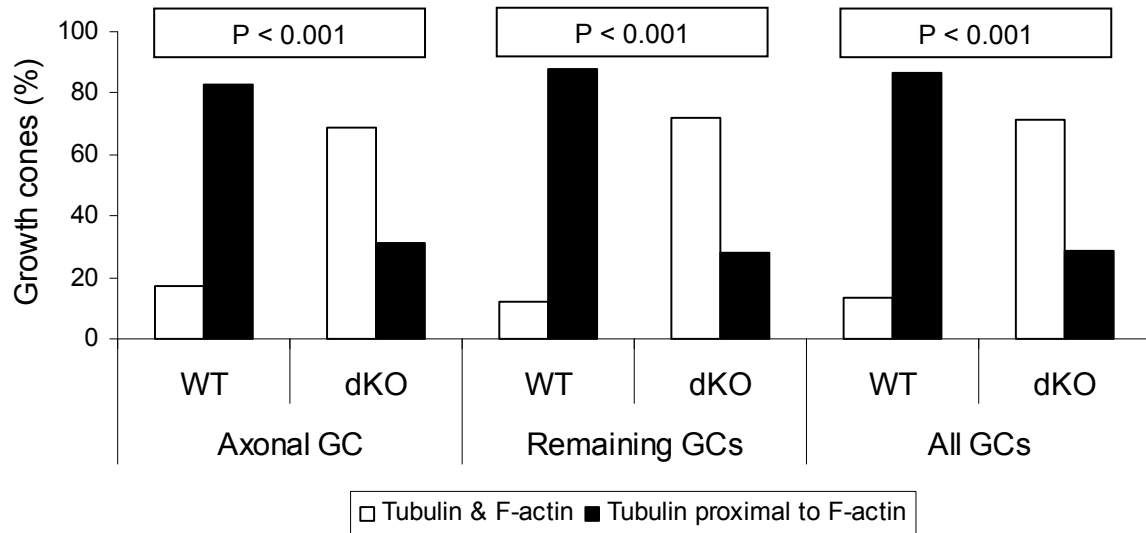


Figure 14. Classification of the neuronal growth cones according to two categories. Evaluation of the tubulin and F-actin localization in 2 DIV cultured primary cortical neurons of E17 mice. Percentage of wild-type (WT) and $Gpm6a^{null/*}Gpm6b^{null}$ (dKO) growth cones of the axon (Axonal GC) as well as the remaining growth cones (Remaining GCs) and the totality of the growth cones (All GCs), according to two categories: (1) tubulin and F-actin in one compartment superimposed or tubulin at the outer tip or (2) tubulin proximal to F-actin localization. There is a very highly significant difference ($P < 0.001$) regarding this two categories between the WT and dKO growth cones of the axons, as well as the dendrites.

An example of this altered growth cone morphology –defined by the localization of tubulin and F-actin– is given in figure 15.

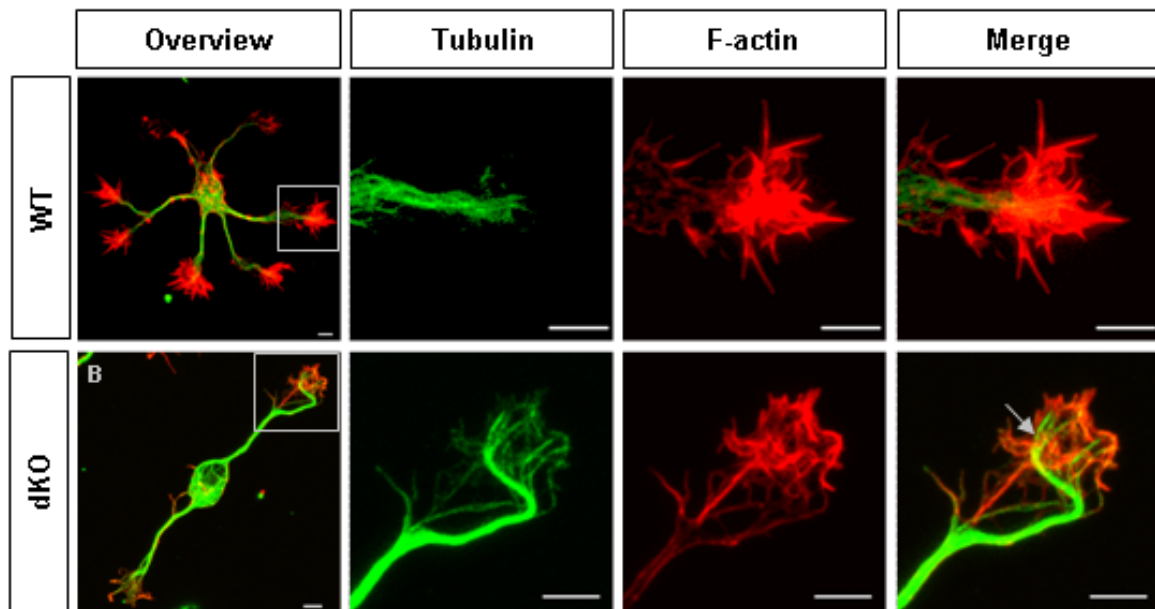


Figure 15. Altered growth cone morphology in $Gpm6a^{null/*}Gpm6b^{null}$ mice. E17 cortical neurons were cultured for 2 DIV and stained against tubulin (Tuj1 antibody) and F-actin (Phalloidin toxin). The overview shows a normal F-actin-tubulin localization on the full cell level, but this is different when focusing at the growth cones. The wild-type (WT) growth cones (A) exhibit a defined and separated F-actin and tubulin localization. But the growth cones of the $Gpm6a^{null/*}Gpm6b^{null}$ (dKO, B) show a strong overlap of tubulin and F-actin. Tubulin partially localizes to the F-actin domain, without having a complete overlap (arrow) with F-actin. Some regions contain more tubulin, others more F-actin. Scale bars = 5 μ m.

As depicted in the representative example of Fig. 15, in Gpm6a^{null*}Gpm6b^{null} cortical neurons the extension of the tubulin compartment into the normally exclusive F-actin domains does not occur with an absolute overlap. Although tubulin covers the majority of the F-actin-positive regions, it occurs in a specific and partially exclusive manner. There are tubulin-positive processes that lack the same F-actin distribution (Fig. 15, arrow). This also provides evidence that this observation is not due to a microscopy artefact.

Consequently, there is an alteration of the normal F-actin and tubulin compartmentalization in the growth cones of Gpm6a^{null*}Gpm6b^{null} cortical neurons. This mislocalization is found in all neurite tips; no matter if they belong to the axons or to the dendrites. It is important to recall that M6A as well as M6B are expressed in basically all cortical neurons and that both neuronal proteolipids are present in axons as well as in dendrites. It is the absence of the M6-proteins in the neurites that leads to modified growth cone morphology. Thereby the M6 neuronal proteolipids are required for the normal segregation of cytoskeletal proteins at the growth cones.

4.1.5. M6A and M6B are required for normal reaction to ephrinA5

To assess if there is a functional response to the altered growth cone morphology and actin-tubulin compartmentalization it was chosen to realize a “growth cone collapse assay”. For the assay ephrinA5, widely known to act as a collapse agent on neurons, was chosen (Knöll *et al.*, 2006; Pandithage *et al.*, 2008). The collapse or non-collapse was defined as the absence or presence, respectively, of a lamellipodium or veil-like structure in the growth cones of the axon or longest neurite. The experiment was performed on primary cortical neurons of E17 mice embryos that were cultured for 2 DIV.

On the representative images (Fig. 16) it can be observed that there is a difference in the responsiveness to ephrinA5 in the Gpm6a^{null*}Gpm6b^{null} cortical neurons, in comparison to the wild-type, Gpm6a^{null} and Gpm6b^{null} single-mutant cortical neurons. These dKO neurons do not react to the commonly used amount of ephrinA5 (1 µg/ml) (Knöll *et al.*, 2006; Pandithage *et al.*, 2008), but they do react to it when it is doubled (2 µg/ml).

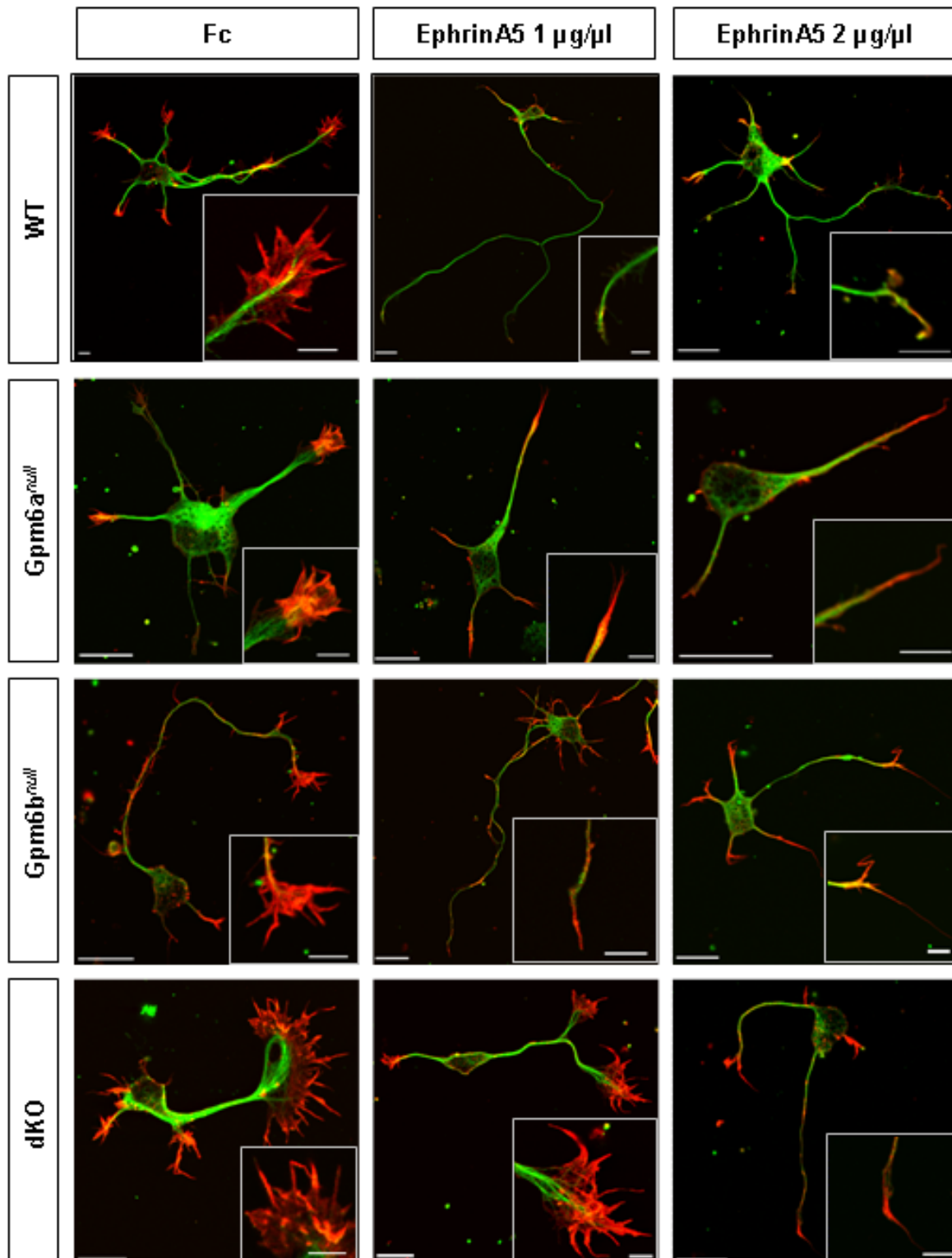


Figure 16. Responsiveness to ephrinA5 induced growth cone collapse assay.

WT, Gpm6a^{null}, Gpm6b^{null} and dKO cortical neurons from E17 mice were cultured and after 2 DIV a “growth cone collapse assay” with ephrinA5 was performed. Cells were then fixed and stained against Tuj1 (in green) and Phalloidin (in red). Examples for each given genotype with the control (recombinant Fc) and ephrinA5 (recombinant ephrinA5/Fc chimera, 1 $\mu\text{g}/\text{ml}$ or 2 $\mu\text{g}/\text{ml}$) treatment. The dKO cortical neurons do not react to ephrinA5 at the same extension as wild-type do. Scale bar = 15 μm ; in inset scale bar = 5 μm .

The quantification of the “growth cone collapse assay” is given in table 4. There is a clear difference in the responsive behaviour of the dKO neurons as they don’t react to the growth cone collapse induction in the same manner than wild-type, Gpm6a^{null} and Gpm6b^{null} single-null mutant cortical neurons.

Table 4. Quantification of the growth cone collapse assay induced by ephrinA5.

Growth cone collapse assay performed on 2 DIV cultured WT, Gpm6a^{null}, Gpm6b^{null} and dKO cortical neurons from E17 mice. dKO cortical neurons react differently to the ephrinA5 induced collapse assay at 1 µg/ml (star). The axonal growth cone was categorized as non-collapsed (Non C) or collapsed (C) regarding the presence or absence of a lamellipodium. The percentage of collapsed (%C) growth cones is given. The experiment was performed on n = 3 per genotype.

	Control			Ephrin A5 [1 µg/ml]			Ephrin A5 [2 µg/ml]		
	Non C	C	%C	Non C	C	%C	Non C	C	%C
WT	34	41	55	15	62	81	9	67	88
Gpm6a ^{null}	49	28	36	18	57	76	19	58	75
Gpm6b ^{null}	57	43	43	12	64	84	16	59	79
dKO	53	23	30	38	38	50*	15	60	80

A chi-square pair wise comparison of the distributions of the cortical neurons regarding their status of being collapsed or non-collapsed under the different conditions was performed (Table 5). When comparing the reaction between the control situation and the standard ephrinA5 dose (1 µg/ml) it is clear that there is a very highly significant difference in the wild-type, Gpm6a^{null} and Gpm6b^{null} null mutant cortical neurons. Most of their growth cones do react to the ephrinA5 collapse induction. The dKO neurons react, but to a much lesser extend to this collapse. Moreover there is no alteration when comparing the responsiveness between the two concentrations of ephrinA5 (1 µg/ml Vs 2 µg/ml) in the wild-type, Gpm6a^{null} and Gpm6b^{null} single-null mutant cortical neurons. However there is a very highly significant difference in the Gpm6a^{null}*Gpm6b^{null} cortical neurons. Most of the axonal growth cones require the higher ephrinA5 dose to respond with an extensive collapse reaction (50 % of collapsed Vs 80 % of collapsed).

Table 5. Chi-square comparison of the growth cone collapse assay induced by ephrinA5.

Growth cone collapse assay performed on 2 DIV cultured WT, Gpm6a^{null}, Gpm6b^{null} and dKO cortical neurons from E17 mice. Chi-square pair-wise comparison (n = 3 per genotype; each ≥ 25 neurons) of ephrinA5 response at 1 µg/ml and 2 µg/ml. dKO neurons required a two-fold increased dose of ephrinA5 to achieve a response comparable to wild-type, Gpm6a^{null} and Gpm6b^{null} cortical neurons. The P-value is shown and in parenthesis the Pearson Chi-Square statistic with the degrees of freedom as subscript.

	Ctrl Vs EphrinA5 [1 µg/ml]	EphrinA5 [1 µg/ml] Vs [2 µg/ml]
WT	8.999 · 10 ⁻⁴ (11.625 ₁)	0.267 (1.599 ₁)
Gpm6a ^{null}	8.592 · 10 ⁻⁷ (24.215 ₁)	1.000 (0.009 ₁)
Gpm6b ^{null}	4.220 · 10 ⁻⁸ (29.284 ₁)	0.539 (0.487 ₁)
dKO	0.013 (6.733 ₁)	1.542 · 10 ⁻⁴ (14.914 ₁)

The result of this experiment is summarized in the diagram bar of figure 17. There is a notable difference in the behaviour of the Gpm6a^{null}*Gpm6b^{null} cortical neurons towards the growth cone inducing agent ephrinA5. These neurons require a much higher dose to achieve comparable results as the wild-type and the Gpm6a^{null} and Gpm6b^{null} single-null mutant cortical neurons.

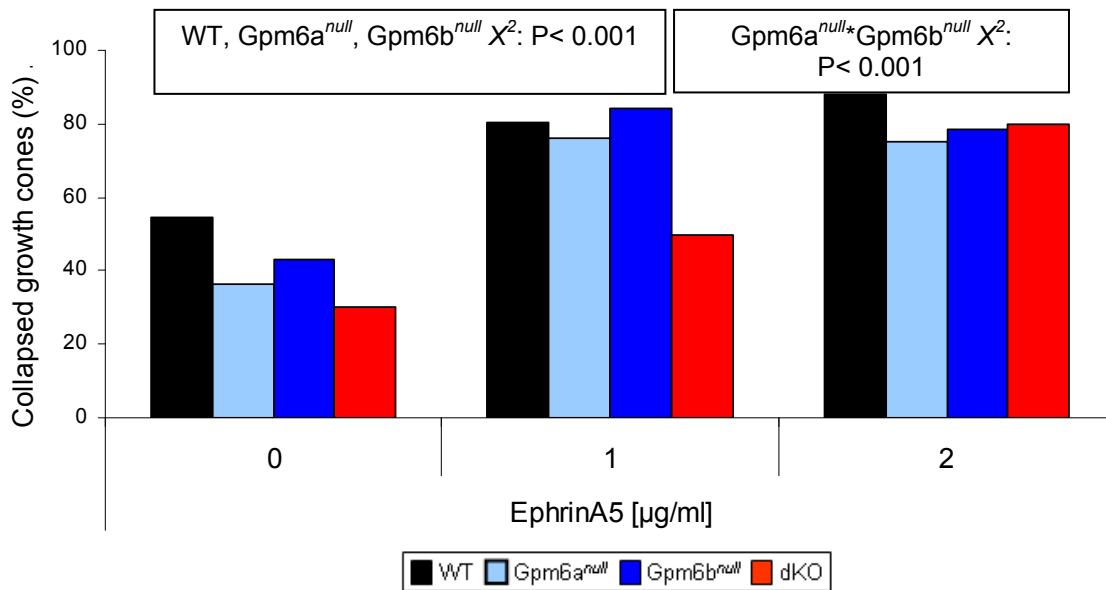


Figure 17. Responsiveness to ephrinA5 induced growth cone collapse assay (diagram)

WT, Gpm6a^{null}, Gpm6b^{null} and dKO cortical neurons from E17 mice were cultured and after 2 DIV a “growth cone collapse assay” with ephrinA5 was performed and assessed on the axonal growth cone (n = 3). dKO-neurons required a two-fold increased dose of ephrinA5 to achieve a response comparable to wild-type, Gpm6a^{null} and Gpm6b^{null} cortical neurons.

Examining the control group, there is a significant difference regarding the axonal growth cones. As the non-collapsed growth cone has been defined as the presence of a lamellipodium, one can observe that the dKO as well as the Gpm6a^{null} cortical neurons have significantly more growth cones with lamellipodia than the wild-type or the Gpm6b^{null} cortical neurons (Table 6).

Table 6. Abundance of axonal growth cones with lamellipodia.

WT, Gpm6a^{null}, Gpm6b^{null} and dKO cortical neurons from E17 mice were cultured and after 2 DIV the presence or absence of a lamellipodium on the axonal growth cone (GC) was assessed. It is shown the percentage of axonal growth cones with a lamellipodium (GC + lamellipodium). dKO and Gpm6a^{null} cortical neurons have more axonal growth cones with a lamellipodium than wild-type or Gpm6b^{null} cortical neurons. Chi-square pair wise comparison of the distribution of frequencies relative to wild-type neurons (n=3 animals per genotype; each ≥ 25 neurons), shown the Pearson χ^2 statistic (Pearson χ^2), the degrees of freedom (df) and the P-value (P).

	GC + lamellipodium (%)	χ^2 : WT Vs		
		Pearson χ^2	df	P
WT	45			
Gpm6a ^{null}	64	5.135	1	0.034
Gpm6b ^{null}	57	2.337	1	0.130
dKO	70	9.880	1	0.003

The difference between the Gpm6a^{null} and the WT is significant (P = 0.0034) and it is highly significant between the Gpm6a^{null}*Gpm6b^{null} cortical neurons and the wild-types (P = 0.003). There is no significant difference when comparing the other groups. This result demonstrates that in the absence of the neuronal proteolipid protein M6A (Gpm6a^{null} and Gpm6a^{null}*Gpm6b^{null}) the axonal growth cones of their cortical neurons show a significantly increased abundance in lamellipodia. And this effect is increased when the ortholog M6B is as well absent.

This result is schematized in the following bar diagram (Fig. 18).

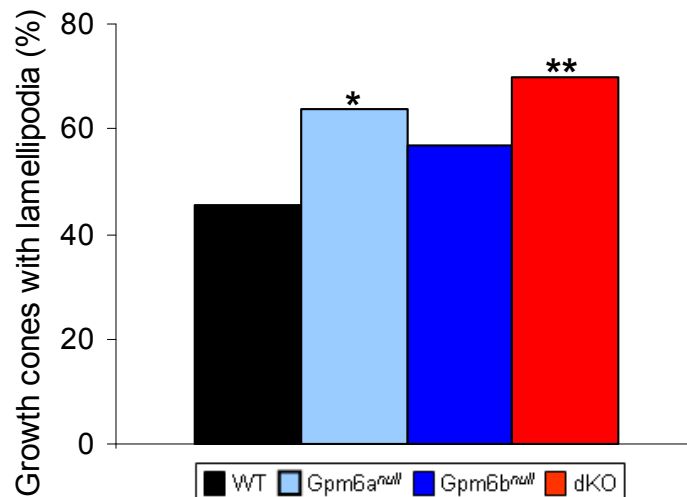


Figure 18. Abundance of axonal growth cones with lamellipodia.

WT, Gpm6a^{null}, Gpm6b^{null} and dKO cortical neurons from E17 mice were cultured and after 2 DIV the presence or absence of a lamellipodium on the axonal growth cone was assessed. In comparison to wild-type or Gpm6b^{null}, Gpm6a^{null} and dKO cortical neurons have significantly more (*) and highly significantly more (**) axonal growth cones with a lamellipodium, respectively. Significance according to chi-square test (n = 3).

The increased number of neuronal growth cones regarding the presence of lamellipodia points once more to a role of M6 proteins in the normal morphology and function of neuronal growth cones.

To further explain the observed altered behaviour of the Gpm6a^{null*}Gpm6b^{null} cortical neurons regarding the ephrinA5 induced growth cone collapse assay, immunoblot analysis was performed on cortical neuron lysates at 2 DIV (from E17 embryos). It was tested whether ephexin-1 levels were altered. Ephexin-1 levels are in relationship with the abundance of Eph receptors (see section 2.1.2., reviewed by Egea & Klein, 2007). This simplified the approach to test if the abundance of Eph-receptors were altered, as ephrinA5 binds to EphA1-8 as well as EphB2 (reviewed by Pasquale, 2004).

As can be observed on figure 19, the preliminary result of the immunoblot performed on the lysates of wild-type and Gpm6a^{null*}Gpm6b^{null} cortical neurons show a decreased abundance of ephexin1 in the Gpm6a^{null*}Gpm6b^{null} cortical neurons. This would argue for a decreased overall level of Eph-receptors in the dKO neurons, a likely explanation why these dKO neurons have an impaired response to the ephrinA5 induced growth cone collapse.

Another downstream event to investigate was the levels of RhoA. RhoA is the key signalling molecule when referring to growth cone collapse (Wahl *et al.*, 2000; reviewed in Hall & Lalli, 2010). Upon its activation, it leads to collapse of the actin filaments. In the dKO cortical neuron lysates, the abundance of RhoA is slightly decreased. The lower levels would argue for less total cellular RhoA, regardless of its activation status. A lower abundance of RhoA may explain the delayed reactivity of the dKO cortical neurons towards ephrinA5.

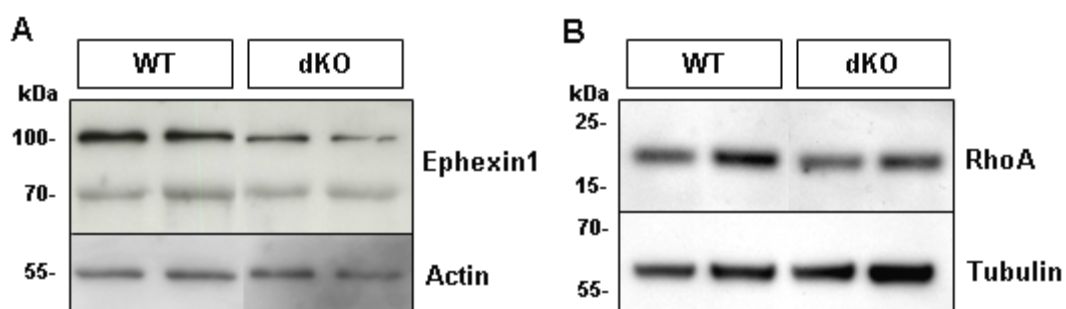


Figure 19. Immunoblot of cortical neuron lysates.

WT and Gpm6a^{null*}Gpm6b^{null} cortical neurons from E17 mice were cultured and lysed after 2 DIV (n = 2 - 3).

A) Immunoblot showing the levels of ephexin-1 and actin as a loading control. It seems that in the dKO cortical neuron lysates the abundance levels of ephexin1 are decreased.

B) Immunoblot against total RhoA with tubulin as a loading control. The RhoA abundance levels seem to be moderately decreased in the dKO cortical neuron lysates.

The immunoblot demonstrates the importance of neuronal M6 proteolipid proteins in the proper function of the growth cone and its associated cytoskeleton proteins as well as the appropriate abundance (and possibly localization) of signalling receptors including Ephs.

4.1.6. Impaired neurite outgrowth in the absence of M6 proteins

Previous results have shown that upon application of the monoclonal M6 antibody against M6A there was a reduced neurite outgrowth of cultured cerebellar wild-type neurons (Lagenauer *et al.*, 1992).

To test if a similar effect exists in the chronic absence of this protein, as well as of the homologue M6B, primary cortical neurons of E15 mice were cultured for 3 DIV to assess their neurite length. This experiment was performed on wild-type, $Gpm6a^{null}$, $Gpm6b^{null}$ and $Gpm6a^{null*}Gpm6b^{null}$ cortical neurons (Fig. 20, with 4 individuals per genotype and three technical replicates each (34 - 47 neurons per individual)).

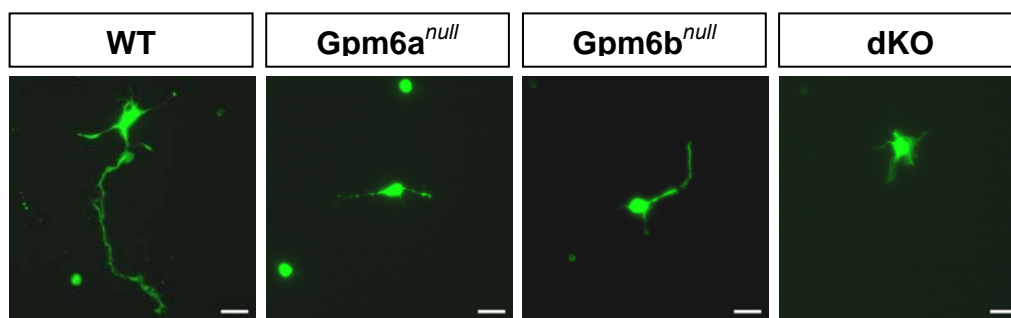


Figure 20. Impaired neurite outgrowth of M6 mutant cortical neurons.

WT, $Gpm6a^{null}$, $Gpm6b^{null}$ and dKO cortical neurons from E15 mice were cultured and after 3 DIV the neurites were immunostained with the antibody Tuj1. Representative examples for each genotype. Scale bar = 25 μ m.

The resulting data (Table 7) show a decreased neurite length in the cortical neurons lacking M6. A two-sided T-test was performed, and the resulting P-values demonstrate a very highly significant and decreased neurite length of the $Gpm6a^{null}$, the $Gpm6b^{null}$ and the $Gpm6a^{null*}Gpm6b^{null}$ cortical neurons in comparison to the wild-types. $Gpm6a^{null}$ and $Gpm6a^{null*}Gpm6b^{null}$ neurites are also significantly shorter than those of $Gpm6b^{null}$ cortical neurons. This shows that the $Gpm6b^{null}$ cortical neurons are affected in their neurite outgrowth by themselves, though more moderately.

Table 7. Impaired neurite outgrowth of M6 mutant cortical neurons.

WT, Gpm6a^{null}, Gpm6b^{null} and dKO cortical neurons from E15 mice were cultured and after 3 DIV the neurite length was measured according to the Tuj1 immunocytochemistry. It is exhibited the mean neurite length (Neurite length, in μm) and the P-value for the two-sided T-test for the different comparisons. The neurites of Gpm6a^{null}, Gpm6b^{null} and dKO cortical neurons are shorter than those of the wild-type. Additionally the neurites of the Gpm6a^{null} and dKO cortical neurons have a decreased length in comparison to the Gpm6b^{null} cortical neurons (n = 4, 3 technical replicates each, 163 - 183 cells were quantified per genotype). Shown T statistic with the degrees of freedom as subscript, and the P-value.

	Neurite length (μm)	P-value for T-test		
		WT	Gpm6a ^{null}	Gpm6b ^{null}
WT	235.253			
Gpm6a ^{null}	102.265	15.375 ₂₄₀ , $1.337 \cdot 10^{-37}$		
Gpm6b ^{null}	138.367	10.010 ₃₀₉ , $1.287 \cdot 10^{-20}$	-5.162 ₃₁₇ , $4.330 \cdot 10^{-7}$	
dKO	98.534	15.989 ₂₃₂ , $2.756 \cdot 10^{-39}$	0.701 ₃₅₉ , 0.484	5.796 ₃₀₅ , $1.689 \cdot 10^{-8}$

Figure 21 shows a bar diagram of the mean neurite length of the four genotypes and the resulting significance levels according to the T-test. Categorizing the neurons regarding their neurite length allows a chi-square pair-wise comparison of all the distributions (Table 8) and this reveals a significantly different frequency distribution of the neurite length of any genotype against any other.

Table 8. Impaired neurite outgrowth of M6 mutant cortical neurons.

WT, Gpm6a^{null}, Gpm6b^{null} and dKO cortical neurons from E15 mice were cultured and after 3 DIV the neurite length was measured according to the Tuj1 immunocytochemistry. It is represented the P-value for the chi-square test and in parenthesis the Pearson χ^2 statistic and the degrees of freedom as subscript. There is a significant difference in the frequency distribution of the neurite length of every genotype towards every other.

	WT	Gpm6a ^{null}	Gpm6b ^{null}
Gpm6a ^{null}	$5.919 \cdot 10^{-30}$ (157.281 ₈)		
Gpm6b ^{null}	$1.161 \cdot 10^{-14}$ (83.098 ₈)	$4.960 \cdot 10^{-5}$ (31.532 ₇)	
dKO	$2.816 \cdot 10^{-33}$ (173.152 ₈)	0.025 (12.787 ₅)	$1.159 \cdot 10^{-6}$ (40.188 ₇)

The following diagrams show the mean neurite length for each genotype and the resulting significance levels after the T-test (Fig. 21A) and the categorized distribution of the cortical neurites of each genotype along nine categories (Fig. 21B).

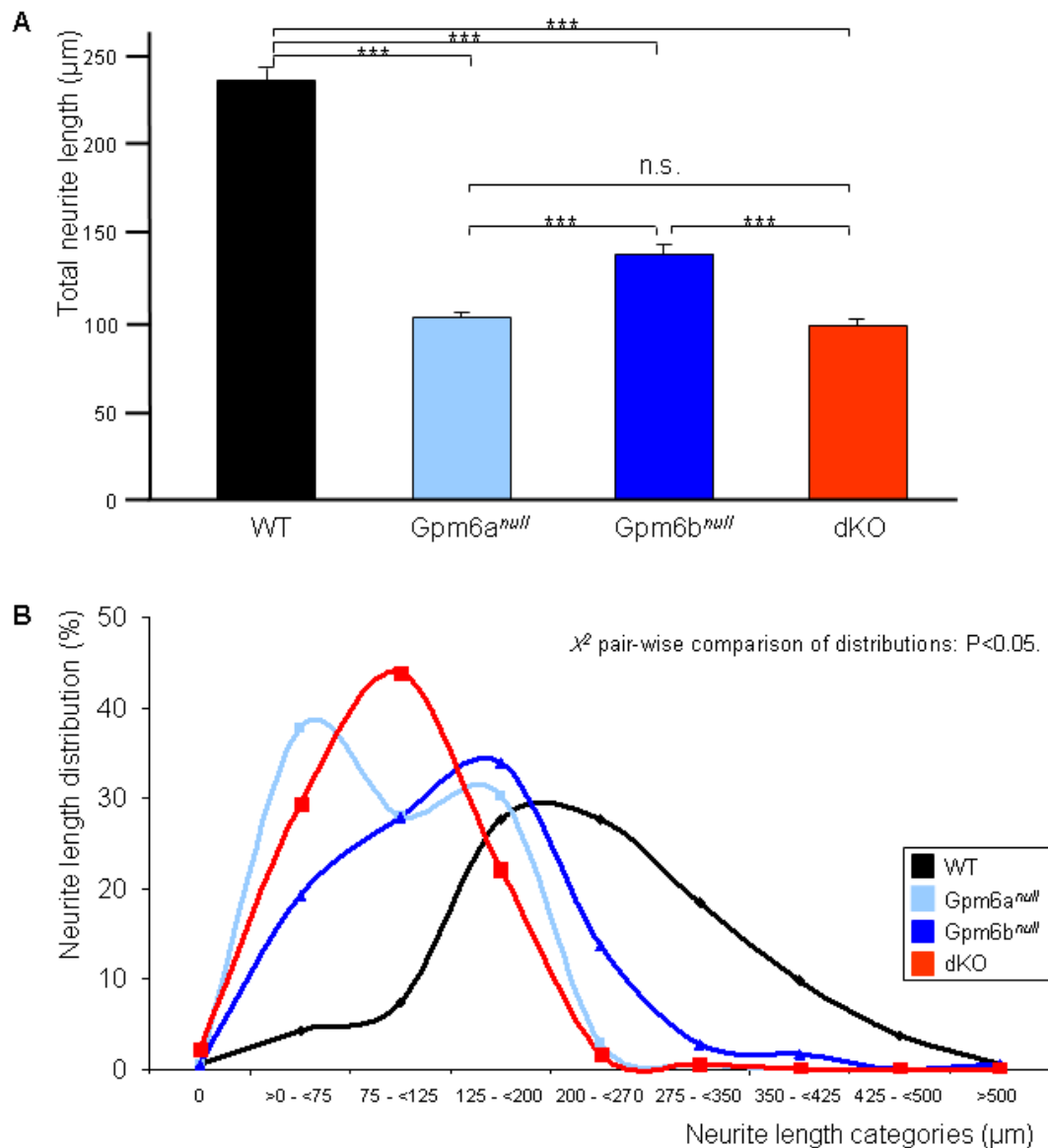


Figure 21. Impaired neurite outgrowth in M6 deficient cortical neurons.

A. Total neurite length analysis (mean \pm SEM), showing a reduced neurite length as indicated (***) = $P < 0.001$, T-test). $n = 4$ animals; 3 technical replicates per genotype.

B. Neurite length distribution in the four genotypes. χ^2 pair-wise comparison determined a significantly different distribution of the neurite length between all genotypes ($P < 0.05$).

The reduced neurite outgrowth displays the requirement of the neuronal M6 proteolipid proteins in this process. The absence of M6B already induces a very significant decrease in the neurite length. However, the lack of M6A has even more drastic consequences. Thus, this evidence suggests that M6 proteins have an important role in the normal neuronal development, including neurite extension.

4.1.7. Neurite outgrowth and cholesterol

As demonstrated above, neurons that lack M6 proteins do have impaired neurite outgrowth. It has been proven before that the oligodendroglial proteolipid protein PLP, ortholog to M6A and M6B, binds directly to cholesterol (Simons *et al.*, 2000; Krämer-Albers *et al.*, 2006). And this has also been shown for M6B (Werner H., pers. comm.).

Cholesterol is essential for the proper neuron function, like e.g. for the maintenance of the plasma membrane itself, for locating ion channels and signalling proteins into lipid rafts, and for the functionality of the synaptic machinery (reviewed in Benarroch, 2008). To assess if there is a relationship between the neuronal proteolipids in their function related to neurite outgrowth and cholesterol, primary cortical neurons were cultured under different concentrations of cholesterol. Wild-type and Gpm6a^{null*}Gpm6b^{null} cortical neurons of E15 mice were cultured for 3 DIV. The experiment was performed with four embryos per genotype and three technical replicates per condition, resulting in 38 - 36 neurons evaluated per animal. The applied cholesterol concentrations were: 0 µg/µl, 0.1 µg/µl and 1 µg/µl of cholesterol and the neurite length was measured.

As depicted in table 9, wild-type cortical neurons show a clear decrease in their neurite outgrowth length once the cholesterol concentration is above 0.1 µg/µl, and this decrease augments with an increasing dose (1 µg/µl). This is in congruence with prior results (Ko *et al.*, 2005) and also shows how critical cholesterol amounts are for proper neuronal function.

It was surprising to observe that the dKO cortical neurons do not react to the modified cholesterol concentrations. They do have a significant reduction in their neurite length *per se* (as proven before), but this stays unaltered and at the same magnitude, no matter the different concentrations of cholesterol. Nonetheless, wild-type neurons have significantly larger neurites than dKO neurons under these conditions.

Table 9. Neurite outgrowth in cortical neurons upon cholesterol application.

E15 mice cortical neurons were cultured for 3 DIV under different cholesterol concentrations and were stained with Tuj1. The neurite outgrowth was measured.

A) Mean neurite length of WT and dKO cortical neurons under the different cholesterol concentrations.

b) Statistical outcome of a T student test, showing the T statistic with the degrees of freedom as subscript, and the P-value.

A

Mean neurite length (μm)		
	WT	dKO
0 $\mu\text{g/ml}$	146.817	77.331
0.1 $\mu\text{g/ml}$	136.822	86.685
1 $\mu\text{g/ml}$	112.580	84.041

B

T-test				
Vs Genotype		Vs Cholesterol concentration		
	WT Vs dKO		WT	dKo
0 $\mu\text{g/ml}$	7.930 ₃₁₈ , $3.746 \cdot 10^{-14}$	0 $\mu\text{g/ml}$ Vs 0.1 $\mu\text{g/ml}$	1.061 ₃₄₆ , 0.289	-1.319 ₃₅₇ , 0.188
0.1 $\mu\text{g/ml}$	6.358 ₃₄₂ , $6.548 \cdot 10^{-10}$	0 $\mu\text{g/ml}$ Vs 1 $\mu\text{g/ml}$	3.694 ₃₄₀ , $2.573 \cdot 10^{-4}$	-0.932 ₃₅₄ , 0.352
1 $\mu\text{g/ml}$	3.654 ₃₄₄ , $2.989 \cdot 10^{-4}$	0.1 $\mu\text{g/ml}$ Vs 1 $\mu\text{g/ml}$	2.868 ₃₅₁ , $4.387 \cdot 10^{-3}$	0.368 ₃₅₄ , 0.713

The figure 22 exposes this clear effect: the neurite length of wild-type cortical neurons decreases upon increasing the cholesterol concentrations, and the dKO cortical neurons behave unaltered, preserving their anyway significantly reduced neurite length.

This result demonstrates that neuronal M6 proteins interact directly or indirectly with cholesterol and this relates to their involvement in neurite outgrowth. The lack of M6 proteins makes cortical neurons not respond in the normal manner, which would mean a reduction in their neurite extension capacities, but it seems to make them indifferent to an increasing cholesterol concentration.

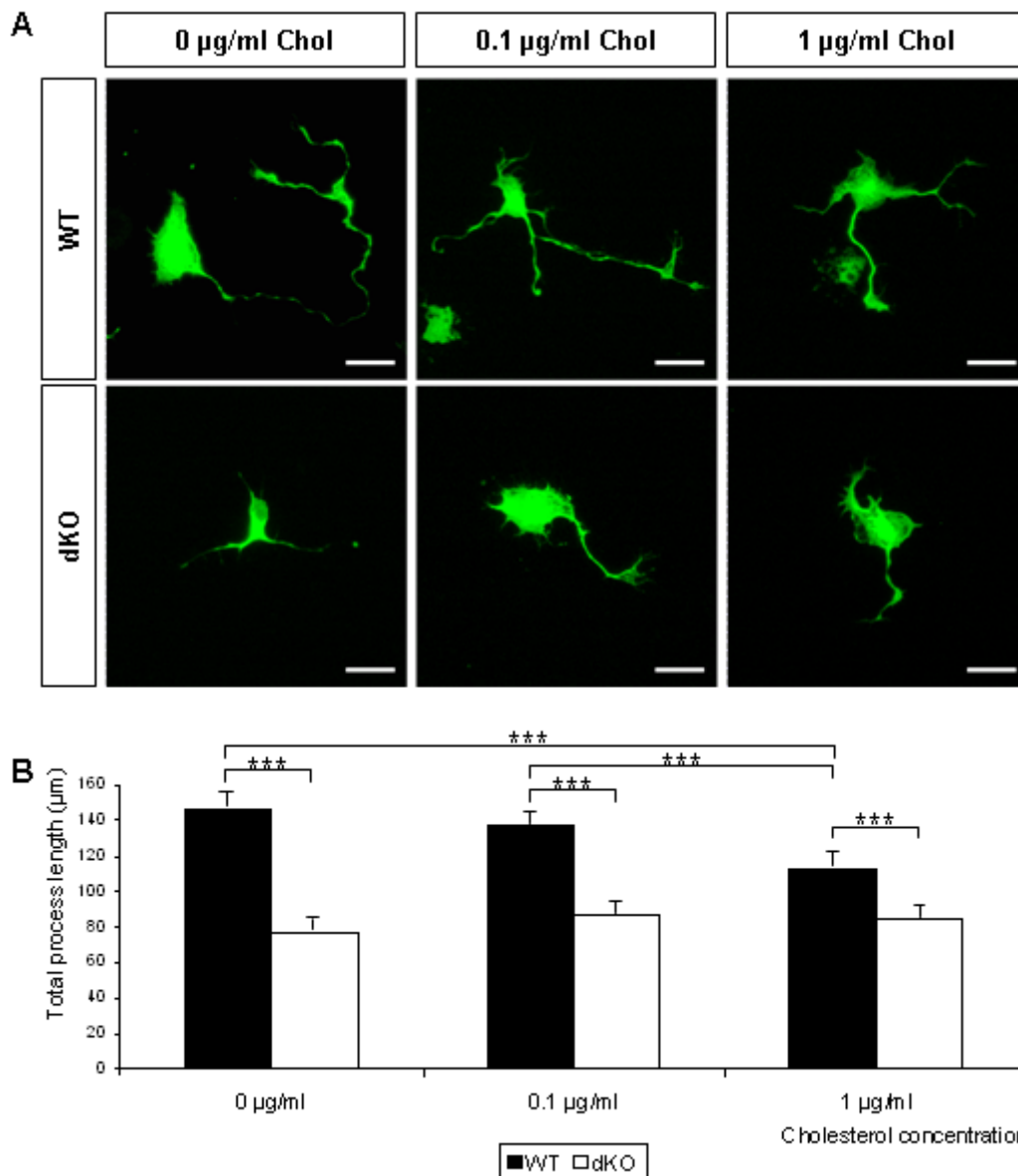


Figure 22. Neurite outgrowth of cortical neurons upon cholesterol application.

E15 mice cortical neurons were cultured for 3 DIV under different cholesterol concentrations and were immunostained with Tuj1. The neurite outgrowth was measured.

A) Representative images of WT and $\text{Gpm6a}^{\text{null}*}\text{Gpm6b}^{\text{null}}$ (dKO) cortical neurons under the different cholesterol concentrations. Scale bars = 20 μm .

B) Bar diagram representing the mean neurite length (with the SEM) of WT and dKO neurons in the different cholesterol concentration.

4.1.8. Growth cone morphology, adhesiveness and motility

An essential evaluation was to prove how the cortical neurons that lack M6 proteins do behave while being in culture, as the prior results demonstrated an altered behaviour of the neurons in their neurite outgrowth and in their growth cone function. Therefore, primary cortical neurons of E17 wild-type and $\text{Gpm6a}^{\text{null}*}\text{Gpm6b}^{\text{null}}$ mice were subjected to *in vivo* imaging after being cultured 2 DIV. The microscopy was performed on a confocal setup and

reflection microscopy was used. As M6 proteins seem to be especially important in the growth cone, the analysis focused on this structure. The individual growth cones were imaged during ten minutes and an image was acquired every three seconds, so that for every growth cones were 201 frames which were converted into a video (Fig. 23A). From the wild-type cortical neurons nine growth cones were imaged, and ten in the $Gpm6a^{null*}Gpm6b^{null}$ ones. The imaging acquisition was chosen to be of a period of ten minutes, as it had already been assessed that the $Gpm6a^{null*}Gpm6b^{null}$ cortical neurons have an impaired neurite extension, so that there would be no masking of the effect of the reduced neurite extension in their motility properties.

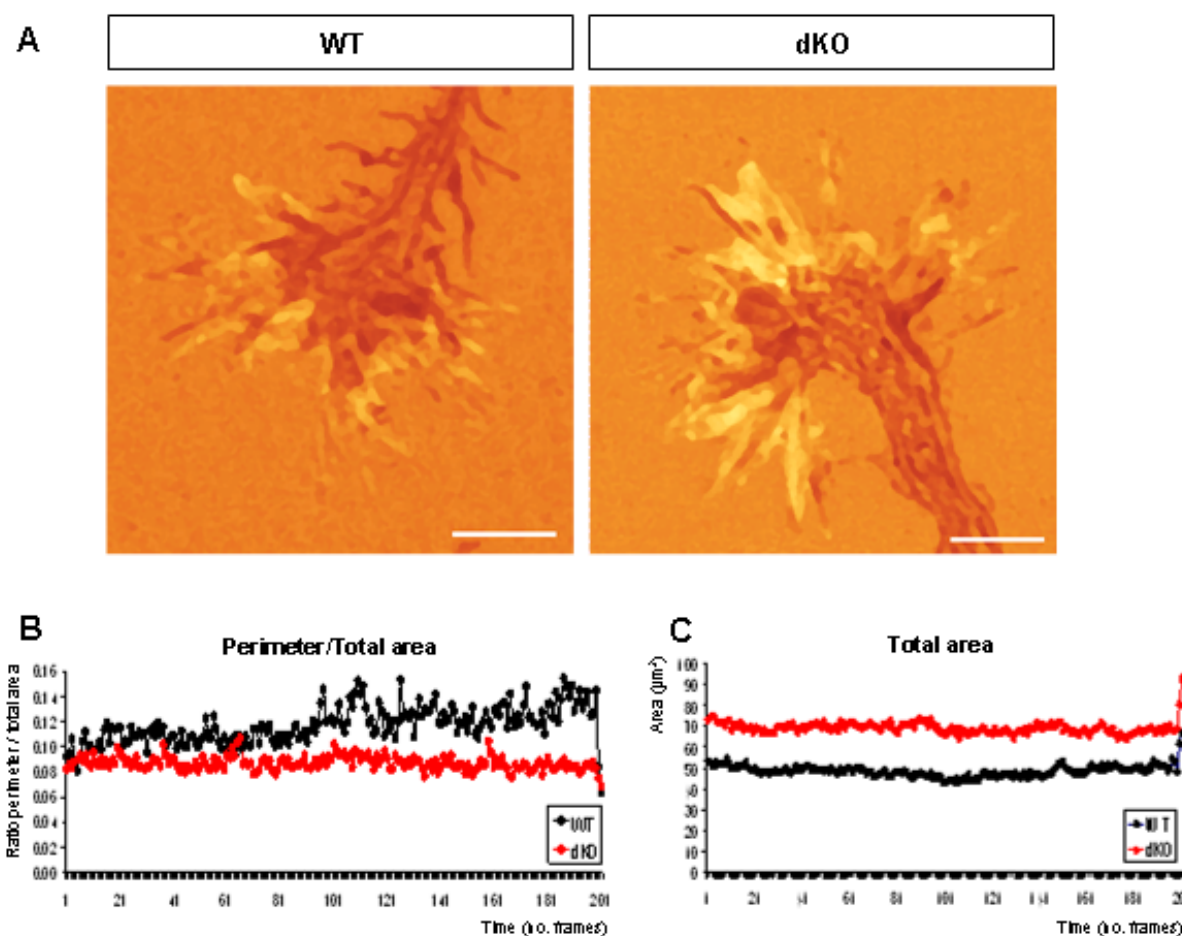


Figure 23. Morphometry of *in vivo* imaged cortical neuron growth cones.

A) Cortical neurons of E17 WT and $Gpm6a^{null*}Gpm6b^{null}$ (dKO) mice were cultured for 2 DIV. *In vivo* imaging of their growth cones during 10 min, performing one image every 3 seconds. Depicted is the first image for one growth cone of each genotype. Scale bars = 5 μ m.

B) Representation of the normalized mean ratio of the perimeter against the total area. No significant differences could be observed.

C) Representation of the normalized mean total area. No significant differences could be observed.

The first approach was to analyse the morphometrical properties. The perimeter of each growth cone in each frame was determined, as well as the total surface. When comparing the normalized values for the ratio of the perimeter against the total area (Fig. 23B), as well

as the total area *per se* (Fig. 23C), no difference could be assessed. This was proven by realizing an ANOVA with repeated measurements (Greenhouse-Geisser) (perimeter / total area: $F = 1.287$, $P = 0.287$; total area: $F = 0.411$, $P = 0.758$). Thus, growth cones of cortical neurons that lack M6 proteins do have the same morphometrical properties than wild-type ones.

Because of employing reflection microscopy, the various levels of attachment to the glass slide could be differentiated. Thereby, the following analysis was based on the different adhesion levels. The area of the growth cones was divided into “adhesive” and “non adhesive” according to the intensity levels on each single image (Fig. 24A). When performing the ratio of the normalized data of the “adhesion area” Vs the “non adhesion area” no differences could be proven (Fig. 24B, C). This was confirmed by means of an ANOVA with repeated measurements (Greenhouse-Geisser) (adhesion area / total area: $F = 1.150$, $P = 0.340$). Consequently, the adhesive properties are also not altered when analysing neuronal growth cones that lack chronically neuronal M6 proteins.

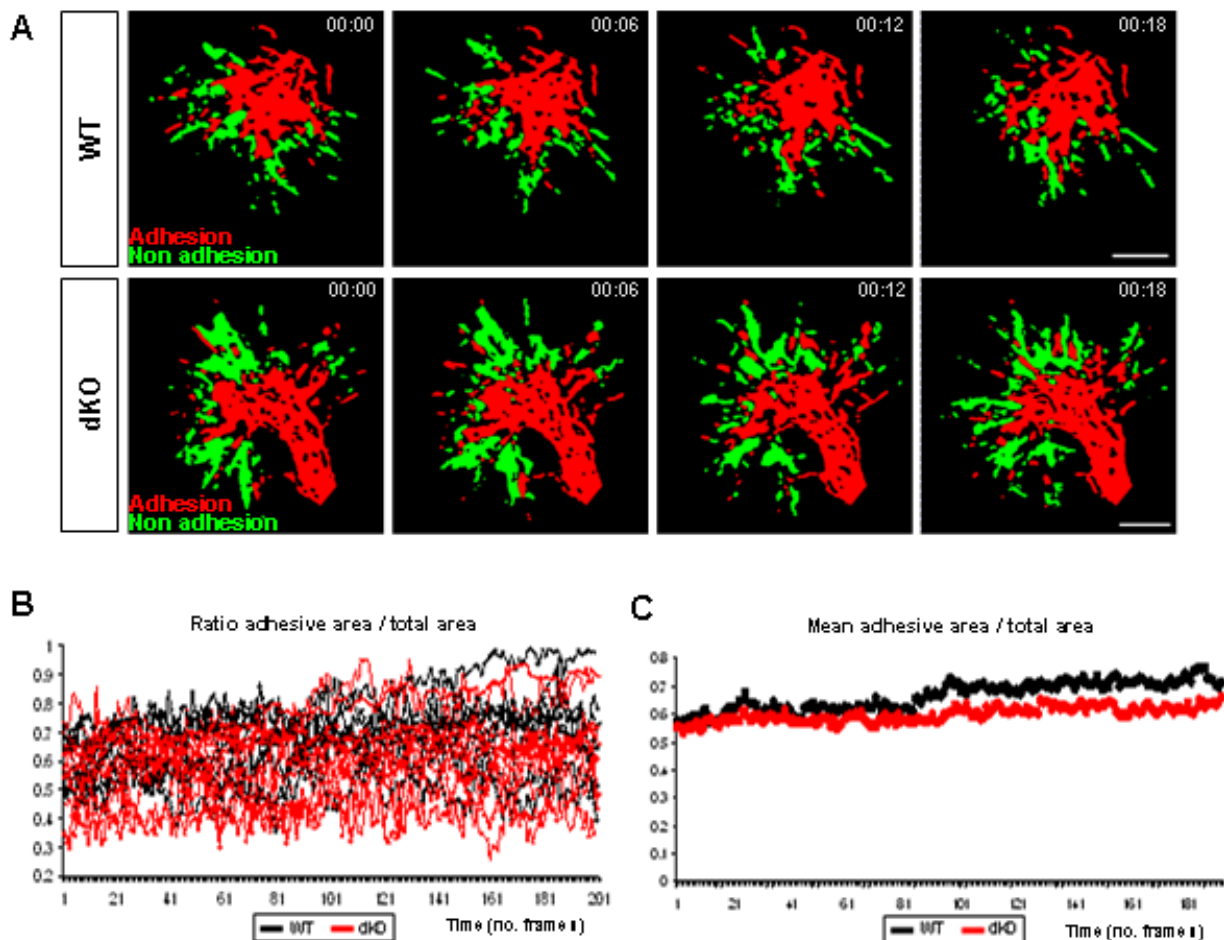


Figure 24. Adhesiveness of *in vivo* imaged cortical neuron growth cones (*cont.*)

Figure 24. Adhesiveness of *in vivo* imaged cortical neuron growth cones (cont.).

A) Cortical neurons of E17 wild-type and Gpm6a^{null*}Gpm6b^{null} (dKO) mice were cultured for 2 DIV. The growth cones were imaged *in vivo* during 10 min, achieving one image every 3 seconds. According to the intensity levels, the growth cone area was classified into “adhesion” (red) and “non adhesion” (green) areas. Depicted are four example images of each genotype, chosen every second frame from the first one on. The time passed is indicated on each image. Scale bars = 5 μ m.

B) Representation of the normalized ratio of the adhesive area against the total area. No significant differences could be observed.

C) Representation of the normalized mean adhesive area against the total area. No significant differences could be observed.

Furthermore, the examination of the videos was performed in such a manner that the motility of the growth cones could be investigated, as this is an essential factor of the growth cone functionality. Between each frame of each single video, the differences from one to the next frame were analysed in such a way that the extension and retraction areas could be assessed (See Fig. 7). As the areas occupied by the growth cone in one frame were subtracted from the prior one, extension was evaluated as values minor than zero and retraction as values larger than zero. If there would be no difference, the sum would be zero. When comparing the growth cones regarding the extension (Fig. 25A-B) and retraction (Fig. 25C-D) levels no differences could be observed between wild-type and Gpm6a^{null*}Gpm6b^{null}. This is obvious when observing the normalized mean alteration of the sum of the retraction and extension values (Fig. 25E), as it is basically identical for the growth cones of wild-type and Gpm6a^{null*}Gpm6b^{null} cortical neurons. Additionally, when plotting the normalized differences of retraction and extension (Fig. 25F) no differences could be observed. An ANOVA with repeated measurements (Greenhouse-Geisser) was performed and validated this (retraction + extension: $F = 0.992$, $P = 0.494$; retraction-extension: $F = 1.184$, $P = 0.286$). Yet again, there is no difference of the *in vivo* behaviour of the Gpm6a^{null*}Gpm6b^{null} cortical neuron growth cones. The way they retract and extend over a period of 10 minutes is equivalent.

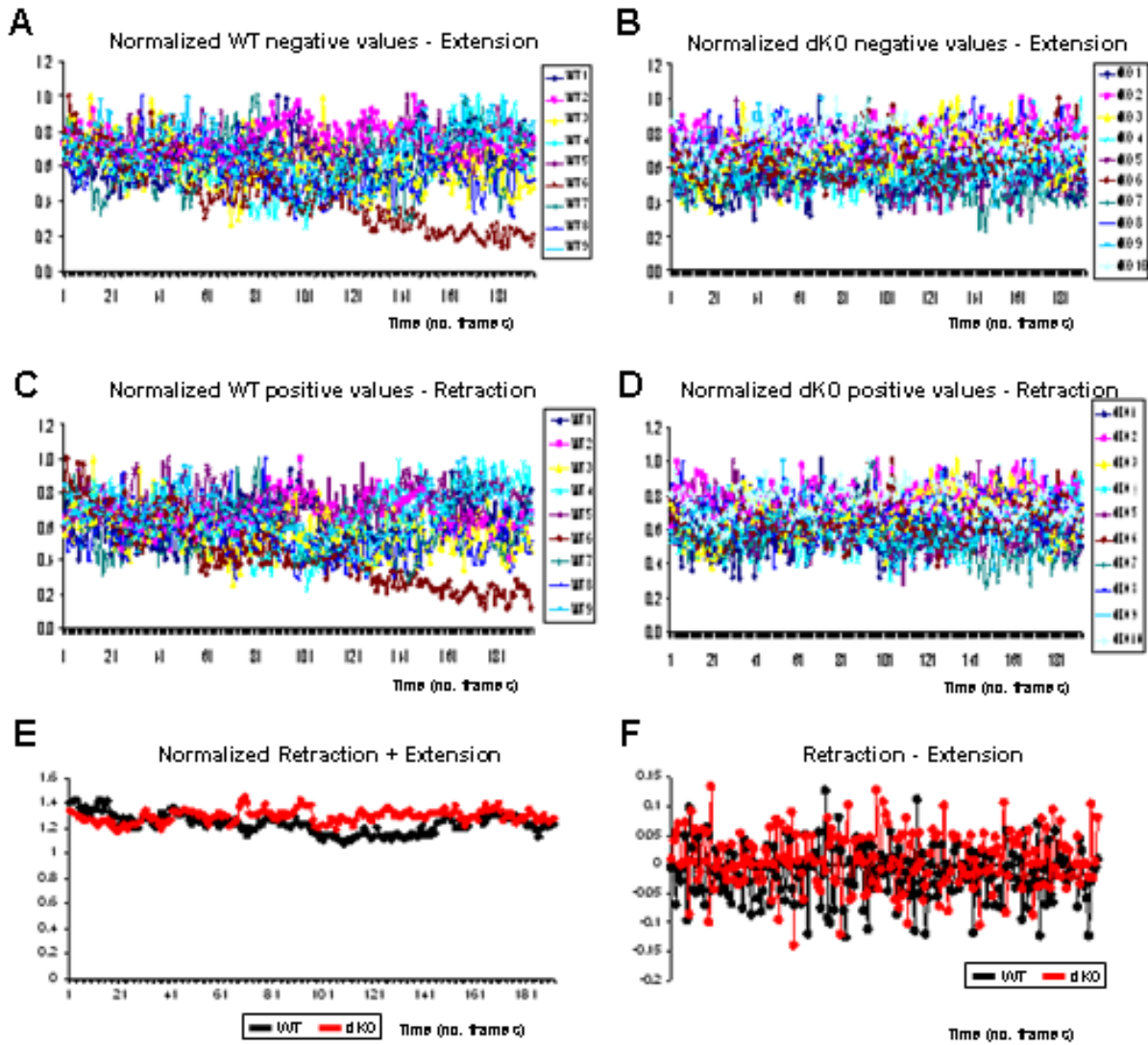


Figure 25. Motility of *in vivo* imaged cortical neuron growth cones.
 Cortical neurons of E17 WT and $Gpm6a^{null*}Gpm6b^{null}$ (dKO) mice were cultured for 2 DIV. Growth cones were imaged *in vivo* during 10 min, performing one image every 3 seconds. The differences in area occupied by the growth cone were assessed between each frame of each single video, by subtracting the occupied area of one frame with the prior one. Thereby positive values measure retraction and negative values measure extension. If there is no net movement, the value would be zero.
 A-B) Representation of the normalized extension values for WT (A) and dKO (B) growth cones.
 C-D) Representation of the normalized retraction values for WT (A) and dKO (B) growth cones.
 E) Representation of the normalized mean sum of the retraction and extension values in WT (black) and dKO (red) growth cones.
 F) Representation of the normalized levels of retraction and extension values in WT (black) and dKO (red) growth cones.

This *in vivo* analysis demonstrates that the short-term morphometry, adhesion and motility is not altered in the growth cones of $Gpm6a^{null*}Gpm6b^{null}$ cortical neurons.

4.1.9. Cortical development and corpus callosum width

The corpus callosum is the largest commissure of the brain that connects most cortical areas of each cerebral hemisphere (Kandel *et al.*, 2000). It was chosen for studying the possible *in vivo* consequences of the effect of the impaired neurite outgrowth and altered growth cone function proven before in cortical neurons that lack chronically neuronal M6 proteins.

Therefore, brains of P5 wild-type (n = 4) and $Gpm6a^{null*}Gpm6b^{null}$ (n = 5) mice were fixed and coronal sections were stained with HE and the width of the corpus callosum was measured. The examination was divided into two regions in the caudorostral axis: sections comprising the corpus callosum anterior to the hippocampus or sections including the corpus callosum and the hippocampus (Fig. 26).

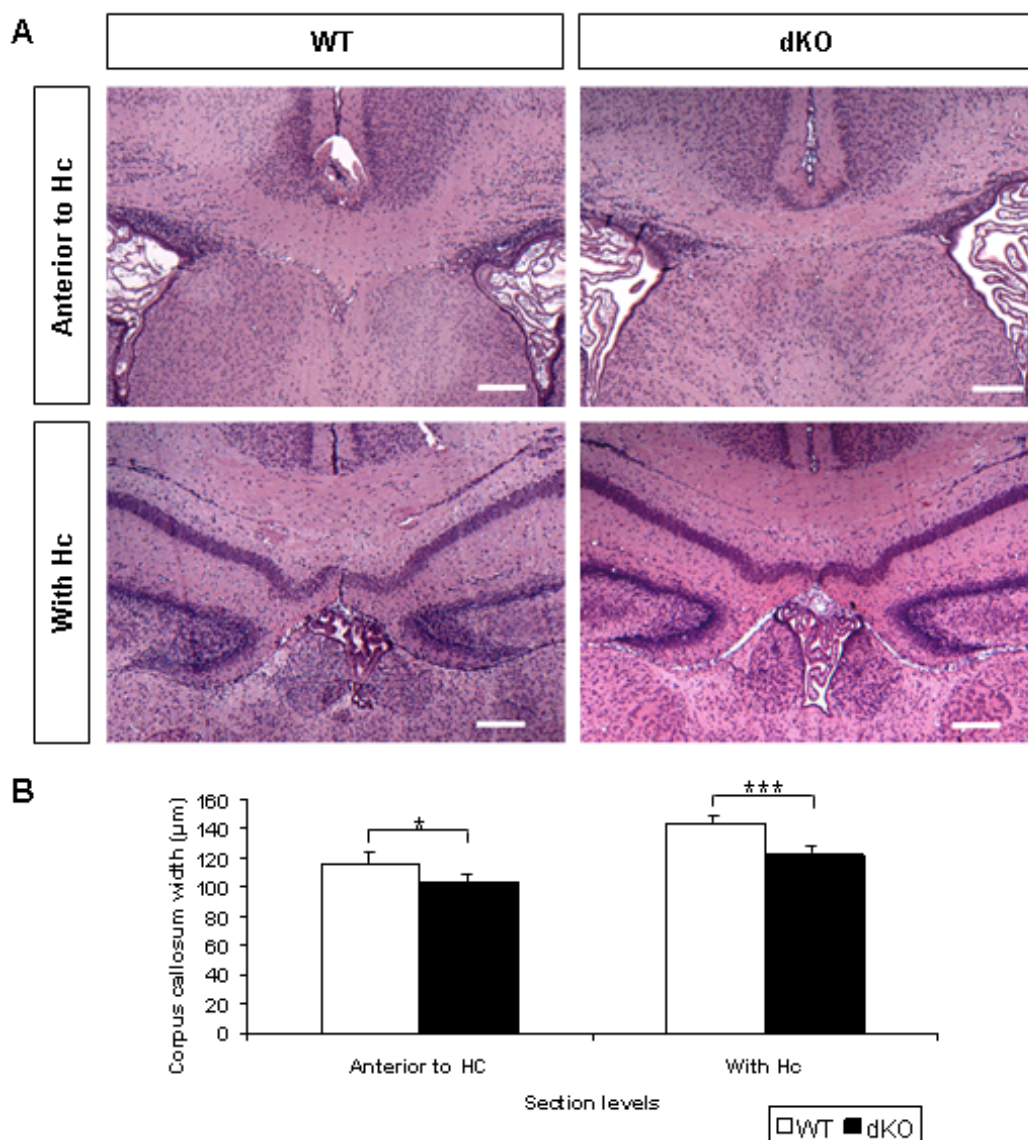


Figure 26. Reduced corpus callosum width at P5 in $Gpm6a^{null*}Gpm6b^{null}$ mice.

P5 brain sections of wild-type (WT) and $Gpm6a^{null*}Gpm6b^{null}$ (dKO) mice were stained with HE and the corpus callosum width was measured. It was differentiated between sections anterior to the hippocampus (Anterior to Hc) or comprising the hippocampus (With Hc).

A) Representative images of the corpus callosum for each genotype and each section level. Scale bar = 100 µm.

B) Bar diagram representing the mean corpus callosum width. The SEM is shown, as well as the levels of significance differences (*, $P < 0.05$; ***, $P > 0.001$) according to a student T-test.

The comparison between the two genotypes by means of a students T-test revealed a significant difference (Table 10), owing to a decreased corpus callosum width in the Gpm6a^{null*}Gpm6b^{null} mice. This occurred in both analyzed section levels and the differences were more significant in the brain levels that comprise the corpus callosum and the hippocampus.

Table 10. Decreased corpus callosum width at P5 in Gpm6a^{null*}Gpm6b^{null} mice.

P5 brain of wild-type (n = 4) and Gpm6a^{null*}Gpm6b^{null} (n = 5) mice were fixed, sectioned and stained with HE. The corpus callosum width was assessed in regions anterior to the hippocampus (Anterior to Hc) or in regions comprising the corpus callosum and the hippocampus (With Hc). Depicted is the mean corpus callosum width in μm , in parenthesis the number of counts per genotype and the T-statistic with the degrees of freedom as subscript. and the P-value.

	Mean corpus callosum width (μm)		Student T-test
	WT	dKO	
Anterior to Hc	116.300 (18)	102.727 (34)	2.285 ₄₀ , 0.028
With Hc	143.405 (15)	121.776 (21)	4.167 ₃₄ , 2.002 · 10 ⁻⁴

This proves that neurons lacking neuronal M6 proteolipid proteins provoke a deficient formation of the major white matter tract in the brain. According to prior experiments this developmental defect in neuronal projections seems to be compensated at P30 (Fünfschilling U., Werner H., pers. comm.), but further investigations will assess this into more detail.

Neuronal M6 proteolipid proteins are required for an efficient and normal development of axonal tracts in the white matter, as is the corpus callosum.

4.2. Tetraspanin2 in CNS myelination

4.2.1. Tetraspanin2 expression in myelin

As a first step to study the function of TSPAN2 in the CNS myelin, P75 old wild-type and PLP^{null} mice were perfused, their brains sectioned and immunostained using an antibody against TSPAN2 (Birling *et al.*, 1999). In wild-type brain sections the TSPAN2 antibody stains profusely white matter regions, containing myelin, like e.g. the corpus callosum or the striatum (Fig. 27). But on PLP^{null} mice sections, the TSPAN2 labelling reveals a much higher TSPAN2 abundance. This effect is found throughout the white matter tracts of the brain. Hence, it is in agreement with prior results obtained in immunoblots of CNS myelin-enriched fractions (Werner H., pers. comm.). This suggests that TSPAN2 could compensate for the

lack of PLP in its absence, as both are structurally similar tetraspan proteins found in CNS compact myelin.

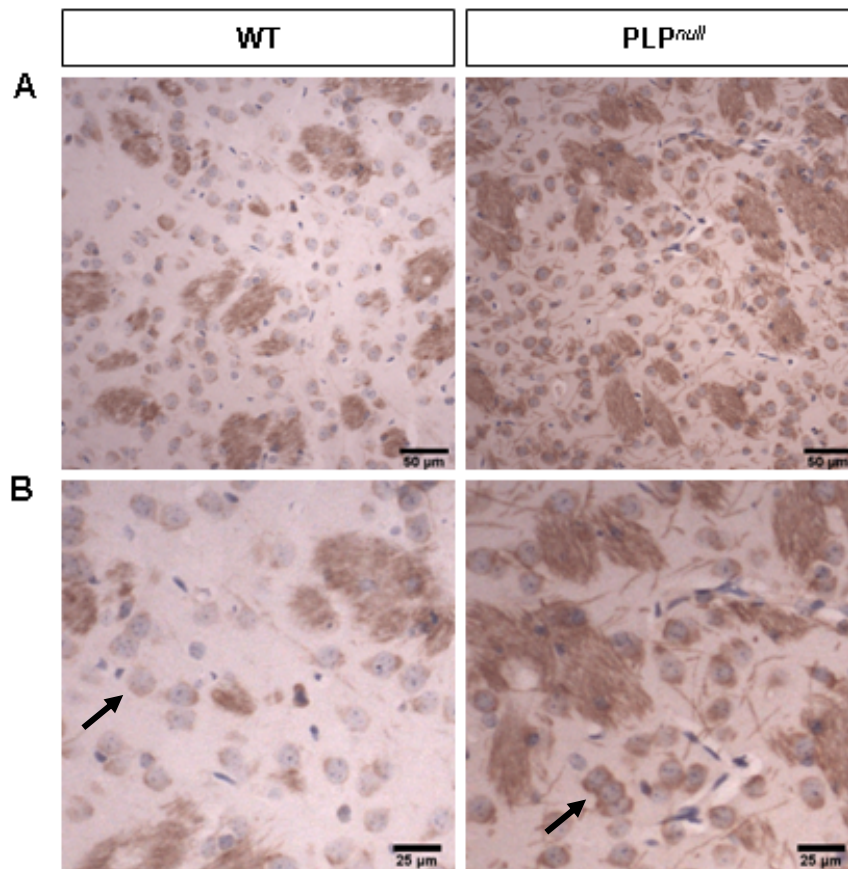


Figure 27. Tspan2 staining in the striatum of WT and PLP^{null} mice.

P75 brain sections of the striatum of WT and PLP^{null} mice were immunostained using a TSPAN2 antibody.

A) PLP^{null} mice have a higher abundance of TSPAN2 labelling. Scale bar = 50 μm .

B) Magnification of A, demonstrating that the increased TSPAN2 labelling in PLP^{null} mice is due to the more profound staining of the white matter bundles, as well as of the OL of the surrounding gray matter (arrow). Scale bar = 25 μm .

4.2.2. Targeted inactivation of the murine *Tspan2* gene

The early onset of the nervous system specific expression of TSPAN2 (Nielsen *et al.*, 2006; Dugas *et al.*, 2006), its distribution in CNS myelin (Birling *et al.*, 1999), as well as its high abundance in PLP^{null} myelin suggests that TSPAN2 is an important protein for CNS myelination and maintenance. To elucidate the function of TSPAN2 *in vivo*, the generation of conventional TSPAN2^{null} mice was pursued.

Briefly, to generate TSPAN2^{null} mice, the *Tspan2* gene had to be modified by homologous recombination of a *Tspan2* gene-comprising targeting vector in embryonic stem (ES) cells *in vitro*. ES cells that are positively targeted are microinjected into host blastocysts, and foster mothers will give rise to ES cell-chimeric mice. These chimeric mice can be distinguished by their spotted fur colour. When breeding chimeras with wild-type mice and with successful

germline transmission, the offspring will be heterozygous for the *Tspan2* gene (represented in Fig. 28).

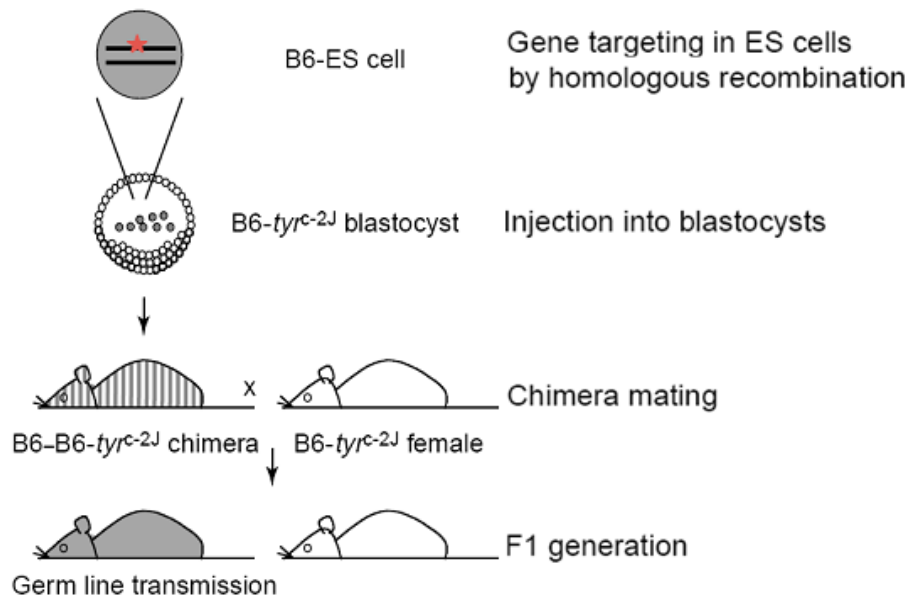


Figure 28. Generation of a C57BL/6 null-mutant mouse by gene targeting

The gene of interest is targeted by homologous recombination (star) in ES cells and these are injected into host blastocysts to produce ES cell–mouse chimeras. When using ES cells derived from C57 black B6 mice and injecting into host blastocysts derived from C57BL/6J-*Tyr^{c-2J}* albino mice, the chimeric offspring will be black-white patched. After breeding these chimeras with albino-C57 mice, the offspring after the germline transmission (F1 generation) will be black, representing the fur colour of the original ES cell (Taken from Seong *et al.*, 2004).

The targeting vector comprised three distinct regions (generated by de Monasterio Schrader P., Werner H. & others): (1) a 5' "short arm", homologous to part of the 5' UTR of the *Tspan2* gene as a template, flanked by XhoI/NotI restriction sites, (2) a neomycin resistance cassette flanked by two FRT sites, which gives upon its integration resistance to the neomycin-analogue G418 (essential for the ES cell positive-selection), and (3) a 3' "long arm" homologous to a sequence in intron 1 of the *Tspan2* gene, flanked by SbfI/Sac2 restriction sites. The vector backbone was the pCom-True (kindly provided by Schwab M.). The targeting vector proper sequence was verified by PCR and sequencing (data not shown). The gene targeting vector replaced most of the 5' UTR, the first coding exon, exon 1, and a large fragment of intron 1. This would, after homologous recombination, impede the *Tspan2* transcription, thereby giving rise to mice lacking TSPAN2.

Following scheme represents the gene targeting strategy followed (Fig. 29).

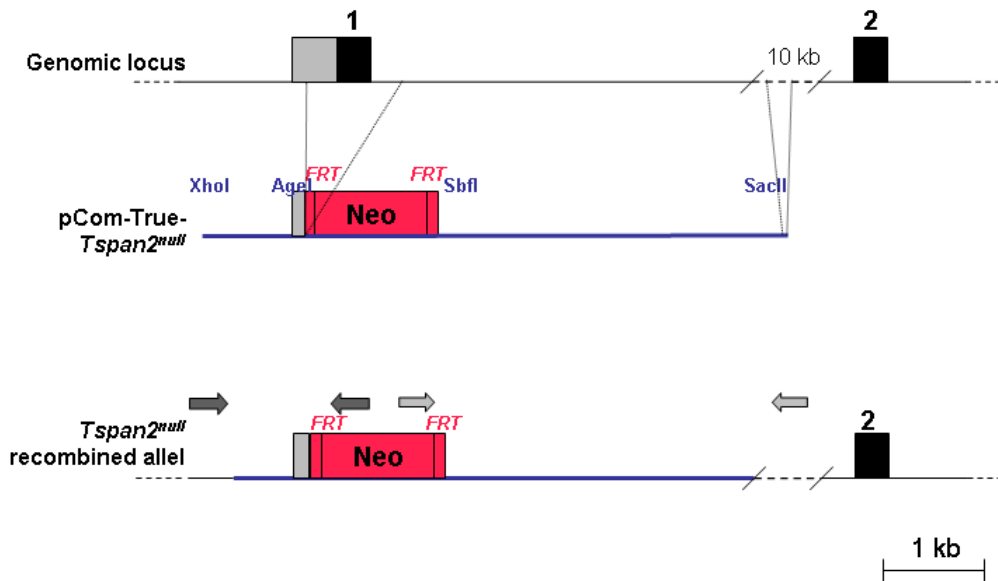


Figure 29. Targeting strategy to inactivate the murine *Tspan2* gene.

Genomic locus showing the 5' UTR (gray box) and the two exons (black box). The pCom-True-*Tspan2*^{null} targeting vector will excise at the 5' side part of the 5' UTR, and at the 3' it will target the large intron 1. Therefore, the *Tspan2*^{null} recombined allele will have a short initial segment of the 5' UTR followed by the neomycin resistance cassette. This will lead to no *Tspan2* transcripts. On the *TSPAN2*^{null} recombined allele are depicted primer locations that lead to identify homologous recombined ES cells (arrows). The PCR results for these are given in Fig. 30.

For the gene targeting, ES cells derived from C57BL/6 mice were used. This was a relative novel technique, as until recently most ES cells used for homologous recombination were derived from SV-129 mice. But the usage of C57BL/6-derived ES cells has several advantages. On one hand it is the reference strain for the mouse genome and thereby all further genetic investigations are facilitated. As well the C57BL/6 strain is the reference strain used in most biological investigations. And by using C57BL/6-derived ES cells, no backcrossing is necessary after germline transmission, which saves months of breeding, but also close to the insertion sites of the target vector there will be no different remaining sequences from the original ES cell strain (reviewed by Seong *et al.*, 2004). Therefore, C57BL/6-derived ES cells were chosen for the *Tspan2* gene inactivation.

Before the electroporation of the C57BL/6-derived ES cells, the targeted vector was linearized with ClaI. Nested PCR screening was performed to detect the ES cell clones containing the correct genomic target insertion. The “positive” clone (clone #5.3; 1 out of 48), where the gene targeted vector was inserted properly at the 5' and 3' ends of the *Tspan2* gene (Fig. 30A), was injected into C57BL/6J-*Tyrc-2J* albino derived blastocysts, which were carried out by foster mothers, and gave rise to chimeric offspring (Fig. 30B). By breeding the 33 resulting chimeras with C57BL/6 mice, germline transmission was achieved in two cases (mice #580, #590; 2 out of 352, Fig. 30C) in the F1 generation. These mice were heterozygous for the *Tspan2* gene (Fig. 31) and were bred to each other, to give rise to homozygous *TSPAN2*^{null} mice.

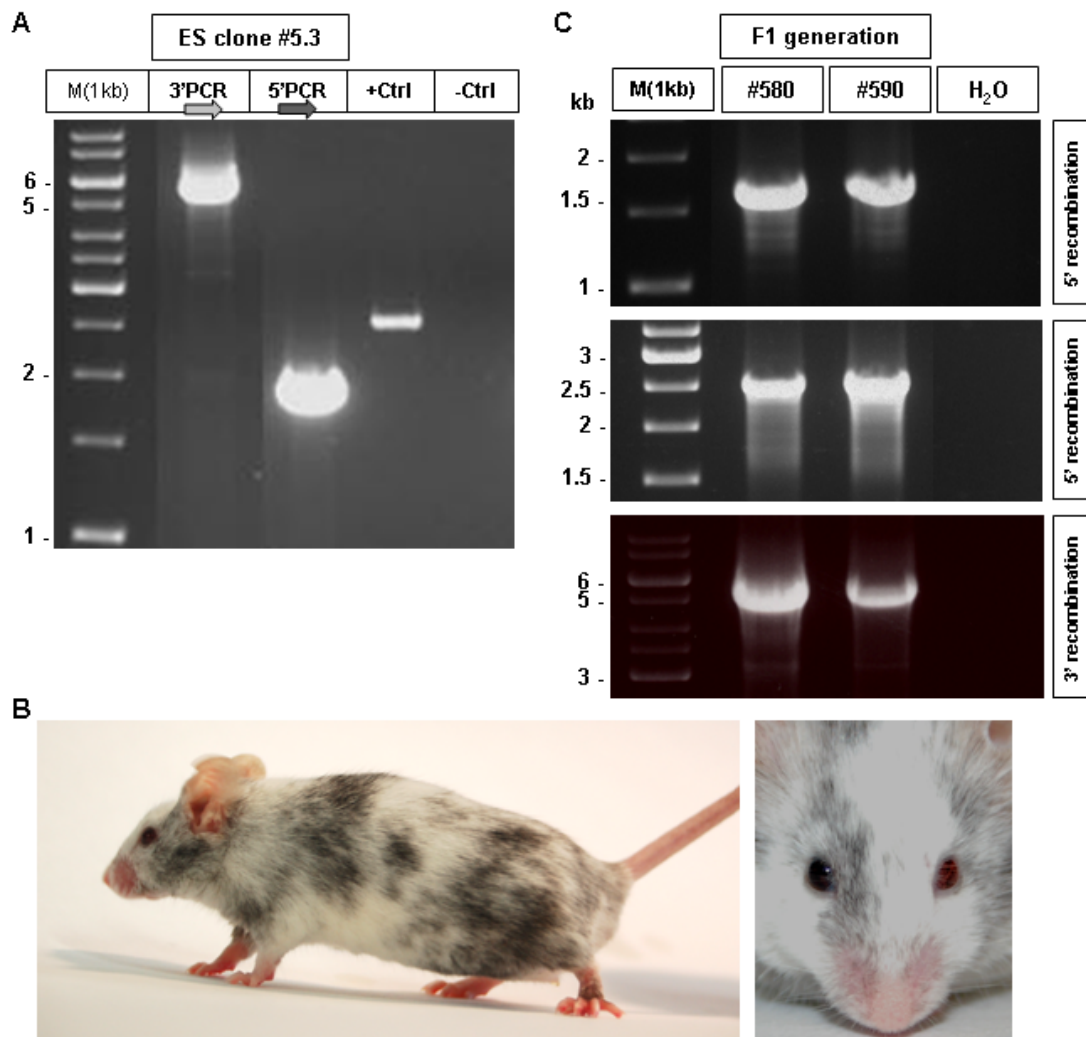


Figure 30. Homologous recombination and germline transmission after *Tspan2* gene targeting.
 A) PCR result of the ES clone #5.3 that showed a homologous recombination in the 5' end (5'PCR) and in the 3' end (3'PCR), the primer pairs are depicted in figure 29, a control vector was used as a positive control.
 B) Chimeric animals resulting from the injection of the homologous targeted clone #5.3 into C57BL/6J-*Tyrc-2J* albino derived blastocysts. Note the black-white patched colour, representing the mosaic genetic properties of the mouse.
 C) PCR results demonstrating the germline transmission in the F1 generation. The top two PCR results verify the 5' recombination, the lower one proves the 3' recombination. PCR performed on genomic DNA of the F1 offspring #580 and #590.

As could already be observed from the F2, and confirmed by the posterior breeding behaviour, the *TSPAN2^{null}* mice are good breeders and give rise to offspring with genotypes according to the Mendelian inheritance rules.

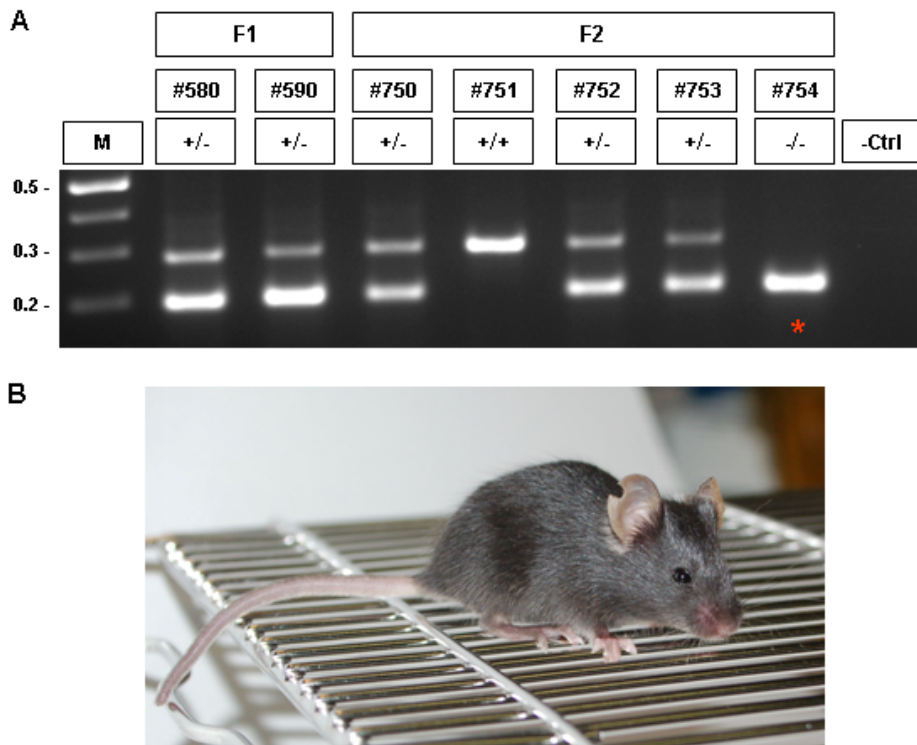


Figure 31. Germline transmission and first TSPAN2^{null} mouse.

A) Genotyping PCR on genomic DNA of the F1 and F2 generation, demonstrated the two heterozygous mice for the recombined *Tspan2* allele of the F1 (#580, #590) and their offspring, the F2. In the F2 appeared mice being homozygous for the wild-type allele (#751), heterozygous for the recombined allele (#750, #752, #753), and homozygous for the recombined allele (#754, star). This was the first complete TSPAN2^{null} mouse.

B) An image of the first TSPAN2^{null} mouse (#764, star on the PCR).

4.2.3. Characterization of TSPAN2^{null} mice

The TSPAN2^{null} mice breed normally, and have no obvious phenotypic abnormalities at least in the first 10 month of age. The fact that there is no obvious phenotype could probably be explained by some compensatory mechanism of other myelin tetraspanins.

To assess the absence of TSPAN2 protein in the TSPAN2^{null} mice, immunoblot of CNS-myelin enriched fractions was performed on P75 mice. The analysis included wild-type, TSPAN^{+/-}, TSPAN2^{null} and PLP^{null} mice. The TSPAN2 immunoblot revealed a clear band in the wild-type mice and, indeed, revealed no band in the TSPAN2^{null} mice (Fig. 32). This demonstrates that the TSPAN2^{null} mice do actually lack the TSPAN2 protein. There is a strong decrease in the intensity of the TSPAN2 band of the TSPAN^{+/-} mice, proving that the heterozygous mice do actually have reduced levels of TSPAN2. Confirming prior results, the levels of TSPAN2 were prominently increased in the PLP^{null} mice. CNP was used as a loading control, as no differences could be observed in the levels of the non-compact myelin protein CNP in these genotypes.

The immunoblot against PLP/DM20 demonstrated the expected absence in the PLP^{null} mice and similar levels in the wild-type and $TSPAN2^{null}$ mice. It seemed that in the $TSPAN2^{+/-}$ mice the levels of PLP/DM20 are reduced. CNP was used as a loading control and showed no differences. Surprisingly, there is an increase in the levels of MBP in the $TSPAN2^{null}$ mice. MBP is the second most abundant protein in compact CNS myelin (after PLP) and acts on compaction, as its positive charges attract the polar cytoplasmic membrane lipids, thereby putting the two membrane bilayers in close apposition (reviewed in Boggs, 2006). This increase in MBP could be a compensatory effect for a potential less compacted myelin in $TSPAN2^{null}$ mice. Further investigations will be needed to study the possible interaction of TSPAN2 and MBP.

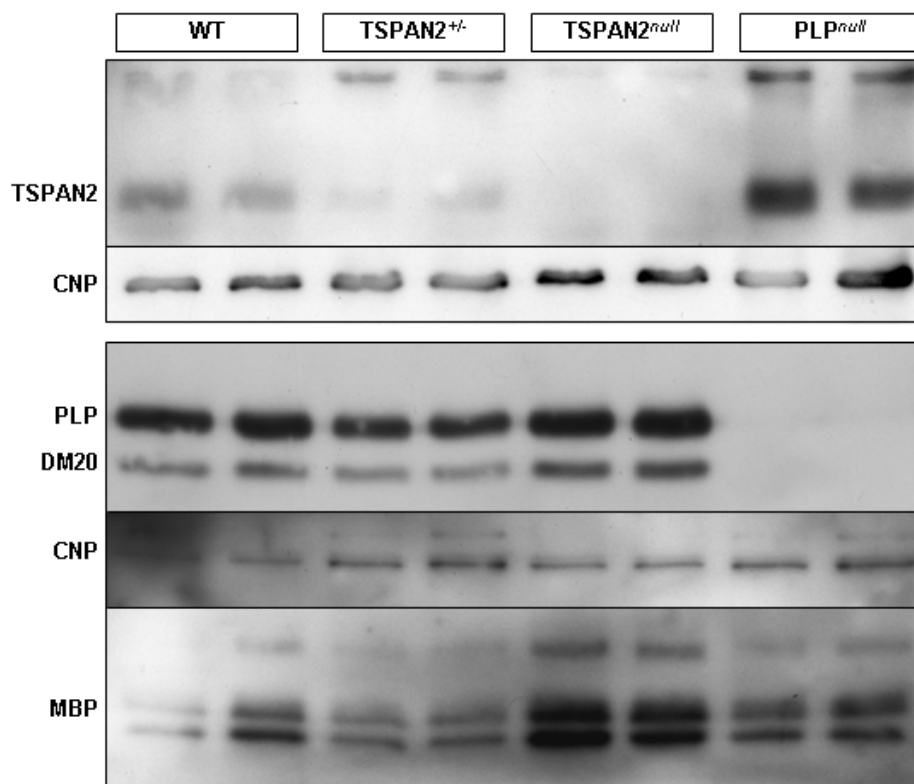


Figure 32. Characterization of $TSPAN2^{null}$ mice.

Immunoblot analysis was performed on P75 CNS-myelin enriched fraction of wild-type (WT), $TSPAN2^{+/-}$, $TSPAN2^{null}$ and PLP^{null} mice (n = 2). TSPAN2 was absent in the $TSPAN2^{null}$ mice, very decreased in the $TSPAN2^{+/-}$ mice and highly increased in PLP^{null} mice, when comparing to WT. There was no positive signal of PLP/DM20 in the PLP^{null} mice (as expected) and the levels seemed to be reduced in the $TSPAN2^{+/-}$ mice, when comparing to WT and $TSPAN2^{null}$ mice. Interestingly, the MBP levels were increased in the $TSPAN2^{null}$ mice. The non-compact CNS myelin protein CNP was used as a loading control.

4.2.4. Weight increase in TSPAN2^{null} mice

As TSPAN2 has been observed to be increased in PLP^{null} mice, the TSPAN2^{null}*PLP^{null} mice were generated by cross-breeding the single-mutants, for permitting the *in vivo* study of the chronic absence of these two CNS myelin tetraspan proteins. These TSPAN2^{null}*PLP^{null} mice do breed normally and have no obvious phenotypes, at least until 10 months of age.

The weight increase was measured in wild-type, TSPAN2^{null}, PLP^{null} and TSPAN2^{null}*PLP^{null} mice, for assessing if the normal body weight increase during development was achieved. The weight was measured every second day between P2 and P30 (n = 16 - 23) in the four genotypes. An ANOVA with repeated measurements was performed and it demonstrated a significant effect of the genotypes on the weight increase. The post-hoc Bonferroni correction demonstrated that the weight increase in wild-type and TSPAN2^{null} mice behaves equally, as well as in the PLP^{null} and TSPAN2^{null}*PLP^{null} mice (Table 11). The latter two genotypes had significantly reduced weight increase levels between P2 and P30.

Table 11. Reduced weight increase in PLP^{null} and TSPAN2^{null}*PLP^{null} mice.

The weight increase was measured in wild-type (WT), TSPAN2^{null}, PLP^{null} and TSPAN2^{null}*PLP^{null} mice every second day between P2 and P30 (n = 16 - 23). The post-hoc Bonferroni correction (given the P-values) demonstrated that the weight increase is similar in (WT), TSPAN2^{null} mice, while it is reduced in PLP^{null} and TSPAN2^{null}*PLP^{null} mice, being equal between them.

	WT	TSPAN2 ^{null}	PLP ^{null}
TSPAN2 ^{null}	P = 0.230		
PLP ^{null}	P = 5.369 · 10 ⁻¹¹	P = 7.918 · 10 ⁻⁷	
TSPAN2 ^{null} *PLP ^{null}	P = 3.934 · 10 ⁻¹⁰	P = 1.192 · 10 ⁻⁵	P = 1.000

The diagram in figure 33A, shows the weight increase above mentioned.

The weight differences were also analysed statistically at P30 (Fig. 33B), and an ANOVA analysis proved a significant differences between the wild-type and the PLP^{null} and TSPAN2^{null}*PLP^{null} mice (with higher weights in wild-type mice), and between TSPAN2^{null} and PLP^{null} mice, with a reduced weight in PLP^{null} mice. This reveals, as in the P2 to P30 evaluation, a similar weight in wild-type and TSPAN2^{null} mice, and a reduced one in PLP^{null} and TSPAN2^{null}*PLP^{null} mice.

The weight was also assessed at ten months of age in these four genotypes (n = 6 - 13) and yet again wild-type and TSPAN2^{null} mice show the same weight (Fig. 33C), while the PLP^{null} and TSPAN2^{null}*PLP^{null} mice had significantly reduced weights.

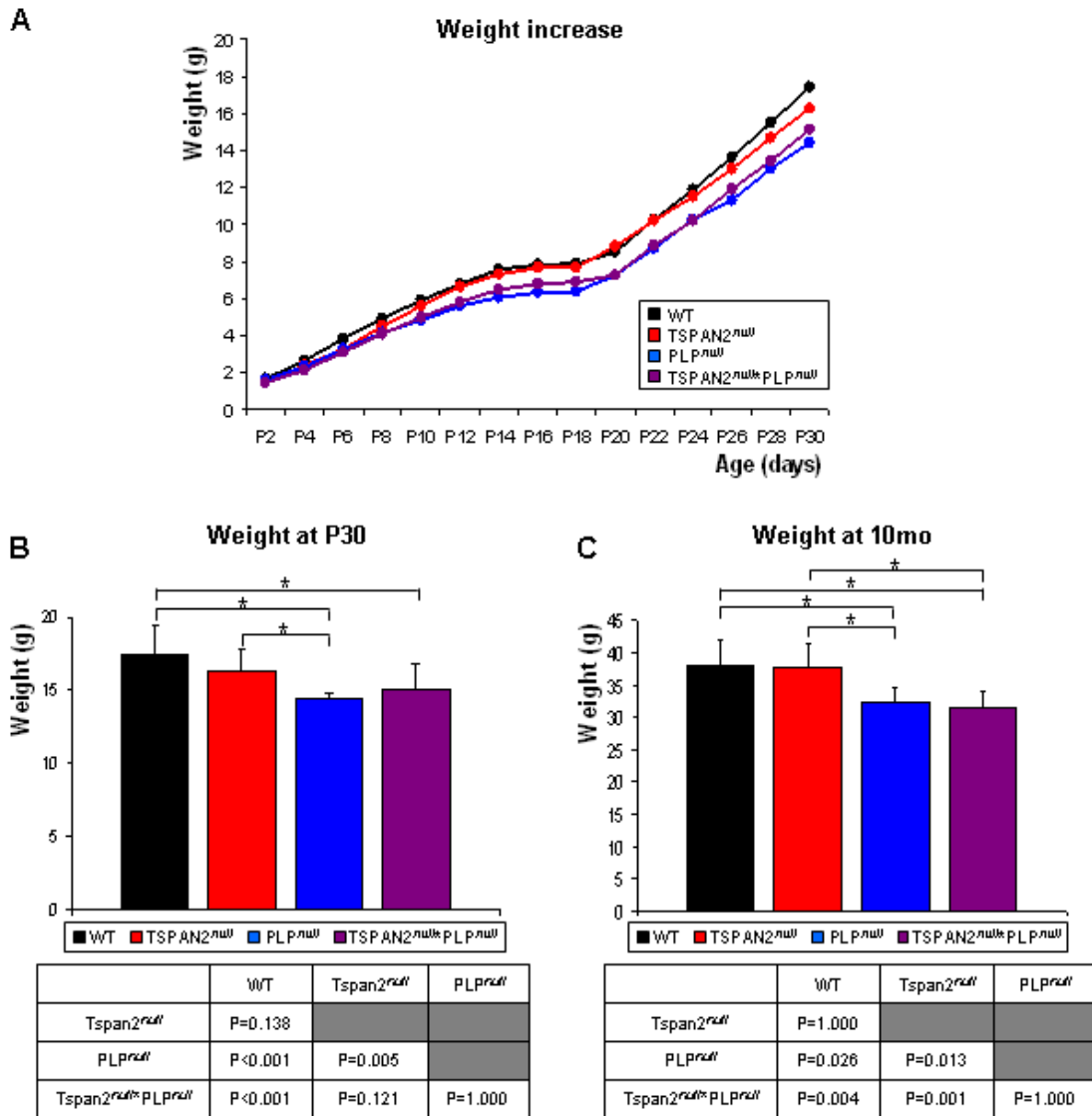


Figure 33. Weight increase in wild-type, TSPAN2^{null}, PLP^{null} and TSPAN2^{null}*PLP^{null} mice.

A) The weight increase was assessed every second day between P2 and P30. Wild-type (WT) and TSPAN2^{null} mice showed similar weights, while PLP^{null} and TSPAN2^{null}*PLP^{null} mice had a significant reduction.

B) Diagram bar representing the weight at P30 (mean ± StDev). The table below depicts the result of the Bonferroni Post-hoc (P-value).

C) Diagram bar representing the weight at 10 months of age (mean ± StDev). The table below depicts the result of the Bonferroni Post-hoc (P-value).

Therefore, regarding their weight increase during early postnatal development and in adulthood, wild-type and TSPAN2^{null} mice behaved in the same manner, while PLP^{null} and TSPAN2^{null}*PLP^{null} mice showed reduced weights at the different time points evaluated.

4.2.5. Protein composition in TSPAN2^{null} mice

To evaluate if the protein composition in CNS myelin was altered in the absence of TSPAN2, silver stainings were performed with CNS-myelin enriched fractions. At P30, no obvious

differences could be observed in the TSPAN2^{null} mice (Fig. 34A), but in PLP^{null} and TSPAN2^{null}*PLP^{null} mice the expected and prominent bands of PLP/DM20 (20 - 23 kDa) were absent. This was equivalent when performing the analysis at P75. Thus, in the absence of TSPAN2 no drastic protein level alteration could be found in the silvergel evaluations.

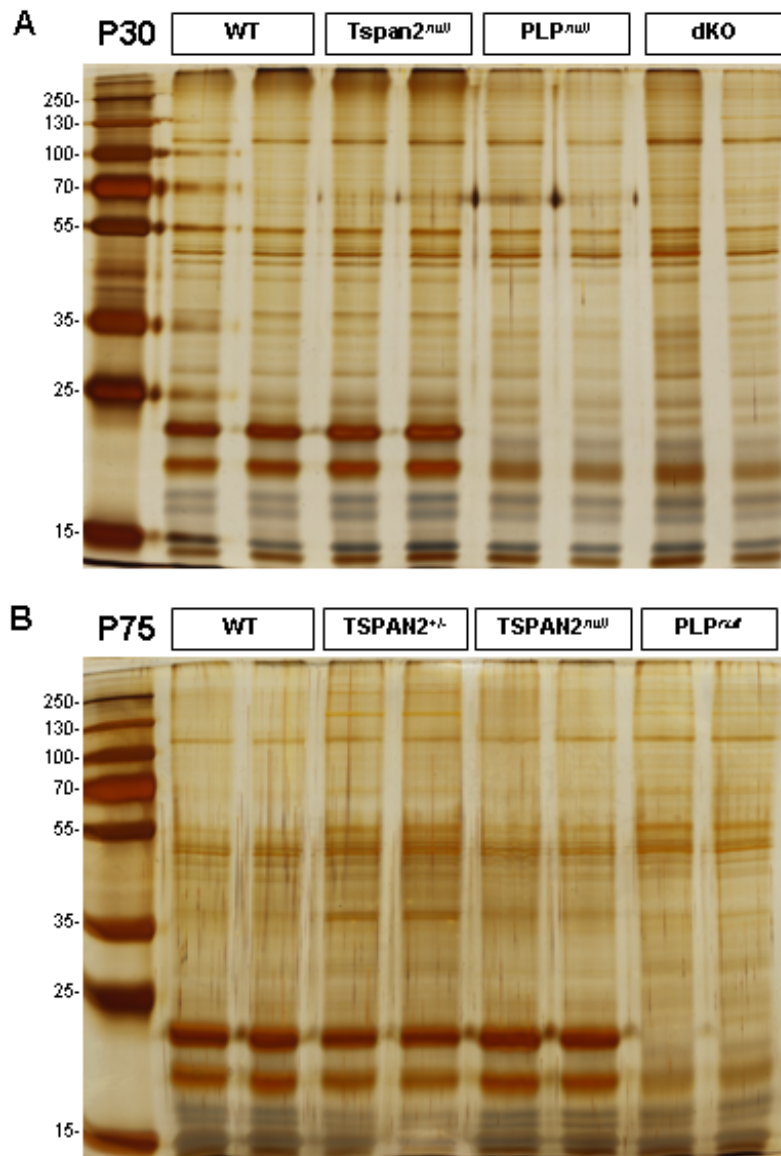


Figure 34. Silver staining of TSPAN2^{null} CNS myelin.

A CNS-myelin enriched fraction was analyzed by means of silver staining (n = 2).

A) Analysis at P30 including wild-type (WT), TSPAN2^{null}, PLP^{null} and TSPAN2^{null}*PLP^{null} (dKO) CNS-myelin enriched fractions. PLP/DM20 is absent in the PLP-null mutations (as expected), no other major differences could be observed.

B) Analysis at P75 including WT, TSPAN2^{+/-}, TSPAN2^{null} and PLP^{null} of CNS-myelin enriched fractions. No obvious differences could be observed, apart from the lack of PLP/DM20 in PLP^{null} mice.

As, on the broad assessment level that a silvergel allows, no differences had been observed, the further evaluations were performed with immunoblots.

Therefore, immunoblots of CNS-enriched myelin fractions were performed on P30 wild-type, TSPAN2^{null}, PLP^{null} and TSPAN2^{null}*PLP^{null} mice (Fig. 35). The closely related to TSPAN2, tetraspanins CD9 and CD81 were assessed (See 2.3.1.). The paranodal protein CD9 revealed no abundance differences in the four genotypes. But CD81 showed an increased abundance in TSPAN2^{null}, PLP^{null} and TSPAN2^{null}*PLP^{null}, and especially its smaller isoform was more abundant in PLP^{null} and TSPAN2^{null}*PLP^{null} mice. CD81 seems to compensate for the absence of TSPAN2 and PLP. As suggested in the immunoblot of P75 CNS-myelin fractions (Fig. 32), the abundance of MBP was also increased at P30. The two smaller isoforms were more abundant in the TSPAN2^{null}, PLP^{null}, and TSPAN2^{null}*PLP^{null} mice, and the larger isoform in the two latter genotypes. Again, this increase in the MBP levels could argue for a manner of compensating for reduced CNS myelin compaction. On the other side, two other myelin tetraspanins, CD82 and CD63 showed no alterations, as well as the non-compact myelin protein CNP.

Fyn was tested, as tetraspanins are integrators and assemblers of signalling molecules, and the tyrosine kinase Fyn is known to be a key downstream signalling element in OLs maturation (reviewed in Krämer-Albers & White, 2011). Thus, TSPAN2 could be involved in the assembly of this kinase. However, the immunoblot did not reveal any differences when TSPAN2 is missing.

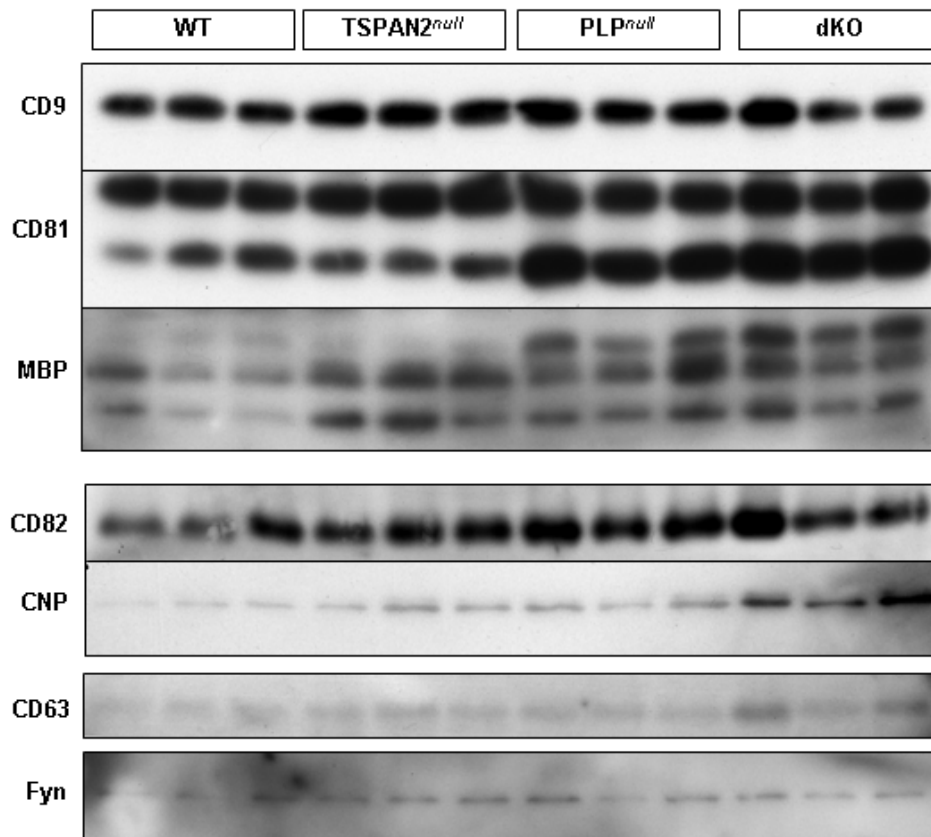


Figure 35. Immunoblot analysis of TSPAN2^{null} mice.

Immunoblots were performed on CNS-myelin enriched fraction at P30 (n = 3) of wild-type (WT), TSPAN2^{null}, PLP^{null} and TSPAN2^{null}*PLP^{null} (dKO) mice. The tetraspanin CD9 showed no difference. The smaller isoform of the tetraspanin CD81 was more abundant in TSPAN2^{null}, PLP^{null} and dKO mice. MBP showed an increased abundance in TSPAN2^{null}, PLP^{null} and dKO mice, as already proven in P75 CNS myelin (Fig. 32), and its larger isoform was even more abundant in PLP^{null} and dKO mice. Probably, MBP compensates for a reduced myelin compaction. The other tested tetraspanins, CD82 and CD63, showed no differences, as well as the non-compact myelin protein CNP and the tyrosine kinase Fyn.

Thus, the prominent signalling protein in OLs, Fyn, is not altered. Additional examinations of different tetraspanin-associated signalling proteins in OLs should be pursued. But the consistent (at P30 and P75) increased abundance of MBP does suggest that the myelin sheaths lacking TSPAN2 need an extra-compaction to be properly functional. This is also apparent, as in the PLP^{null} (known to have a myelin compaction deficiency; Klugmann *et al.*, 1997) and TSPAN2^{null}*PLP^{null} mice the larger MBP isoform is additionally increased. The possible compaction deficit should be further assessed, as well as the role of MBP in TSPAN2^{null} mice. Furthermore, it seems that CD81 is the tetraspanin that compensated for the chronic lack of TSPAN2. The role of CD81 in TSPAN2^{null} mice ought to be evaluated in more detail.

5. Discussion

5.1. Neuronal M6A and M6B proteolipids are abundant in cortical neurons

The neuronal proteolipids M6A and M6B were known to be highly expressed throughout the neurons in the brain (Baumrind *et al.*, 1992; Yan *et al.*, 1996; Huminiecki *et al.*, 2003), but it had to be proven that this was also the case in primary cortical neurons, the chosen *ex vivo* culture system. To define their exact localization, I immunostained primary cortical neurons with antibodies against M6A and M6B.

Indeed, most neurons do express both proteolipids, but at different expression levels. On the whole, neurons express both M6 proteins in an equivalent manner, and some express majorly M6A or M6B. In the case of the predominant M6B expression, two types of neurons could be differentiated: some with a broad cellular expression and others with a more plasma membrane restricted expression. It could also be verified that M6A as well as M6B are evenly distributed on axons and dendrites. Hence, this demonstrated that the chosen *ex vivo* culture system is optimal for studying the role of neuronal proteolipids in the neuronal development.

To reveal the precise localization of the neuronal proteolipids in the different neuronal domains, I performed co-localization studies. M6A or M6B were co-labelled with tubulin, a marker for the axonal and dendritic shafts (Dent & Gertler, 2003), and revealed a large expression of both M6 proteins in tubulin rich domains. The co-localization with F-actin, which is mainly present in distal regions like growth cones (Dent *et al.*, 2010), proved that both proteins are found in F-actin rich compartments. But M6A was notably located at F-actin free membrane protrusions. Consequently, M6A and M6B are abundantly expressed in most primary cortical neurons and they share a broad distribution, but this is not identical.

5.2. M6A defines F-actin free membrane protrusions

As the localization of M6A had been observed on F-actin free membrane extensions, a more profound examination was pursued. Hence, I immunostained primary cortical neurons with an antibody against M6A and the F-actin binding toxin phalloidin. Detailed confocal analysis including reflection microscopy, allowed analysing the potential co-localization of M6A and F-actin with the simultaneous confirmation of the outer plasma membrane extension. This was

indispensable as it enabled defining the outer membrane of the processes on which M6A and F-actin could be confined.

This examination revealed that on many tubular processes (filopodia) M6A and F-actin co-localize. However, oftentimes M6A has been found on F-actin free membrane extensions with intact and continuous membranes. There has been a diversity regarding this partial co-localization: some tips are M6A and F-actin positive, while the neighbouring one would lack F-actin completely, and in some tips the proximal part could be labelled by both, but only M6A was found in the distal domains or even just at the distal tip end. Also the length of this extension varied, as M6A-positive F-actin-negative processes have been observed to be larger than 10 μm . Moreover, this prominent finding is not restricted to tubular processes, but has also been observed in flattened membrane extensions. Subsequently, as F-actin has been supposed “to compose the core of filopodia” (cited after Dent & Gertler, 2003), M6A defines novel F-actin free M6A-rich membrane protrusions.

In the case of M6B, this distinct localization could not be observed. In most membrane tips, M6B has been found in the neuronal membrane extension at F-actin-positive domains. Some membrane extension lacked both M6B and F-actin, presumably being M6A-positive.

Hence, membrane extensions on cortical neurons express both M6 proteolipids, and M6A defines F-actin free membrane protrusions whereas M6B does not.

5.3. M6A and M6B are required for growth cone compartmentalization

Since M6A and M6B had been located extensively on neuronal growth cones (Sheetz *et al.*, 1990; Baumrind *et al.*, 1992; and current analysis) and especially M6A was found to have a very particular localization at F-actin free membrane protrusions, the examination continued by analysing the neuronal growth cones in the chronic absence of these proteins. The growth cone structure is mainly compartmentalized by MTs being present in the extending axon shaft and central growth cone regions, and F-actin concentrated in the peripheral growth cone regions, lamellipodia and filopodia (Dent & Kalil, 2001; Dent & Gertler, 2003). Wild-type and Gpm6a^{null}*Gpm6b^{null} cortical neurons were immunostained against tubulin and F-actin.

For the evaluation, initially three categories of tubulin and F-actin localization were established, where (1) tubulin and F-actin were overlapping in one compartment, (2) tubulin and F-actin were being in two distinct compartments and (3) tubulin was being present at the distal domain. Most wild-type cortical neurons, as expected, belonged to the second

category, with tubulin and F-actin in distinct domains, and tubulin was extremely seldom found in the distal regions. Intriguingly, most growth cones of Gpm6a^{null*}Gpm6b^{null} cortical neurons fell into the category of tubulin and F-actin being superimposed. And even frequently, growth cones contained tubulin at their most distal domains. In both genotypes, this result was consistent no matter the growth cones of the axon or longest neurite or of the remaining neurites was assessed.

The comparison was also evaluated after merging the two categories that involved unusual tubulin to F-actin localization, as no statistical analysis could be performed with the prior data set because of the data points being zero or one in wild-type neurons. This evaluation demonstrated significant differences in the distribution of tubulin and F-actin at the growth cones. Gpm6a^{null*}Gpm6b^{null} cortical neurons have frequently tubulin partially superimposed to F-actin or even tubulin at the distal end of their growth cones, both on the axon or dendrites, while this is not the case for wild-type cortical neurons.

Therefore, the normal F-actin and tubulin compartmentalization in the growth cones of Gpm6a^{null*}Gpm6b^{null} cortical neurons is altered, and this occurred in all process endings, either axonal or dendritic. This mislocalization of tubulin and F-actin represents a very profound modification of the proper growth cone structure, as the localization of these two proteins mainly define distinct morphological and functional growth cone domains. M6A and M6B are expressed on most cortical neurons and located throughout the axon, dendrites and growth cones, and in their chronic absence, the tubulin to F-actin compartmentalization at the growth cones is altered. Hence, the neuronal proteolipids M6A and M6B are required for the proper separation of cytoskeletal proteins at the growth cones.

5.4. M6A and M6B are required for normal reaction to ephrinA5

Is there a functional consequence to the altered growth cone compartmentalization? To evaluate this, I performed a “growth cone collapse assay” induced by ephrinA5, a well-know collapse inducing agent (Knöll *et al.*, 2006) and defined collapse or non-collapse as the absence or presence, respectively, of a lamellipodium in the growth cones of the axon or longest neurite.

In wild-type, Gpm6a^{null} and Gpm6b^{null} single-mutant cortical neurons ephrinA5 induced a significant collapse of their growth cones, with the same extend when applying the standard or the doubled dose. Surprisingly, the Gpm6a^{null*}Gpm6b^{null} cortical neurons react differently, they react to a much lesser extend at the standard dose. But they undergo a highly

significant increase in the abundance of collapsed growth cones when applying the double concentration of ephrinA5.

The present data suggest that although Gpm6a^{null*}Gpm6b^{null} cortical neurons reacted to an ephrinA5 induced “growth cone collapse assay”, they required a greater dose to achieve equivalent effects as in the wild-type and the Gpm6a^{null} and Gpm6b^{null} single-null mutant cortical neurons. Thereby, it seemed that M6 proteolipids are important for the proper growth cone function.

Another significant difference could be observed when comparing the number of non-collapsed (defined as presence of a lamellipodium) growth cones in the control group. Gpm6a^{null} and even more the Gpm6a^{null*}Gpm6b^{null} cortical neurons presented a significant increased abundance of growth cones with lamellipodia, in comparison to wild-type or Gpm6b^{null} cortical neurons. Therefore, the chronic absence of M6A lead to an increase in the number of growth cones presenting lamellipodia. This effect is more pronounced when M6A and M6B are missing in the cortical neurons. Once more, these involved the neuronal M6 proteolipids in the maintenance of the proper growth cone morphology, and thereby function.

To elucidate the reason of the altered responsiveness of Gpm6a^{null*}Gpm6b^{null} cortical neurons to the ephrinA5 induced “growth cone collapse assay”, cortical neuron lysates were analysed with immunoblots. To simplify the approach for studying the Eph receptors that could bind to ephrinA5, as ephrinA5 binds to EphA1-8 and EphB2 (reviewed by Pasquale, 2004), the levels of ephexin-1 were assessed, as they relate to the abundance of Eph receptors (reviewed by Egea & Klein, 2007). The initial result showed a moderately decreased abundance of ephexin-1 in Gpm6a^{null*}Gpm6b^{null} cortical neurons, when compared to wild-type. This would signify a reduction in the overall Eph-receptor levels in the chronic absence of M6 proteins, and would thereby be a possible explanation to the altered responsiveness of these Gpm6a^{null*}Gpm6b^{null} cortical neurons in the ephrinA5 induced growth cone collapse.

RhoA, as key downstream element acting in growth cones collapse (Wahl *et al.*, 2000; reviewed in Hall & Lalli, 2010), was investigated next. Preliminary results showed a slight decrease in the RhoA levels in cortical neuron lysates, which would mean that the total levels of RhoA would be decreased in the Gpm6a^{null*}Gpm6b^{null} cortical neurons. Less RhoA could account for the delayed reactivity of the Gpm6a^{null*}Gpm6b^{null} cortical neurons towards the ephrinA5 induced growth cone collapse.

Thus, the immunoblot analysis provides preliminary results for the significance of M6 proteins in growth cone function, potentially by associating to cytoskeleton proteins in lipid rafts and thereby regulating the localization and abundance of signalling receptors, like Ephs, and signalling proteins, like RhoA.

5.5. M6A and M6B are required for neurite outgrowth

The next step was to assess the functional relevance of the neuronal M6 proteolipids in neurite extension, a hallmark in neuronal development. It had been previously demonstrated an *in vitro* involvement of M6A, upon application of the monoclonal M6 antibody against M6A (Lagenauer *et al.*, 1992) as well as in overexpression studies (Zhao *et al.*, 2008), in neurite outgrowth. For this examination, the neurite length was measured on wild-type, Gpm6a^{null}, Gpm6b^{null} and Gpm6a^{null}*Gpm6b^{null} cortical neurons, so that the effect of the absence of M6A as well as M6B could be assessed.

Interestingly, there is a very significant reduction in neurite length when the M6 proteolipids are missing, and this occurs in a gradient manner: from wild-type, to neurons lacking M6B, and to neurons lacking M6A or both M6A and M6B. When categorizing the neurons according to their neurite extension length, all four genotypes had a significant different frequency distribution pattern.

The diminished neurite outgrowth revealed the need of M6 proteins in this important neuronal task. The absence of M6B generated a very significant decrease in the neurite length. Nevertheless, the neurite extension was even more reduced in the absence of M6A. Hence, this suggested an important role of both neuronal M6 proteolipids in the proper neuronal development, including neurite extension.

5.6. M6A and M6B are required for the response to cholesterol in neurite outgrowth

Cholesterol is essential for the neuronal function, including the maintenance of the plasma membrane and the extension of membrane processes during development (reviewed in Benarroch, 2008), plus PLP, ortholog to M6A and M6B, interacts directly with cholesterol (Simons *et al.*, 2000; Krämer-Albers *et al.*, 2006), as well as M6B itself (Werner H., pers. comm). Therefore, I hypothesized that the impact of the impaired neurite outgrowth in the absence of M6 proteins could be related to their potential cholesterol association.

To evaluate this, cortical neurons of wild-type and Gpm6a^{null*}Gpm6b^{null} mice were cultured under increasing cholesterol concentrations and their neurite extension was measured. In agreement with prior results (Ko *et al.*, 2005), wild-type cortical neurons show a decrease in their neurite length upon an increasing cholesterol dose. This confirmed the importance of the regulation of the cholesterol levels for proper neuronal function. Unexpectedly, the Gpm6a^{null*}Gpm6b^{null} cortical neurons did not react to the increasing cholesterol amounts and preserved their reduced neurite extension (as described above) at the same levels. Even under this conditions, which reduced the length of the wild-type neurites, the Gpm6a^{null*}Gpm6b^{null} neurons were still significantly more impaired in their neurite extension capacities.

Hence, when cortical neurons lacked chronically M6 proteins they could not respond in the normal manner to alterations in the cholesterol concentration. Thus it seemed that M6 proteins associate directly or indirectly with cholesterol and this relates to their role in neurite outgrowth.

5.7. M6A and M6B are not required for growth cone morphology, adhesiveness and motility

The prior observed differences in growth cone compartmentalization and function, and the impaired neurite extension in the chronic absence of neuronal M6 proteins, led to the hypothesis of an impaired *in vivo* behaviour. For that reason, wild-type and Gpm6a^{null*}Gpm6b^{null} cortical neuron growth cones were imaged *in vivo* with confocal reflection microscopy in a short time-frame (10 min), to avoid camouflaging effects of the lack of M6 proteins in the overall neurite extension.

When comparing the morphometrical properties like e.g. the perimeter in relation to the total growth cone area, as well as the total area itself, no significant differences could be observed. Thus, the absence of M6 proteins does not alter the growth cone morphometry in a short-time window. The evaluation of the adhesive area in relationship to the total area in the growth cones, demonstrated again no significant differences between wild-type and Gpm6a^{null*}Gpm6b^{null} cortical neurons. The adhesiveness was not altered when neuronal growth cones lack chronically M6 proteins. As a next step, the motility of the growth cones was assessed, by evaluating the retraction and extension between each single image of the taken videos. Surprisingly, the motility of growth cones of wild-type and Gpm6a^{null*}Gpm6b^{null} cortical neurons is essentially identical.

Thus, unexpectedly, the short-term *in vivo* analysis of the growth cones of cultured Gpm6a^{null*}Gpm6b^{null} cortical neurons demonstrated similar morphometry, adhesion and motility as in wild-type neurons. Therefore, the investigations performed on the *ex vivo* cortical neuron culture system have proven that M6A and M6B are important for several aspects of neuronal development, including growth cone compartmentalization and function, neurite extension, and the response to the cholesterol levels in neurite extension. But they seemed not to be relevant for the short-term morphometry, adhesion and motility.

5.8. M6A and M6B are required for proper corpus callosum formation

To assess if the described alterations of cultured cortical neurons in the chronic absence of M6 proteins could be observed *in vivo*, the corpus callosum of wild-type and Gpm6a^{null*}Gpm6b^{null} mice was analyzed, as it is the largest cortical brain commissure. The observed reduced neurite extension, as well as the altered growth cone compartmentalization and response to ephrinA5 in Gpm6a^{null*}Gpm6b^{null} cortical neurons, led to the hypothesis of an impaired axonal pathfinding, and thereby a reduction in axons crossing the hemispheres at the corpus callosum. So, the corpus callosum width was measured at two regions, anterior to the hippocampus and containing the hippocampus.

The comparison of wild-type and Gpm6a^{null*}Gpm6b^{null} corpora callosa width demonstrated a significant reduction of the corpus callosum in Gpm6a^{null*}Gpm6b^{null} mice. This was found at both analyzed levels, although it was even more prominent in the more caudal levels comprising the hippocampus. It seemed from prior investigations that in the young adult mice no developmental defects could be observed (Fünfschilling U., Werner H., pers. comm.), which would argue for a developmental delay in the absence of M6 proteins that is compensated throughout development. More detailed analysis in the adult mice should be performed, for clarifying if the developmental effect of reduced corpora callosa is actually compensated over time.

In the current investigation, M6 proteins seemed to be important for the formation of the major white matter tract in the brain, the corpus callosum, thereby being required for the efficient and normal development of axonal tracts in the brain.

5.9. Tetraspanin2 in CNS myelin

Tetraspanin2 has been shown to be present in CNS compact myelin (Birling *et al.*, 1999) and was found to be enriched in PLP^{null} CNS-enriched myelin fractions by immunoblot analysis (Werner H., pers. comm.). Hence, the localization of TSPAN2 was assessed on brain sections. TSPAN2 appeared to be present in all white matter tracts in wild-type mice, and to some extent in OLs of the gray matter. In the PLP^{null} mice the levels of TSPAN2 were strongly increased, confirming the prior results. TSPAN2 is more abundant in the white matter tracts and much more in the OLs of the gray matter. This upregulation of TSPAN2 in the absence of PLP suggests that, as both are structurally similar tetraspan proteins found in CNS compact myelin, TSPAN2 could structurally and functionally compensate for PLP in its absence.

5.10. Targeted inactivation of the murine Tspan2 gene

The upregulation of TSPAN2 in PLP^{null} mice and its early onset of expression during OL development (Nielsen *et al.*, 2006; Dugas *et al.*, 2006), suggests that TSPAN2 could be a relevant protein for CNS myelination. To test this hypothesis, I successfully generated TSPAN2^{null} mice by homologous recombination of the murine *Tspan2* gene in ES cells. The absence of TSPAN2 was proven on the genomic DNA by PCR and on the protein level by immunoblot analysis. The TSPAN2^{null} mice breed normally and give rise to offspring with genotypes according to the Mendelian inheritance rules. Until known so far, TSPAN2^{null} mice showed no obvious phenotypic abnormalities. The fact that there is no obvious phenotype could probably be explained by some compensatory mechanism of other myelin tetraspanins. Therefore, it would be e.g. interesting to analyze the TSPAN2^{null}*CD9^{null} or the TSPAN2^{null}*CD81^{null} mice.

Because the function or at least the abundance of TSPAN2 seemed to be correlating with the presence of PLP, TSPAN2^{null}*PLP^{null} mice were generated by cross-breeding the single-mutants. These mice were also included in the pursued studies to evaluate the *in vivo* consequence of the chronic lack of these two tetraspan proteins of compact CNS myelin. TSPAN2^{null}*PLP^{null} mice do breed normally and have no obvious phenotypes, as known so far.

5.11. Weight increase in TSPAN2^{null} mice

To evaluate if the normal weight increase does occur during early postnatal development in the absence of TSPAN2, the weight increase was measured between P2 and P30 in wild-type, TSPAN2^{null}, PLP^{null} and TSPAN2^{null}*PLP^{null} mice. During this period, TSPAN2^{null} weighted similarly to wild-type mice, and both PLP^{null} and TSPAN2^{null}*PLP^{null} mice had a reduced weight increase. This was also the case when assessing their weight at P30 and at ten months of age. Hence, TSPAN2 has no influence on the weight increase during development, as well as on the weight in adult mice. The reduced levels in PLP^{null} and TSPAN2^{null}*PLP^{null} mice probably refer to a minor phenotype in the mice, not yet proven, as the weight is related to the overall health of the animals.

5.12. Protein composition in TSPAN2^{null} mice

To assess if the lack of TSPAN2 altered the protein composition of CNS myelin, silver staining was performed. These demonstrated no major differences in the protein abundance in CNS-myelin enriched fractions, neither at P30 (TSPAN2^{+/-} and TSPAN2^{null}) nor at P75 (TSPAN2^{null} and TSPAN2^{null}*PLP^{null}). PLP/DM20 was, as expected, absent in the lack of PLP (PLP^{null} and TSPAN2^{null}*PLP^{null}).

To perform an examination in more detail, immunoblots on P30 CNS-myelin enriched fractions of wild-type, TSPAN2^{null}, PLP^{null} and TSPAN2^{null}*PLP^{null} mice were performed. The most related myelin tetraspanin to TSPAN2, CD9, did not show, surprisingly, any abundance difference. This was an unexpected result, as CD9 was the primary candidate to potentially compensate for the absence of TSPAN2, as both are very similar structurally and are found in the same domains of CNS myelin (Birling *et al.*, 1999; Ishibashi *et al.*, 2004). However, the abundance of the myelin tetraspanin CD81, the next close related tetraspanin (Garcia-España *et al.*, 2008), was augmented in TSPAN2^{null}, PLP^{null} and TSPAN2^{null}*PLP^{null} mice. And the smaller isoform is additionally increased in PLP^{null} and TSPAN2^{null}*PLP^{null}. Therefore, CD81 does seem to compensate for TSPAN2. The myelin tetraspanins CD82 and CD63 revealed no differences at all. CD82 has been involved in the early stages of OL development (Mela & Goodman, 2009) and possibly its abundance levels could be regulated at earlier postnatal stages. CD63 is known to be in CNS myelin (Baer *et al.*, 2009), but until now, the investigations have related CD63 mainly to exosomes and late lysosomes (reviewed in Pols & Klumperman, 2008) and it is unknown if CD63 is actually present at the compact CNS myelin. The two CNS myelin tetraspanins, CD151 and OAP-1 could not be assessed while performing this characterization. CD151 is an important regulator of cell morphology in an integrin-dependent manner (reviewed in Hemler, 2005), but there is no

evidence of its exact localization in the CNS myelin domains, as well as its function in the nervous system. And OAP-1 has been involved in OL proliferation (Tiwari-Woodruff *et al.*, 2001). It is very tempting to suggest that these two, CD151 and OAP-1, that are known to bind integrins (a typical characteristic of tetraspanins, Hemler, 2005), could compensate for the lack of TSPAN2 in the CNS myelin. Further investigation should assess this interesting question.

In addition, the abundance of Fyn, a tyrosine kinase important in OL maturation (reviewed in Krämer-Albers & White, 2011) was also not altered. This was, yet again, an unexpected result, as tetraspanins assemble signalling molecules and Fyn was a major candidate to be regulated by TSPAN2.

Beside, the non-compact myelin protein CNP has also no different abundance levels in the absence of TSPAN2 at P30 and at P75. However, the MBP levels demonstrated a notably augmented abundance in the CNS-myelin enriched fractions of TSPAN2^{null}, PLP^{null}, and TSPAN2^{null}*PLP^{null} mice. And in the latter two, the abundance of the larger isoform was as well increased. MBP is the second most abundant compact myelin protein and it is involved in myelin compaction and is essential for myelination (reviewed in Boggs, 2006). The augmented MBP levels suggested a compensation for an altered compaction in TSPAN2^{null}, PLP^{null}, and TSPAN2^{null}*PLP^{null} mice. This would be in accordance to the prior knowledge of PLP^{null} mice having a reduced CNS myelin compaction (Klugmann *et al.*, 1997). This unexpected and promising result should be assessed in more detail, for understanding the manner TSPAN2 and MBP do possibly interact.

Therefore, an obvious abundance difference was found regarding MBP, which is strongly increased in the absence of TSPAN2, at P30 and at P75. MBP could compensate for a reduced CNS compaction in the TSPAN2^{null} mice. And it is the tetraspanin CD81 that seemed to compensate for the lack of TSPAN2. This altered regulation of MBP and CD81 should be further assessed.

6. Summary and conclusions

The neuronal tetraspan proteolipids M6A and M6B were previously characterized regarding their cellular expression, and by acute manipulation *in vitro*. However, little was known of their function during neuronal development *in vivo*. I have analysed primary cortical neurons of mice chronically lacking M6A, M6B, or both. The absence of M6-proteins led to an altered morphology of the axonal growth cones regarding actin/tubulin compartmentalization, and an augment in growth cones with lamellipodia. The latter feature was also apparent in growth cones lacking only M6A. Interestingly in this regard, M6A defines an F-actin free subcompartment of the growth cone filopodia. Importantly, M6-deficient growth cones did not collapse normally upon the application of the known collapsing agent ephrinA5, which can be explained by the finding that the abundance of the Eph-receptor signalling-mediator ephexin1 is reduced in cortical neurons devoid of M6-proteolipids. By live-cell imaging I could assess that chronic lack of M6-proteins does not impair the normal adhesiveness or motility of neuronal growth cones. Nevertheless, cortical neurons lacking M6 proteins were impaired regarding neurite outgrowth, which cannot be ameliorated by the addition of cholesterol. *In vivo*, there is a reduced width of the corpus callosum, which connects most cortical areas of the two brain hemispheres, in GPM6A^{null*}GPM6B^{null} double null mutant mice, at least during early postnatal development. Together, M6 proteins are required for normal growth cone morphology and function and for neurite outgrowth, but not for normal growth cone motility.

The third member of the proteolipid protein family is proteolipid protein (PLP), the most abundant constituent of CNS myelin. Mice and humans lacking PLP are largely normally myelinated, which has been difficult to explain. In a candidate approach the low-abundant myelin tetraspan tetraspanin-2 (TSPAN2) has been identified as a candidate to compensate for PLP-deficiency because of its dramatically increased abundance in PLP-deficient myelin. To investigate the role of TSPAN2 in myelination, I generated TSPAN2^{null} mutant mice by homologous recombination in embryonic stem cells. These mice are viable, breed normally and the initial evaluation at the protein level shows several alterations. The abundance of the closely related tetraspanin CD81 as well as that of the major myelin protein MBP is increased in myelin isolated from TSPAN2^{null} mice, indicating molecular changes that may compensate for the absence of TSPAN2 function. Therefore, TSPAN2 seems to play a role at the oligodendrocyte early development. Further investigations will be necessary to elucidate the molecular mechanisms of how TSPAN2 acts during myelin biogenesis.

Together, structurally related tetraspan proteins, including the neuronal proteolipids M6A and M6B, and the oligodendroglial PLP and TSPAN2, are required for the normal formation of cellular processes in neural cells.

7. References

- Alfonso J, Pollevick GD, Van Der Hart MG, Flügge G, Fuchs E, Frasch AC. Identification of genes regulated by chronic psychosocial stress and antidepressant treatment in the hippocampus. *Eur J Neurosci*. 2004 Feb;19(3):659-66.
- Alfonso J, Fernández ME, Cooper B, Flugge G, Frasch AC. The stress-regulated protein M6a is a key modulator for neurite outgrowth and filopodium/spine formation. *Proc Natl Acad Sci U S A*. 2005 Nov 22;102(47):17196-201.
- Alfonso J, Frick LR, Silberman DM, Palumbo ML, Genaro AM, Frasch AC. Regulation of hippocampal gene expression is conserved in two species subjected to different stressors and antidepressant treatments. *Biol Psychiatry*. 2006 Feb 1;59(3):244-51.
- Arroyo EJ, Scherer SS. On the molecular architecture of myelinated fibers. *Histochem Cell Biol*. 2000 Jan;113(1):1-18.
- Baer AS, Syed YA, Kang SU, Mitteregger D, Vig R, Ffrench-Constant C, Franklin RJ, Altmann F, Lubec G, Kotter MR. Myelin-mediated inhibition of oligodendrocyte precursor differentiation can be overcome by pharmacological modulation of Fyn-RhoA and protein kinase C signalling. *Brain*. 2009 Feb;132(Pt 2):465-81.
- Baumrind NL, Parkinson D, Wayne DB, Heuser JE, Pearlman AL. EMA: a developmentally regulated cell-surface glycoprotein of CNS neurons that is concentrated at the leading edge of growth cones. *Dev Dyn*. 1992 Aug;194(4):311-25.
- Benarroch EE. Brain cholesterol metabolism and neurologic disease. *Neurology*. 2008 Oct 21;71(17):1368-73.
- Benson DL, Colman DR, Huntley GW. Molecules, maps and synapse specificity. *Nat Rev Neurosci*. 2001 Dec;2(12):899-909.
- Birling MC, Tait S, Hardy RJ, Brophy PJ. A novel rat tetraspan protein in cells of the oligodendrocyte lineage. *J Neurochem*. 1999 Dec;73(6):2600-8.
- Birnboim HC, Doly J. A rapid alkaline extraction procedure for screening recombinant plasmid DNA. *Nucleic Acids Res*. 1979 Nov 24;7(6):1513-23.
- Blum H, Beier H, Gross HJ. Improved silver staining of plant proteins, RNA and DNA in polyacrylamide gels. *Electrophoresis* 1987, 8:93-99.
- Boggs J. Myelin basic protein: a multifunctional protein. *Cell Mol Life Sci*. 2006 Sep;63(17):1945-61.
- Boks MP, Hoogendoorn M, Jungerius BJ, Bakker SC, Sommer IE, Sinke RJ, Ophoff RA, Kahn RS. Do mood symptoms subdivide the schizophrenia phenotype? Association of the GMP6A gene with a depression subgroup. *Am J Med Genet B Neuropsychiatr Genet*. 2008 Sep 5;147B(6):707-11.
- Brocco MA, Fernández ME, Frasch AC. Filopodial protrusions induced by glycoprotein M6a exhibit high motility and aids synapse formation. *ur J Neurosci*. 2010 Jan;31(2):195-202.
- Carrel L, Willard HF. X-inactivation profile reveals extensive variability in X-linked gene expression in females. *Nature*. 2005 Mar 17;434(7031):400-4.
- Charrin S, Manié S, Thiele C, Billard M, Gerlier D, Boucheix C, Rubinstein E. A physical and functional link between cholesterol and tetraspanins. *Eur J Immunol*. 2003 Sep;33(9):2479-89.
- Charrin S, le Naour F, Silvie O, Milhiet PE, Boucheix C, Rubinstein E. Lateral organization of membrane proteins: tetraspanins spin their web. *Biochem J*. 2009 May 13;420(2):133-54.
- Cooper B, Werner HB, Flügge G. Glycoprotein M6a is present in glutamatergic axons in adult rat forebrain and cerebellum. *Brain Res*. 2008 Mar 4;1197:1-12.

Cooper B, Fuchs E, Flügge G. Expression of the axonal membrane glycoprotein M6a is regulated by chronic stress. *PLoS One*. 2009;4(1):e3659.

Deissler H, Blass-Kampmann S, Kindler-Röhrborn A, Meyer HE, Rajewsky MF. Characterization of rat NCA/CD9 cell surface antigen and its expression by normal and malignant neural cells. *J Neurosci Res*. 1996 Mar 15;43(6):664-74.

Dent EW, Kalil K. Axon branching requires interactions between dynamic microtubules and actin filaments. *J Neurosci*. 2001 Dec 15;21(24):9757-69.

Dent EW, Gertler FB. Cytoskeletal dynamics and transport in growth cone motility and axon guidance. *Neuron*. 2003 Oct 9;40(2):209-27.

Dent EW, Kwiatkowski AV, Mebane LM, Philippar U, Barzik M, Rubinson DA, Gupton S, Van Veen JE, Furman C, Zhang J, Alberts AS, Mori S, Gertler FB. Filopodia are required for cortical neurite initiation. *Nat Cell Biol*. 2007 Dec;9(12):1347-59.

Dent EW, Gupton SL, Gertler FB. The growth cone cytoskeleton in axon outgrowth and guidance. *Cold Spring Harb Perspect Biol*. 2011 Mar 1;3(3).

Dhaunchak AS, Nave KA. A common mechanism of PLP/DM20 misfolding causes cysteine-mediated endoplasmic reticulum retention in oligodendrocytes and Pelizaeus-Merzbacher disease. *Proc Natl Acad Sci U S A*. 2007 Nov 6;104(45):17813-8.

Dhaunchak AS, Huang JK, De Faria Junior O, Roth AD, Pedraza L, Antel JP, Bar-Or A, Colman DR. A proteome map of axoglial specializations isolated and purified from human central nervous system. *Glia*. 2010 Dec;58(16):1949-60.

Dickson BJ. Molecular mechanisms of axon guidance. *Science*. 2002 Dec 6;298(5600):1959-64.

Dugas JC, Tai YC, Speed TP, Ngai J, Barres BA. Functional genomic analysis of oligodendrocyte differentiation. *J Neurosci*. 2006 Oct 25;26(43):10967-83.

Edgar JM, McLaughlin M, Yool D, Zhang SC, Fowler JH, Montague P, Barrie JA, McCulloch MC, Duncan ID, Garbern J, Nave KA, Griffiths IR. Oligodendroglial modulation of fast axonal transport in a mouse model of hereditary spastic paraplegia. *J Cell Biol*. 2004 Jul 5;166(1):121-31.

Egea J, Klein R. Bidirectional Eph-ephrin signaling during axon guidance. *Trends Cell Biol*. 2007 May;17(5):230-8.

Feldheim DA, O'Leary DD. Visual map development: bidirectional signaling, bifunctional guidance molecules, and competition. *Cold Spring Harb Perspect Biol*. 2010 Nov;2(11):a001768.

Fernández ME, Alfonso J, Brocco MA, Frasch AC. Conserved cellular function and stress-mediated regulation among members of the proteolipid protein family. *J Neurosci Res*. 2010 May 1;88(6):1298-308.

Fiori LM, Zouk H, Himmelman C, Turecki G. X chromosome and suicide. *Mol Psychiatry*. 2011 Feb;16(2):216-26.

Fjorback AW, Müller HK, Wiborg O. Membrane glycoprotein M6B interacts with the human serotonin transporter. *J Mol Neurosci*. 2009 Mar;37(3):191-200.

Folch J, Lees M. Proteolipides, a new type of tissue lipoproteins; their isolation from brain. *J Biol Chem*. 1951 Aug;191(2):807-17.

Fradkin LG, Kamphorst JT, DiAntonio A, Goodman CS, Noordermeer JN. Genomewide analysis of the *Drosophila* tetraspanins reveals a subset with similar function in the formation of the embryonic synapse. *Proc Natl Acad Sci U S A*. 2002 Oct 15;99(21):13663-8.

- Fuchsova B, Fernández ME, Alfonso J, Frasch AC. Cysteine residues in the large extracellular loop (EC2) are essential for the function of the stress-regulated glycoprotein M6a. *J Biol Chem*. 2009 Nov 13;284(46):32075-88.
- Garbern JY. Pelizaeus-Merzbacher disease: Genetic and cellular pathogenesis. *Cell Mol Life Sci*. 2007 Jan;64(1):50-65.
- Garcia-España A, Chung PJ, Sarkar IN, Stiner E, Sun TT, Desalle R. Appearance of new tetraspanin genes during vertebrate evolution. *Genomics*. 2008 Apr;91(4):326-34.
- Geisert EE Jr, Williams RW, Geisert GR, Fan L, Asbury AM, Maecker HT, Deng J, Levy S. Increased brain size and glial cell number in CD81-null mice. *J Comp Neurol*. 2002 Nov 4;453(1):22-32.
- Gilbert SF. *Developmental Biology*. 7th Edition. Sinauer Associates. 2003.
- Griffiths I, Klugmann M, Anderson T, Thomson C, Vouyiouklis D, Nave KA. Current concepts of PLP and its role in the nervous system. *Microsc Res Tech*. 1998a Jun 1;41(5):344-58.
- Griffiths I, Klugmann M, Anderson T, Yool D, Thomson C, Schwab MH, Schneider A, Zimmermann F, McCulloch M, Nadon N, Nave KA. Axonal swellings and degeneration in mice lacking the major proteolipid of myelin. *Science*. 1998b Jun 5;280(5369):1610-3.
- Hall A, Lalli G. Rho and Ras GTPases in axon growth, guidance, and branching. *Cold Spring Harb Perspect Biol*. 2010 Feb;2(2):a001818.
- Hartline DK, Colman DR. Rapid conduction and the evolution of giant axons and myelinated fibers. *Curr Biol*. 2007 Jan 9;17(1):R29-35.
- Hemler ME. Specific tetraspanin functions. *J Cell Biol*. 2001 Dec 24;155(7):1103-7.
- Hemler ME. Tetraspanin functions and associated microdomains. *Nat Rev Mol Cell Biol*. 2005 Oct;6(10):801-11.
- Hemler ME. Targeting of tetraspanin proteins--potential benefits and strategies. *Nat Rev Drug Discov*. 2008 Sep;7(9):747-58.
- Henneke M, Wehner LE, Hennies HC, Preuss N, Gärtner J. Mutation analysis of the M6b gene in patients with Pelizaeus-Merzbacher-like syndrome. *Am J Med Genet A*. 2004 Jul 15;128A(2):156-8.
- Huang S, Yuan S, Dong M, Su J, Yu C, Shen Y, Xie X, Yu Y, Yu X, Chen S, Zhang S, Pontarotti P, Xu A. The phylogenetic analysis of tetraspanins projects the evolution of cell-cell interactions from unicellular to multicellular organisms. *Genomics*. 2005 Dec;86(6):674-84.
- Huber AB, Kolodkin AL, Ginty DD, Cloutier JF. Signaling at the growth cone: ligand-receptor complexes and the control of axon growth and guidance. *Annu Rev Neurosci*. 2003;26:509-63.
- Huminiacki L, Lloyd AT, Wolfe KH. Congruence of tissue expression profiles from Gene Expression Atlas, SAGEmap and TissueInfo databases. *BMC Genomics*. 2003 Jul 29;4(1):31.
- Innocenti GM, Price DJ. Exuberance in the development of cortical networks. *Nat Rev Neurosci*. 2005 Dec;6(12):955-65.
- Isensee J, Witt H, Pregla R, Hetzer R, Regitz-Zagrosek V, Noppinger PR. Sexually dimorphic gene expression in the heart of mice and men. *J Mol Med*. 2008 Jan;86(1):61-74.
- Ishibashi T, Ding L, Ikenaka K, Inoue Y, Miyado K, Mekada E, Baba H. Tetraspanin protein CD9 is a novel paranodal component regulating paranodal junctional formation. *J Neurosci*. 2004 Jan 7;24(1):96-102.
- Israels SJ, McMillan-Ward EM. Platelet tetraspanin complexes and their association with lipid rafts. *Thromb Haemost*. 2007 Nov;98(5):1081-7.

- Jahn O, Tenzer S, Werner HB. Myelin proteomics: molecular anatomy of an insulating sheath. *Mol Neurobiol.* 2009 Aug;40(1):55-72.
- Jessell TM. Neuronal specification in the spinal cord: inductive signals and transcriptional codes. *Nat Rev Genet.* 2000 Oct;1(1):20-9.
- Jung M, M., I. Sommer, M. Schachner, and K.A. Nave. Monoclonal antibody O10 defines a conformationally sensitive cell-surface epitope of proteolipid protein (PLP): evidence that PLP misfolding underlies dysmyelination in mutant mice. *J Neurosci.* 1996. 16:7920-9.
- Kagawa T, Mekada E, Shishido Y, Ikenaka K. Immune system-related CD9 is expressed in mouse central nervous system myelin at a very late stage of myelination. *J Neurosci Res.* 1997 Oct 15;50(2):312-20.
- Kalil K, Dent EW. Touch and go: guidance cues signal to the growth cone cytoskeleton. *Curr Opin Neurobiol.* 2005 Oct;15(5):521-6.
- Kandel ER, Schwartz JH, Jessell TM (Ed.). Principles of neural science, 4th Edition. McGraw Hill. 2000.
- Kang R, Wan J, Arstikaitis P, Takahashi H, Huang K, Bailey AO, Thompson JX, Roth AF, Drisdell RC, Mastro R, Green WN, Yates JR 3rd, Davis NG, El-Husseini A. Neural palmitoyl-proteomics reveals dynamic synaptic palmitoylation. *Nature.* 2008 Dec 18;456(7224):904-9.
- Kitagawa K, Sinoway MP, Yang C, Gould RM, Colman DR. A proteolipid protein gene family: expression in sharks and rays and possible evolution from an ancestral gene encoding a pore-forming polypeptide. *Neuron.* 1993 Sep;11(3):433-48.
- Klämbt C. Modes and regulation of glial migration in vertebrates and invertebrates. *Nat Rev Neurosci.* 2009 Nov;10(11):769-79.
- Klugmann M, Schwab MH, Pühlhofer A, Schneider A, Zimmermann F, Griffiths IR, Nave KA. Assembly of CNS myelin in the absence of proteolipid protein. *Neuron.* 1997 Jan;18(1):59-70.
- Knöll B, Kretz O, Fiedler C, Alberti S, Schütz G, Frotscher M, Nordheim A. Serum response factor controls neuronal circuit assembly in the hippocampus. *Nat Neurosci.* 2006 Feb;9(2):195-204.
- Ko M, Zou K, Minagawa H, Yu W, Gong JS, Yanagisawa K, Michikawa M. Cholesterol-mediated neurite outgrowth is differently regulated between cortical and hippocampal neurons. *J Biol Chem.* 2005 Dec 30;280(52):42759-65.
- Kopczynski CC, Davis GW, Goodman CS. A neural tetraspanin, encoded by late bloomer, that facilitates synapse formation. *Science.* 1996 Mar 29;271(5257):1867-70.
- Kovalenko OV, Metcalf DG, DeGrado WF, Hemler ME. Structural organization and interactions of transmembrane domains in tetraspanin proteins. *BMC Struct Biol.* 2005 Jun 28;5:11.
- Krämer-Albers EM, Gehrig-Burger K, Thiele C, Trotter J, Nave KA. Perturbed interactions of mutant proteolipid protein/DM20 with cholesterol and lipid rafts in oligodendroglia: implications for dysmyelination in spastic paraplegia. *J Neurosci.* 2006 Nov 8;26(45):11743-52.
- Krämer-Albers EM, White R. From axon-glial signalling to myelination: the integrating role of oligodendroglial Fyn kinase. *Cell Mol Life Sci.* 2011 Jun;68(12):2003-12.
- Laemmli UK. Cleavage of structural proteins during the assembly of the head of bacteriophage T4. *Nature.* 1970 Aug 15;227(5259):680-5.
- Lagenaur C, Kunemund V, Fischer G, Fushiki S, Schachner M. Monoclonal M6 antibody interferes with neurite extension of cultured neurons. *J Neurobiol.* 1992 Feb;23(1):71-88.

- Lappe-Siefke C, Goebbels S, Gravel M, Nicksch E, Lee J, Braun PE, Griffiths IR, Nave KA. Disruption of Cnp1 uncouples oligodendroglial functions in axonal support and myelination. *Nat Genet.* 2003 Mar;33(3):366-74.
- Lee JC, Mayer-Proschel M, Rao MS. Gliogenesis in the central nervous system. *Glia.* 2000 Apr;30(2):105-21.
- Levy S, Shoham T. The tetraspanin web modulates immune-signalling complexes. *Nat Rev Immunol.* 2005a Feb;5(2):136-48.
- Levy S, Shoham T. Protein-protein interactions in the tetraspanin web. *Physiology (Bethesda).* 2005b Aug;20:218-24.
- Liang YJ, Wu DF, Stumm R, Höllt V, Koch T. Membrane glycoprotein M6A promotes mu-opioid receptor endocytosis and facilitates receptor sorting into the recycling pathway. *Cell Res.* 2008 Jul;18(7):768-79.
- López-Bendito G, Molnár Z. Thalamocortical development: how are we going to get there? *Nat Rev Neurosci.* 2003 Apr;4(4):276-89.
- Lowry OH, Rosebrough NJ, Farr AL, Randall RJ. Protein measurement with the Folin phenol reagent. *J Biol Chem.* 1951 Nov;193(1):265-75.
- Lowery LA, Van Vactor D. The trip of the tip: understanding the growth cone machinery. *Nat Rev Mol Cell Biol.* 2009 May;10(5):332-43.
- Lund RD, Perry VH, Lagenaur CF. Cell surface changes in the developing optic nerve of mice. *J Comp Neurol.* 1986 May 22;247(4):439-46.
- Maecker HT, Todd SC, Levy S. The tetraspanin superfamily: molecular facilitators. *FASEB J.* 1997 May;11(6):428-42.
- Mattila PK, Lappalainen P. Filopodia: molecular architecture and cellular functions. *Nat Rev Mol Cell Biol.* 2008 Jun;9(6):446-54.
- Mela A, Goldman JE. The tetraspanin KAI1/CD82 is expressed by late-lineage oligodendrocyte precursors and may function to restrict precursor migration and promote oligodendrocyte differentiation and myelination. *J Neurosci.* 2009 Sep 9;29(36):11172-81.
- Mi ZP, Weng W, Hankin MH, Narayanan V, Lagenaur CF. Maturation changes in cell surface antigen expression in the mouse retina and optic pathway. *Brain Res Dev Brain Res.* 1998 Mar 12;106(1-2):145-54.
- Michibata H, Okuno T, Konishi N, Wakimoto K, Kyono K, Aoki K, Kondo Y, Takata K, Kitamura Y, Taniguchi T. Inhibition of mouse GPM6A expression leads to decreased differentiation of neurons derived from mouse embryonic stem cells. *Stem Cells Dev.* 2008 Aug;17(4):641-51.
- Michibata H, Okuno T, Konishi N, Kyono K, Wakimoto K, Aoki K, Kondo Y, Takata K, Kitamura Y, Taniguchi T. Human GPM6A is associated with differentiation and neuronal migration of neurons derived from human embryonic stem cells. *Stem Cells Dev.* 2009 May;18(4):629-39.
- Möbius W, Patzig J, Nave KA, Werner HB. Phylogeny of proteolipid proteins: divergence, constraints, and the evolution of novel functions in myelination and neuroprotection. *Neuron Glia Biol.* 2008 May;4(2):111-27.
- Mortz E, Krogh TN, Vorum H, Görg A. Improved silver staining protocols for high sensitivity protein identification using matrix-assisted laser desorption/ionization-time of flight analysis. *Proteomics.* 2001 Nov;1(11):1359-63.
- Mullis K, Faloona F, Scharf S, Saiki R, Horn G, Erlich H. Specific enzymatic amplification of DNA in vitro: the polymerase chain reaction. *Cold Spring Harb Symp Quant Biol.* 1986;51 Pt 1:263-73.

Nakamura Y, Iwamoto R, Mekada E. Expression and distribution of CD9 in myelin of the central and peripheral nervous systems. *Am J Pathol.* 1996 Aug;149(2):575-83.

Narayanan V, Olinsky S, Dahle E, Naidu S, Zoghbi HY. Mutation analysis of the M6b gene in patients with Rett syndrome. *Am J Med Genet.* 1998 Jun 30;78(2):165-8.

Nave KA, Lai C, Bloom FE, Milner RJ. Jimpy mutant mouse: a 74-base deletion in the mRNA for myelin proteolipid protein and evidence for a primary defect in RNA splicing. *Proc Natl Acad Sci U S A.* 1986 Dec;83(23):9264-8.

Nave KA, Lai C, Bloom FE, Milner RJ. Splice site selection in the proteolipid protein (PLP) gene transcript and primary structure of the DM-20 protein of central nervous system myelin. *Proc Natl Acad Sci U S A.* 1987 Aug;84(16):5665-9.

Nave KA. Myelination and the trophic support of long axons. *Nat Rev Neurosci.* 2010a Apr;11(4):275-83.

Nave KA. Myelination and support of axonal integrity by glia. *Nature.* 2010b Nov 11;468(7321):244-52.

Nielsen JA, Maric D, Lau P, Barker JL, Hudson LD. Identification of a novel oligodendrocyte cell adhesion protein using gene expression profiling. *J Neurosci.* 2006 Sep 27;26(39):9881-91.

Norton WT, Poduslo SE. Myelination in rat brain: method of myelin isolation. *J Neurochem.* 1973 Oct;21(4):749-57.

Norton WT. Recent advances in myelin biochemistry. *Ann N Y Acad Sci.* 1984;436:5-10.

Olinsky S, Loop BT, DeKosky A, Ripepi B, Weng W, Cummins J, Wenger SL, Yan Y, Lagenaur C, Narayanan V. Chromosomal mapping of the human M6 genes. *Genomics.* 1996 May 1;33(3):532-6.

Pandithage R, Lilischkis R, Harting K, Wolf A, Jedamzik B, Lüscher-Firzlaff J, Vervoorts J, Lasonder E, Kremmer E, Knöll B, Lüscher B. The regulation of SIRT2 function by cyclin-dependent kinases affects cell motility. *J Cell Biol.* 2008 Mar 10;180(5):915-29.

Pasquale EB. Eph-ephrin promiscuity is now crystal clear. *Nat Neurosci.* 2004 May;7(5):417-8.

Pfenninger KH. Plasma membrane expansion: a neuron's Herculean task. *Nat Rev Neurosci.* 2009 Apr;10(4):251-61.

Poliak S, Peles E. The local differentiation of myelinated axons at nodes of Ranvier. *Nat Rev Neurosci.* 2003 Dec;4(12):968-80.

Pols MS, Klumperman J. Trafficking and function of the tetraspanin CD63. *Exp Cell Res.* 2009 May 15;315(9):1584-92.

Popot JL, Pham Dinh D, Dautigny A. Major Myelin proteolipid: the 4-alpha-helix topology. *J Membr Biol.* 1991 Mar;120(3):233-46.

Ramón y Cajal S. *Histología del sistema nervioso del hombre y de los vertebrados. Volume I. (Re-edition of 1899-1904 and 1909-1911).* Consejo Superior de Investigaciones Científicas. 2008.

Readhead C, Schneider A, Griffiths I, Nave KA. Premature arrest of myelin formation in transgenic mice with increased proteolipid protein gene dosage. *Neuron.* 1994 Mar;12(3):583-95.

Rosenbluth J, Nave KA, Mierzwa A, Schiff R. Subtle myelin defects in PLP-null mice. *Glia.* 2006 Aug 15;54(3):172-82.

Roth AD, Ivanova A, Colman DR. New observations on the compact myelin proteome. *Neuron Glia Biol.* 2006 Feb;2(1):15-21.

Roussel G, Trifilieff E, Lagenaur C, Nussbaum JL. Immunoelectron microscopic localization of the M6a antigen in rat brain. *J Neurocytol.* 1998 Sep;27(9):695-703.

- Rowe DD, Leonardo CC, Hall AA, Shahaduzzaman MD, Collier LA, Willing AE, Pennypacker KR. Cord blood administration induces oligodendrocyte survival through alterations in gene expression. *Brain Res.* 2010 Dec 17;1366:172-88.
- Rubinstein E, Le Naour F, Lagaudrière-Gesbert C, Billard M, Conjeaud H, Boucheix C. CD9, CD63, CD81, and CD82 are components of a surface tetraspan network connected to HLA-DR and VLA integrins. *Eur J Immunol.* 1996 Nov;26(11):2657-65.
- Saher G, Brügger B, Lappe-Siefke C, Möbius W, Tozawa R, Wehr MC, Wieland F, Ishibashi S, Nave KA. High cholesterol level is essential for myelin membrane growth. *Nat Neurosci.* 2005 Apr;8(4):468-75.
- Saher G, Quintes S, Nave KA. Cholesterol: a novel regulatory role in myelin formation. *Neuroscientist.* 2011 Feb;17(1):79-93.
- Schneider A, Länder H, Schulz G, Wolburg H, Nave KA, Schulz JB, Simons M. Palmitoylation is a sorting determinant for transport to the myelin membrane. *J Cell Sci.* 2005 Jun 1;118(Pt 11):2415-23.
- Schneider A, Montague P, Griffiths I, Fanarraga M, Kennedy P, Brophy P, Nave KA. Uncoupling of hypomyelination and glial cell death by a mutation in the proteolipid protein gene. *Nature.* 1992 Aug 27;358(6389):758-61.
- Scorticati C, Formoso K, Frasch AC. Neuronal glycoprotein M6a induces filopodia formation via association with cholesterol-rich lipid rafts. *J Neurochem.* 2011 Mar 23. [Epub ahead of print]
- Sebastiani P, Wang L, Nolan VG, Melista E, Ma Q, Baldwin CT, Steinberg MH. Fetal hemoglobin in sickle cell anemia: Bayesian modeling of genetic associations. *Am J Hematol.* 2008 Mar;83(3):189-95.
- Seigneuret M, Delaguillaumie A, Lagaudrière-Gesbert C, Conjeaud H. Structure of the tetraspanin main extracellular domain. A partially conserved fold with a structurally variable domain insertion. *J Biol Chem.* 2001 Oct 26;276(43):40055-64.
- Seong E, Saunders TL, Stewart CL, Burmeister M. To knockout in 129 or in C57BL/6: that is the question. *Trends Genet.* 2004 Feb;20(2):59-62.
- Sheetz MP, Baumrind NL, Wayne DB, Pearlman AL. Concentration of membrane antigens by forward transport and trapping in neuronal growth cones. *Cell.* 1990 Apr 20;61(2):231-41.
- Sherman DL, Brophy PJ. Mechanisms of axon ensheathment and myelin growth. *Nat Rev Neurosci.* 2005 Sep;6(9):683-90.
- Simons K, Ikonen E. Functional rafts in cell membranes. *Nature.* 1997 Jun 5;387(6633):569-72.
- Simons K, Toomre D. Lipid rafts and signal transduction. *Nat Rev Mol Cell Biol.* 2000 Oct;1(1):31-9.
- Simons M, Krämer EM, Thiele C, Stoffel W, Trotter J. Assembly of myelin by association of proteolipid protein with cholesterol- and galactosylceramide-rich membrane domains. *J Cell Biol.* 2000 Oct 2;151(1):143-54.
- Simons M, Kramer EM, Macchi P, Rathke-Hartlieb S, Trotter J, Nave KA, Schulz JB. Overexpression of the myelin proteolipid protein leads to accumulation of cholesterol and proteolipid protein in endosomes/lysosomes: implications for Pelizaeus-Merzbacher disease. *J Cell Biol.* 2002 Apr 15;157(2):327-36.
- Snell, RS. *Neuroanatomía clínica*, 5ª ed. Lippincott Williams & Wilkins, Inc. USA, 2001.
- Squire LR, Bloom FE, McConnell SK, Roberts JL, Spitzer NC, Zigmond MJ (Ed.). *Fundamental Neuroscience*, 2nd Edition. Academic Press. 2002.
- Stipp CS, Kolesnikova TV, Hemler ME. Functional domains in tetraspanin proteins. *Trends Biochem Sci.* 2003 Feb;28(2):106-12.

- Sullivan CD, Geisert EE Jr. Expression of rat target of the antiproliferative antibody (TAPA) in the developing brain. *J Comp Neurol*. 1998 Jul 6;396(3):366-80.
- Tarrant JM, Robb L, van Spriel AB, Wright MD. Tetraspanins: molecular organisers of the leukocyte surface. *Trends Immunol*. 2003 Nov;24(11):610-7.
- Taylor CM, Marta CB, Claycomb RJ, Han DK, Rasband MN, Coetzee T, Pfeiffer SE. Proteomic mapping provides powerful insights into functional myelin biology. *Proc Natl Acad Sci U S A*. 2004 Mar 30;101(13):4643-8.
- Terada N, Baracska K, Kinter M, Melrose S, Brophy PJ, Boucheix C, Bjartmar C, Kidd G, Trapp BD. The tetraspanin protein, CD9, is expressed by progenitor cells committed to oligodendrogenesis and is linked to beta1 integrin, CD81, and Tspan-2. *Glia*. 2002 Dec;40(3):350-9.
- Tessier-Lavigne M, Goodman CS. The molecular biology of axon guidance. *Science*. 1996 Nov 15;274(5290):1123-33.
- Timsit SG, Bally-Cuif L, Colman DR, Zalc B. DM-20 mRNA is expressed during the embryonic development of the nervous system of the mouse. *J Neurochem*. 1992 Mar;58(3):1172-5.
- Tiwari-Woodruff SK, Buznikov AG, Vu TQ, Micevych PE, Chen K, Kornblum HI, Bronstein JM. OSP/claudin-11 forms a complex with a novel member of the tetraspanin super family and beta1 integrin and regulates proliferation and migration of oligodendrocytes. *J Cell Biol*. 2001 Apr 16;153(2):295-305.
- Tiwari-Woodruff SK, Kaplan R, Kornblum HI, Bronstein JM. Developmental expression of OAP-1/Tspan-3, a member of the tetraspanin superfamily. *J Neurosci Res*. 2004 Jul 15;77(2):166-73.
- Tole S, Patterson PH. Distribution of CD9 in the developing and mature rat nervous system. *Dev Dyn*. 1993 Jun;197(2):94-106.
- Towbin H, Staehelin T, Gordon J. Electrophoretic transfer of proteins from polyacrylamide gels to nitrocellulose sheets: procedure and some applications. *Proc Natl Acad Sci U S A*. 1979 Sep;76(9):4350-4.
- Trapp BD, Nave KA. Multiple sclerosis: an immune or neurodegenerative disorder? *Annu Rev Neurosci*. 2008;31:247-69.
- Turner G, Gedeon A, Kerr B, Bennett R, Mulley J, Partington M. Syndromic form of X-linked mental retardation with marked hypotonia in early life, severe mental handicap, and difficult adult behavior maps to Xp22. *Am J Med Genet A*. 2003 Mar 15;117A(3):245-50.
- Vanrobaeys F, Van Coster R, Dhondt G, Devreese B, Van Beeumen J. Profiling of myelin proteins by 2D-gel electrophoresis and multidimensional liquid chromatography coupled to MALDI TOF-TOF mass spectrometry. *J Proteome Res*. 2005 Nov-Dec;4(6):2283-93.
- Wahl S, Barth H, Ciossek T, Aktories K, Mueller BK. Ephrin-A5 induces collapse of growth cones by activating Rho and Rho kinase. *J Cell Biol*. 2000 Apr 17;149(2):263-70.
- Weimbs T, Stoffel W. Proteolipid protein (PLP) of CNS myelin: positions of free, disulfide-bonded, and fatty acid thioester-linked cysteine residues and implications for the membrane topology of PLP. *Biochemistry*. 1992 Dec 15;31(49):12289-96.
- Werner H, Dimou L, Klugmann M, Pfeiffer S, Nave KA. Multiple splice isoforms of proteolipid M6B in neurons and oligodendrocytes. *Mol Cell Neurosci*. 2001 Dec;18(6):593-605.
- Werner HB, Kuhlmann K, Shen S, Uecker M, Schardt A, Dimova K, Orfaniotou F, Dhaunchak A, Brinkmann BG, Möbius W, Guarente L, Casaccia-Bonnel P, Jahn O, Nave KA. Proteolipid protein is required for transport of sirtuin 2 into CNS myelin. *J Neurosci*. 2007 Jul 18;27(29):7717-30.
- Woodward KJ. The molecular and cellular defects underlying Pelizaeus-Merzbacher disease. *Expert Rev Mol Med*. 2008 May 19;10:e14.

Wu DF, Koch T, Liang YJ, Stumm R, Schulz S, Schröder H, Höllt V. Membrane glycoprotein M6a interacts with the micro-opioid receptor and facilitates receptor endocytosis and recycling. *J Biol Chem.* 2007 Jul 27;282(30):22239-47.

Yan Y, Lagenaur C, Narayanan V. Molecular cloning of M6: identification of a PLP/DM20 gene family. *Neuron.* 1993 Sep;11(3):423-31.

Yan Y, Narayanan V, Lagenaur C. Expression of members of the proteolipid protein gene family in the developing murine central nervous system. *J Comp Neurol.* 1996 Jul 8;370(4):465-78.

Yáñez-Mó M, Barreiro O, Gordon-Alonso M, Sala-Valdés M, Sánchez-Madrid F. Tetraspanin-enriched microdomains: a functional unit in cell plasma membranes. *Trends Cell Biol.* 2009 Sep;19(9):434-46.

Yin X, Baek RC, Kirschner DA, Peterson A, Fujii Y, Nave KA, Macklin WB, Trapp BD. Evolution of a neuroprotective function of central nervous system myelin. *J Cell Biol.* 2006 Jan 30;172(3):469-78.

Zappia MP, Brocco MA, Billi SC, Frasca AC, Ceriani MF. M6 membrane protein plays an essential role in *Drosophila* oogenesis. *PLoS One.* 2011;6(5):e19715.

Zhang SC. Defining glial cells during CNS development. *Nat Rev Neurosci.* 2001 Nov;2(11):840-3.

Zhao J, Iida A, Ouchi Y, Satoh S, Watanabe S. M6a is expressed in the murine neural retina and regulates neurite extension. *Mol Vis.* 2008 Sep 3;14:1623-30.

Zheng Y, Cheng XR, Zhou WX, Zhang YX. Gene expression patterns of hippocampus and cerebral cortex of senescence-accelerated mouse treated with Huang-Lian-Jie-Du decoction. *Neurosci Lett.* 2008 Jul 11;439(2):119-24.

Appendix 1: List of publications

de Monasterio-Schrader* P, Fünfschilling* U, Mitskovski M, Burzynska AZ, Dimou L, Papiol S, Klugmann M, Nave K-A, Werner HB. Neuronal proteolipids M6A and M6B are required for neurite extension and proper growth cone function (in preparation).

Patzig* P, Jahn* O, Tenzer* S, Wichert SV, **de Monasterio-Schrader P**, Rosfa S, Kuharev J, Yan K, Bormuth I, Bremer J, Aguzzi A, Orfaniotou F, Hesse D, Schwab MH, Möbius W, Nave K-A, Werner HB. Quantitative and integrative proteome analysis of peripheral nerve myelin identifies novel myelin proteins and candidate neuropathy loci. *Journal of Neuroscience* (in revision).

Werner HB, Krämer-Albers E-M, **de Monasterio-Schrader P**, Strenzke N, Saher S, Möbius W, Tenzer S, Ohno-Iwashita Y, Moser T, Griffiths IR, Nave K-A. A critical role for the cholesterol-associated proteolipids PLP and M6B in myelination of the central nervous system (in preparation).

de Monasterio-Schrader P, Kasapoglu B, Jahn O, Tenzer S, Wichert SP, Werner HB. Systematic approaches to myelin. *Cellular and Molecular Life Sciences*, Invited Review, in preparation.

Yague JG, Muñoz A, **de Monasterio-Schrader P**, DeFelipe J, Garcia-Segura LM, Azcoitia I. Aromatase Expression In The Human Temporal Cortex. *Neuroscience*; 138: 389-401 (2006).

Appendix 2: *Curriculum vitae*

Personal Data:

Name: Patricia de Monasterio Schrader
Address: Weender Strasse 23, 37073 Göttingen
Email-address: monasterio@em.mpg.de
Date of Birth : 19th April 1980
Place of Birth: Madrid

Education:

2007-current **Graduate student**
Prof. Nave, Dept. Neurogenetics,
Max-Planck-Institute of Experimental Medicine, Göttingen

2005-2007 **Diploma de Estudios Avanzados**
University Complutense of Madrid, Neuroscience PhD Program
Laboratory of Prof. Azcoitia, Dept. Cell Biology

1998-2005 **Diploma in Biology**
Speciality of Neurobiology and Medical Biology
University Complutense of Madrid

1998 **German Abitur and Spanish Selectividad**
Secondary-school examinations, German School of Madrid

1990 – 1998 **Gymnasium**
German School of Madrid

Professional Qualifications:

2004 – 2007 **Research assistant**
Prof. Azcoitia, Dept. Cell Biology, Faculty of Biology,
University Complutense of Madrid

2005 – 2007 **Research assistant**
Prof. Nave, Dept. Neurogenetics,
Max-Planck-Institute of Experimental Medicine, Göttingen

2004 **Internship**
Prof. Nave, Dept. Neurogenetics,
Max-Planck-Institute of Experimental Medicine, Göttingen

2003 **Internship**
Prof. Beisiegel, Institute of Biochemistry and Molecular Biology II:
Molecular Cell Biology,
University Medical Center Hamburg-Eppendorf

Publications:

Yague JG, Muñoz A, de Monasterio-Schrader P, DeFelipe J, Garcia-Segura LM, Azcoitia I. Aromatase Expression In The Human Temporal Cortex. *Neuroscience*; 138: 389-401 (2006).

Meeting abstracts:

de Monasterio-Schrader* P, Fünfschilling* U, Mitskovski M, Burzynska AZ, Klugmann M, Dimou L, Papiol S, Nave K-A, Werner HB. Neuronal growth cones and neurite extension require M6-glycoproteins. 9th Göttingen Meeting of the German Neuroscience Society, March 2011.

P. de Monasterio-Schrader, U. Fünfschilling, M. Mitkovski, A.Z. Burzynska, M. Klugmann, L. Dimou, S. Papiol, K.-A. Nave, and H.B. Werner. Growth cones require M6-glycoproteins for normal structure and function. 40th Annual Meeting of the Society for Neuroscience, November 2010, San Diego, California.

P. de Monasterio-Schrader, W.B. Werner, E.M. Krämer-Albers, N. Strenzke, G. Saher W. Möbius, S. Tenzer, Y. Ohno-Iwashita, T. Moser, I.R. Griffiths, K.-A. Nave. High-level expression of the proteolipids PLP and M6B is sufficient to induce oligodendroglial process outgrowth *in vitro* and required for normal myelination *in vivo*. 9th European Meeting on Glial Cells in Health and Disease, September 2009, Paris.

P. de Monasterio-Schrader, U. Fünfschilling, A. Burzynska, L. Dimou, M. Klugmann, K.-A. Nave, H.B. Werner. Neuronal M6-proteolipids are required for neurite extension. 8th Göttingen Meeting of the German Neuroscience Society, March 2009.

García Yagüe J., de Monasterio Schrader P., Alonso Nanclares L., Muñoz Céspedes A., DeFelipe Oroquieta J., García Segura L.M., Azcoitia I. Expresión de aromatasa (estradiol sintasa) en corteza cerebral y en gliomas humanos. XI Congreso Nacional de Neurociencia, Málaga, 2005. Spain.

Teaching:

2009	Lab-rotation supervision Project: "Analysis of neurodegeneration and neuroinflammation in the brains of Tetraspanin 2 knockout mice"
2008	Lab-rotation supervision Project: "Proteolipid interactions in Pelizaeus-Merzbacher disease and their cholesterol –binding properties"
1994-2005	Biology and German private lessons, Madrid

Courses:

October 2009	CME Course "Leukoencephalopathies" European Confederation of Neuropathological Societies, Amsterdam
--------------	---

Languages:

German	native language
Spanish	native language
English	Very good knowledge June 2008, Cambridge Certificate of Proficiency in English (B)
French	Good knowledge, 2008, Basic Level 3, Ernst-August University Göttingen